COMPUTING THE FUNDAMENTAL INTERACTIONS

BETWEEN CARBON NANOTUBES AND

PULMONARY SURFACTANT PROTEINS

Bhushan V. Dharmadhikari

Under the Supervision of: Dr. Prabir Patra

DISSERTATION

SUBMITTED IN PARTIAL FULFILMENT OF THE REQUIRMENTS

FOR THE DEGREE OF DOCTOR OF PHILOSOPHY IN COMPUTER SCIENCE

AND ENGINEERING

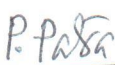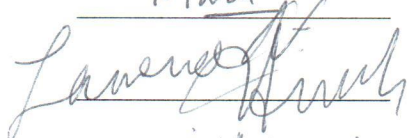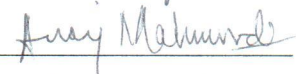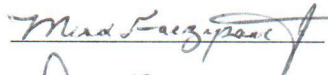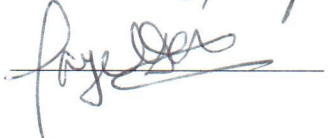THE SCHOOL OF ENGINEERING

UNIVERSITY OF BRIDGEPORT

CONNECTICUT

April 2015

COMPUTING THE FUNDAMENTAL INTERACTIONS BETWEEN CARBON NANOTUBES AND PULMONARY SURFACTANT PROTEINS

Approvals

Committee Members

Name	Signature	Date
Dr. Prabir Patra	*P. Patra*	4/24/15
Dr. Lawrence Hmurcik	*Lawrence Hmurcik*	4/24/15
Dr. Ausif Mahmood	*Ausif Mahmood*	4-24-2015
Dr. Xingguo Xiong	*Xingguo Xiong*	04/24/2015
Dr. Miad Faezipour	*Miad Faezipour*	4, 24, 2015
Dr. Payel Das	*Payel Das*	4/24/15

Ph.D. Program Coordinator

Dr. Khaled M. Elleithy	*Khaled E.*	5/5/15

Chairman, Computer Science and Engineering Department

Dr. Ausif Mahmood	*Ausif Mahmood*	4-24-2015

Dean, School of Engineering

Dr. Tarek M. Sobh	*T. Sobh*	5/5/15

COMPUTING THE FUNDAMENTAL INTERACTION OF CARBON NANOTUBES AND PULMONARY SURFACTANT PROTEINS

II ॐ गम गणपतये नमः II

You cannot believe in God until you believe in yourself.

— Swami Vivekananda

Dedicated to my family

For their endless love, support and encouragement

COMPUTING THE FUNDAMENTAL INTERACTION OF CARBON NANOTUBES AND PULMONARY SURFACTANT PROTEINS

ABSTRACT

Molecular dynamic computation is one of the most direct and detailed approaches for investigating protein and carbon nanotube interaction at the atomic level. Molecular dynamic computation can address the events occurring in a protein's structure and on the surface of the carbon nanotube. Molecular dynamic computation can also explain the structural changes in protein, including (i) secondary and tertiary structure changes, (ii) orientation and reorientation of the protein before and after adsorption, (iii) behavior of each amino acid residual group, (iv) hydrogen-bonding, (v) pi-pi stacking of carbon atoms of proteins and carbon nanotube, and other things as well. These fundamental properties have to address the adsorption of protein on a carbon nanotube surface, and estimates of this process are produced by molecular dynamic computations. Also, molecular dynamic computation is an attractive method for 3D imaging in bio-nanotechnology because it can give a complete trajectory over time (tens or hundreds of nanoseconds) of all atoms of protein interacting with carbon nanotubes and thus clarify their behavior in a given environment.

This work presents the fundamental understanding of the human pulmonary surfactant proteins SP-A, SP-B, SP-C, and SP-D and their interaction with a single-walled carbon nanotube. This is accomplished using nanoscale molecular dynamic computation. Atomistic molecular dynamic simulation is performed and a trajectory over 100 ns is computed. Results show that all four pulmonary surfactant proteins are adsorbed on the surface of a carbon nanotube. The main driving force of interaction is the Van der Waals force of attraction. From the root mean square deviation of all four protein trajectories, stability is achieved. Both hydrophobic and hydrophilic residues of proteins are adsorbed on the surface of a carbon nanotube. These results will be helpful in developing nano-electro-chemical biosensors in the future.

ACKNOWLEDGEMENTS

First, I would like to express my sincere thanks to my PhD advisor **Dr. Prabir Patra** for his guidance and for encouraging my research. Dr. Patra is the reason why I decided to go to pursue a career in research. He is lively, enthusiastic, and energetic nature kept me motivated all the time.

I would like to thank **Dr. Lawrence Hmurcik** for his unconditional support throughout my MS and PhD life.

I would like to thank my PhD thesis Committee members **Dr. Ausif Mahmood**, **Dr. Xingguo Xiong,** and **Dr. Miad Faezipour** for their expert advice and time.

I would like to extend my thanks and appreciation to external committee member **Dr. Payel Das** (IBM, Thomas J. Watson Research Center, Yorktown Heights, NY USA). She provided me with her expert advice on molecular dynamics computations.

I would also like to thank **Dr. Michael McGuigan** (Deputy Director) Computational Science Center Brookhaven National Laboratory for giving us access for NY Blue IBM Blue Gene super computer. I would like to extend my thanks to **Leonard Slatest** (Sr. Technology Engineer) Computational Science Center Brookhaven National Laboratory for providing tech support with NY Blue Gene super computer.

TABLE OF CONTENTS

LIST OF TABLES

LIST OF FIGURES

positively charged carbon nanotube after 100 ns. The carbon nanotube horizontal and the protein structure is represented in purple and secondary structure color scheme

electrochemical

CHAPTER 1: INTRODUCTION

A fundamental and important step in developing any carbon nanotube based protein biosensor is to investigate how the targeted protein molecule interacts with a carbon nanotube. The adsorption or binding process of protein to a carbon nanotube may change the structure and properties of protein. This may lead to faulty results in electrochemically sensing protein by the carbon nanotube sensor. Advancement in laboratory instruments has produced many new experimental ideas, and these experiments greatly improve the understanding of the interaction between proteins and the carbon nanotube surface. Yet, the atomic details of interaction occurring at the molecular level are still ambiguous due to limitations in instruments and experimental methods. For instance, changes in the function and in the conformation of protein as well as spatial orientation of protein residues that are not covalently adsorb on the surface of carbon nanotube are poorly understand by experimental methods. Protein folding and the dynamics of protein adsorption on the surface of a carbon nanotube occur in picoseconds, and present day experimental setups cannot explain this interaction. Understanding this phenomenon is of great value to the study of a biomolecule's behavior in the presence of a carbon nanotube and to their application in nano-electrochemical biosensor fabrication.

Motivation behind this project started with the question of why premature babies develop infant respiratory distress syndrome (IRDS) after birth, which results in death of a newly born infant if necessary treatment is not received in time.

Infants affected by IRDS have a deficiency of pulmonary surfactant, and this may be the result of premature delivery, or it may be genetically transferred. Pulmonary surfactant is the substance inside the lungs, which is necessary to maintain surface tension between the air-water interface. This is a host defense mechanism. Pulmonary surfactant is a complex material made up of lipids and proteins. Proteins constitute 10% of total pulmonary surfactant, but they play a very vital role in the functioning of the respiratory system. A pulmonary surfactant complex consists of four protein named in order of their discovery SP-A, SP-B, SP-C and SP-D. SP-A and SP-D are big and heavy protein molecules and hydrophilic in nature; they play a role in host defense mechanism by fighting infections and pathogen attacks. SP-B and SP-C are smaller. SP-C is the smallest. SP-B and SP-C play an important role in homeostasis of the air-fluid interface, and they prevent the lungs from collapsing. These proteins become active after birth at the first breath of the newborn. If a newborn has a deficiency of protein SP-B, this results in a lack of surface tension between the air-fluid interface. After birth, the lungs of a newborn are filled with fluid and with no surface tension, air rushes into the pulmonary system and compresses the lungs. After this, the lungs fail to trap carbon dioxide and other gases and this results in death of the newborn, assuming proper treatment is not provided on time.

Development of pulmonary surfactant proteins starts during the fourth month of pregnancy at the beginning of organogenesis. Early detection of a deficiency of these proteins is possible by extracting a fetal serum sample and measuring the amount of the pulmonary surfactant proteins for normal functioning of lungs after birth. In addition, this test predicts abnormalities that may lead to IRDS or other respiratory related disorders.

During this stage of fetus development, a large quantity of serum sample from the fetus cannot be extracted without leading to complications in pregnancy. A solution to this problem is to extract the minimum amount of sample (micro to nano liters) and extract proteins from it for measurement. The size of pulmonary surfactant protein molecules ranges from 2 to 10 nm. In order to detect pulmonary surfactant protein molecules that have a size range within a few nanometers, there is a need to have nanostructures that are suitable for protein sensing applications. From the wide range of nanostructures available at the present time, carbon nanotubes are most suitable because of their sensing properties produced by their large specific surface area, which provides binding sites for protein residues. Carbon nanotubes are chemically very stable with biomolecules and provide faster electron transfer. Carbon nanotubes also have excellent mechanical stiffness, thermal conductivity, and electrical conductivity, which make carbon nanotube an ideal nanostructure for electrochemical biosensor.

Potential contributions of this work are:

1. Computational understanding of specific and non-specific binding events of human pulmonary surfactant proteins with carbon nanotubes from single molecule computations

2. The structural evolution of these human pulmonary surfactant proteins on a carbon nanotube's surface for a 100 ns trajectory, in order to elucidate the exact mode of binding (using IBM Blue Gene).

3. Proposed research work will enable specific understanding of hydrophilic and hydrophobic interaction forces between different

protein residues and carbon nanotubes, and this information will be used to design novel biosensors.

4.   Carbon nanotube based biosensors have quickly developed in the past decade; much research work and funding has been spent each year on developing biosensor applications using carbon nanotubes. Research on carbon nanotubes for protein detection or for the detection of other biomolecules is still a very active research area in nanoscience, both biomedical and biomaterial. Carbon nanotubes have found applications in a wide variety of areas from drug delivery systems to VLSI circuits computer chips.

CHAPTER 2: PULMONARY SURFACTANT SYSTEM

Surfactant is an agent that reduces the surface tension between two surfaces. The surface tension between a gas and water interface in the lungs is decreased by the presence of a thin film of fluid known as a pulmonary surfactant. Pulmonary surfactants are produced by type – II Pneumocytes in alveolar cells [1].

A pulmonary surfactant is a complex mixture of phospholipids and proteins, and it creates a unique interface, separating alveolar gas and liquids at the alveolar cell surface, reducing surface tension, and maintaining lung volumes at end expiration. Reduction of the surface tension at the air-liquid interface is a requirement for respiratory function following birth. Deficiency of pulmonary surfactant causes respiratory failure in premature infants, also called infantile respiratory distress syndrome (IRDS) [2]. The adequacy of pulmonary surfactant is maintained by a unique and highly regulated system mediating the synthesis, secretion, re-uptake, re-utilization, and catabolism of surfactant. Loss of pulmonary surfactant later in life occurs in the adult respiratory distress syndrome (ARDS), a significant cause of morbidity and mortality following infection, shock, or trauma [2, 3].

In 1929, Van Neergaard recognized the critical role of surface tension as a "retractile force" in the lung, observing the marked difference in inflation pressures required to inflate the air- versus water-filled lung. Avery and Mead associated the lack

of a lipid-rich material in the lungs of infants dying from IRDS with alveolar collapse and respiratory failure. In the absence of pulmonary surfactant, molecular forces at the air-liquid interface create a region of high surface tension because intermolecular forces between water molecules are unopposed at the air-liquid interface, and an area of high retractile force at the surface is created [4-6]. In 1950's Avery and Mead [7] demonstrated that IRDS or hyaline membrane diseases of a new born is associated with surfactant deficiency. In 1955 Pattle [8] and 1957 Clements [9] also investigated pulmonary surfactant's capacity for reducing surface tension and also recognized the ability of a pulmonary surfactant to adsorb and spread rapidly to form an insoluble surface film. They also demonstrated that reduction in surface area resulted in a corresponding fall in surface tension to surprisingly low values.

2.1 Composition of Pulmonary Surfactant

Pulmonary surfactant consists of highly heterogeneous forms of phospholipid-protein aggregates of distinct sizes, structural characteristics, and composition. Tubular myelin is the most abundant form of alveolar phospholipid and consists of large, relatively dense aggregates composed of phospholipids and surfactant proteins [10]. The main components of the complexes are phospholipids(90%) and proteins(10%) [11]. Phospholipids mainly contain phosphatidylcholine, and 40% of them are dipalmitoyl phosphatidylcholine (DPPC). There are still other forms of phospholipids such as phosphatidyl glycerol (PE), Phosphatidylinositol (PI) and sphingomyelin (SM) [12].

In the adult lung, phosphatidylcholine 70 to 80 % and phosphatidylglycerol 10 % are the most abundant phospholipid constituents. Lesser amounts of phosphatidylserine,

phosphatidylethanolamine, sphingomyelin, neutral lipids, and glycolipids are also detected in the surfactant. The lung content of surfactant phospholipids increases markedly with advancing gestation [13].

2.2 Pulmonary Surfactant Proteins

Proteins represent approximately 10 to 15 % of the mass of pulmonary surfactant and include serum proteins and proteins that are produce by respiratory epithelial cells. Four surfactant proteins—SP-A, SP-B, SP-C, and SP-D— are produced by respiratory epithelial cells, each playing specific roles in surfactant homeostasis or host defense [14].

Four distinct proteins have been isolated from pulmonary surfactant. Their cDNAs, genes, and structures have been identified and are well characterized. Pulmonary surfactant proteins are expressed in a lung epithelial cell–selective manner and are secreted into the airspace, where they influence the structure, metabolism, and function of the surfactant. Two classes of proteins have been distinguished on the basis of their structures [8, 15, 16].

SP-A and SP-D are in abundance, hydrophilic, structurally related proteins that are members of the calcium-dependent lectin family of proteins from collagenous domains. These molecules have weak surfactant like qualities, but are able to specifically bind complex carbohydrates, lipids, and glycolipids, including those found on the surface of pathogens like bacteria, viruses, fungi, and other lung pathogens [17]. They act as opsonins, activate alveolar macrophages, and play important roles in host defense in the lung. In contrast, SPB and SP-C are small, hydrophobic proteins that play vital roles in enhancing the rate of spreading and stability of surfactant phospholipids. SP-B and SP-C

7

are the protein components of the animal-derived surfactant replacement preparations used for the treatment of IRDS [15, 18, 19].

2.3 Pulmonary Surfactant Protein SP-A

Surfactant protein A (SP-A) has been found in every vertebrate species. Protein SP-A is a hydrophilic 26-kD (monomer) glycoprotein that functions in the host defense and regulates surfactant lipid structure [20]. Sequence comparison of the cDNAs for SP-A isolated from human, dog, rabbit, guinea pig and mouse reveal extensive homology [21]. The primary structure of SP-A is defined by four well structured domains: a short N-terminal segment containing inter-chained disulfide bonds, a proline rich collagen like region, a hydrophobic neck domain and a carbohydrate recognition domain (CRD) with a high degree of homology to several members of the Ca^{2+} dependent C-type mammalian lectins, especially mannose binding protein A (MBP-A) [20]. Deletion of the SP-A protein gene (Sftpa) in mice does not alter survival or lung function after birth. While tubular myelin is absent in newborns, surfactant function and secretion are not influenced by deletion of SP-A. SP-A -/- new born mice are highly susceptible to lung infection by bacterial, viral, and fungal pathogens, indicating that SP-A plays a primary role in innate host defense of the lung. [22]

2.4 Pulmonary Surfactant Protein SP-B

Surfactant protein B (SP-B) is a small homodimeric protein that is found tightly associated with surfactant lipids in the alveolar space. SP-B is a hydrophobic 8.8-kD protein produced from a single gene (SFTPB) located on human chromosome 2. The SP-B mRNA is expressed in bronchioles and type II alveolar cells and is translated to

produce a 40- to 42-kD precursor that is proteolytically processed (breakdown of proteins into smaller polypeptides or amino acids) to form the active 79-amino acid peptides found in surfactant. Almost 50 percent of the protein is in an, α-helical conformation, with approximately 20 percent β-sheet and 16 percent turns. As SP-B is associated with phospholipids, the positively charged amino acid residues of SP-B selectively interact with negatively charged phospholipid DPPC. Carboxy-terminal regions of SP-B 1 to 20 and 53 to 78, which contain the predicted amphipathic helices. Synthetic peptides that contain these two regions have surface-tension lowering activity similar to that of native SP-B [23].

To further assess the role of SP-B in lung function, the SP-B gene was disrupted by homologous recombination in murine mouse embryonic stem cells. Mice with a single mutated SP-B allele +/- were unaffected, whereas homozygous SP-B -/- offspring died of respiratory failure immediately after birth. Newborn mice exhibited normal appearance in weight and other bodily functions; they also initiated normal respiratory efforts but failed to inflate their lungs. In contrast newborn mice with SP-B +/- and SP-B +/+ showed normal respiratory functions. This demonstrates the critical role of pulmonary surfactant protein SP-B in homeostasis and in the initiation of lung inflation at birth [24].

SP-B deficient infants and mice die of respiratory failure following birth. For SP-B deficient mice in utero, the lungs shows normal development and proceeds normally, but the lack of SPB causes atelectasis (partial or complete collapse of the lung) and respiratory failure in the immediate postnatal period [24]. As recently reported by Yin Xiaojuan et al. 2013, in the RDS group, SP-B protein expression was reduced or deficient in eight neonates of which 6 had no SP-B protein expression. In the control group, only 1

had reduced SP-B protein expression [25]. SP-B deficiency, inherited as an autosomal-recessive mutation in the SFTPB gene, generally presents itself in full-term infants with IRDS. The disorder is refractory to surfactant replacement therapy and is generally lethal within the first several months of life. Several infants have undergone lung transplantation [26, 27]. Up until now 13 novel mutations in the SP-B gene have been characterized which are responsible for hereditary SP-B deficiency; some of these allowed production of reduced amounts of mature SP-B as well as precursor protein SP-B that was not processed to the functional, mature SP-B peptide, indicating a greater degree of allelic and biochemical heterogeneity in this disorder than previously appreciated [27, 28]. Hereditary SP-B deficiency is an autosomal recessive disorder in which affected infants develop severe respiratory disease that clinically and radiographically resembles RDS in premature infants. However, while premature infants with RDS may be successfully treated with surfactant replacement and supportive care, infants with hereditary SP-B deficiency develop progressive respiratory failure that is refractory to all treatment modalities except to a lung transplant [26-28].

2.5 Pulmonary Surfactant Protein SP-C

Pulmonary surfactant contains less than 1 wt% of the very non-polar surfactant protein C (SP-C) [29]. SP-C enhances the surface-active properties of lipid mixtures by lowering surface tension and enhancing the adsorption rate of a lipid film at the air-water interface. SP-C and SP-B reduce surface tension of a lipid film to near zero, and they increase lung compliance in premature animals [30, 31]. The structure reveals one very regular α-helix with nearly ideal helix geometry. The human SP-C polypeptide chain contains 35 amino acid residues; the carboxy-terminal, two-thirds of SP-C, is generally in

an α-helical conformation, but depalmitoylation reduces the α-helical content of native SP-C [32, 33].

Deletion of SP-C in transgenic mice perturbs surfactant function and causes severe interstitial lung disease. While SP-C -/- mice survive after birth. The SP-C -/- mice were viable at birth and grew normally to adulthood without apparent pulmonary abnormalities. When pulmonary surfactant protein SP-C is absence in mice lungs, they survive and grow normally with no adverse effects on health, reproduction, or pulmonary function. As both SP-B and SP-C are hydrophobic and surface active proteins and help in reducing the surface tension between air-water interface dramatically. Survival of SP-C -/- mice to adulthood indicates that SP-C is not required for surface properties of alveolar phospholipids film which is required to normal functioning of respiratory system [34]. As deficiency of SP-C may not result in loss of surface activity and loss of surface tension but may result in other respiratory complications. A study reported by Lawson et al. 2005 and Glasser et al. 2013 SP-C -/- mice may develop respiratory complications such as airspace abnormalities, pulmonary inflammation, and abnormal lipid accumulations in alveolar macrophages, and epithelial and stromal cells. While surfactant properties are only modestly perturbed, severe and progressive remodeling, emphysema, and fibrosis occur in these mice [35, 36].

2.6 Pulmonary Surfactant Protein SP-D

Surfactant protein-D is a collagenous $Ca2^+$ dependent carbohydrate-binding protein that is structurally related to SP-A and other C-type lectins. SP-D is synthesized by alveolar type II epithelial cells and is found in the endoplasmic reticulum and Golgi of Clara cells, but it is also expressed in many other tissues. SP-D forms large oligomers that bind carbohydrates and glycolipids on the surface of bacteria, fungi, and viruses [37, 38].

In contrast to surfactant proteins SP-A, SP-B, and SP-C, SP-D is not strongly associated with surfactant lipids in the alveolus but plays an important role in determining surfactant structure and phospholipid homeostasis. Deletion of SP-D in mice has provided insight into its important role in surfactant and alveolar homeostasis. SP-D -/- mice survive after birth, but develop severe pulmonary disease associated with macrophage activation, airspace enlargement, and lipid accumulation. Newborn mice born healthy and infection free, after several months, started showing abnormalities in surfactant homeostasis and alveolar cell morphology. There was a gradual accumulation of surfactant phospholipids and apo-proteins in the alveolar air space, hyperplasia of type II cells with massive augmentation of intracellular lamellar bodies, and an accumulation of foamy alveolar macrophages [39-41].

CHAPTER 3: CARBON NANOTUBE BASED BIOSENSORS

Since the discovery of carbon nanotubes in 1991 by Iijima [42], carbon nanotubes have attracted the attention of many researcher scientists. Carbon nanotubes have become one of the most widely studied nano-materials, and they have found applications in fields like energy storage, high-speed electronic circuits, medical machine and many other applications, including space exploration and radiation shielding. It is estimated that nanotechnology could become a $2.6 trillion business in 2014 [43, 44]. Carbon nanotube based electronic sensors have seen an increase in research in the past few years. By the year 2010 nearly 1800 US patents were filed referencing carbon nanotubes [45]. See Figure 3.1. By 2014, this number is expected to be 21,000. Figure 3.2, shows the trend of the number of publications dealing with carbon nanotubes and the estimated quantity of carbon nanotubes produced per year [46].
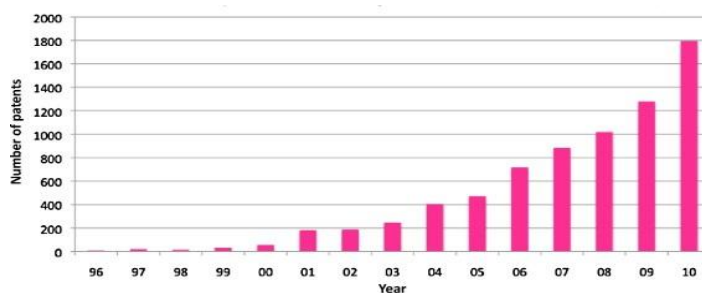
Figure 3.1: Trend of patents filed [source: Patent search engine] [45]
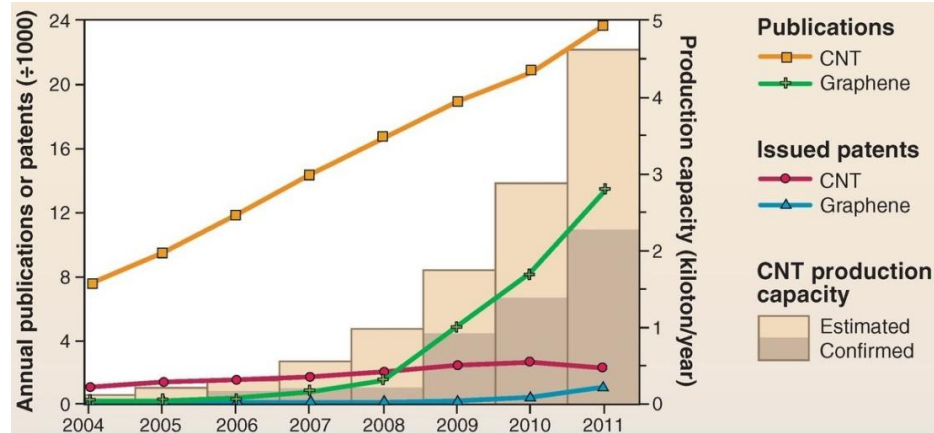
Figure 3.2: Trends in Carbon nanotube research and commercialization, Journal publications and issued worldwide patents per year, along with estimated annual production capacity [46]

3.1 Carbon nanotube and their properties

The carbon nanotube is the result of graphene layer folded into a carbon cylinder. Carbon nanotubes have found many applications because of their unique properties, such as mechanical stiffness [47], high carrier mobility [48], and thermal conductivity [49]. There have been many types of carbon nanotubes, since their initial discovery. Carbon nanotubes can be divided into single-walled carbon nanotubes and multiple-walled carbon nanotubes. Due to the different chiral structure of carbon nanotubes (n, m), they can also be divided into zigzag, armchair, and helix forms. From the standpoint of charge transport properties, there are metal and semiconductor carbon nanotubes.

If we use as a comparison the SP3 hybrid of common carbonization (such as methane and diamond), carbon atoms in a carbon nanotube use the SP2 hybrid, and this gives the carbon nanotube high stiffness. The tensile strength of a carbon nanotube can reach up to 50-200Pa, which is 100 times more than steel, while its density is only 1/6 of steel. Due to the SP2 hybrid form, the electrons in the P-orbital of a carbon nanotube form a large delocalized pi-bond which gives the carbon nanotube several unique

14

electrical properties. The electrical conductivity of a carbon nanotube is determined by the helical angle between the pipe diameter and pipe wall. When the diameter is less than 6nm, the electrical conductivity is high. If the diameter is more than 6nm, the electrical conductivity begins to decrease. The carbon nanotube has a large length-to-diameter ratio (called the aspect ratio) that gives it good thermal conductivity in the length-direction. By adjusting its orientations, a carbon nanotube can be used in synthesizing composite materials of different thermal conductivity.

3.2 Application of carbon nanotube as biosensors

A carbon nanotube can attach itself to many organic and non-organic functional groups, and this process is known as functionalization. Carbon nanotubes are built from sp2 carbon and present a seamless structure with a hexagonal honeycomb lattice. They are a few nanometers in diameter and many microns in length [50]. Britto et al. 1999, showed that a carbon nanotube's closed topology and tubular structure make them very efficient in charge transfer, and they predicted a possible use in electrode applications [51].

Development of nano-biosensors occurred in three stages: first generation sensors depend on dissolved oxygen, nitrogen or other element in a solvent; second generation sensors depend on the direct electron transfer from the enzyme to the electrode via nano-connectors, and these can sense the current corresponding to enzyme oxidation. Third generation biosensors utilize the unique property of large surface area offered by the nanomaterials. In these biosensors, the redox reaction caused by the enzyme or protein is electrically connected to the electrode via the nano-connectors. [52-56]

Initial research on the fabrication of enzyme electrode has begun, and this electrode can exhibit very high selectivity, sensitivity and long term stable response. Ping Loh et al. 2004, fabricated glucose sensors on both boron-doped diamond and CNT electrodes by the immobilization of glucose oxidase (GOD) on the DAB-modified surfaces [57]. A. Bhattacharya et al. 2014, showed that gold coated ZnO nano-rod heterostrutures show improved sensitivity, a lower detection limit. and wider linear detection range as compared to earlier reports on pristine ZnO nano-rod biosensors tested under the same conditions [58].

Single walled and multi walled carbon nanotubes are also used in detecting signals from neurotransmitter and the reactions of neurochemicals. W. Xue and T Cui, 2008 developed a very sensitive, low cost thin-film single wall carbon nanotube based transistor for detection of Acetylcholine [59]. Yogeswaran et al. 2007 developed a novel nano-composite material with fictionalization of multi-wall carbon nanotube with nafion, Platinum nano-particles and Gold nano-particles for simultaneously detecting ascorbic acid, epinephrine, and uric acid from an aqueous buffer solution [60].

3.2.1   Carbon nanotube as protein sensor

Shuqing Dong et al. 2008 showed the electrochemical behavior or nineteen different kinds of natural amino acids (arginine, tryptophan, histidine, threonine, serine, tyrosine, etc) with multi-walled carbon nanotubes. Most proteins are non-electroactive and show an oxidation current response with a modified (with CU_2O [61] carbon nanotube electrode. Wang et al. 2007, showed the electrochemical detection of insulin with a carbon nanotube modified with Ruthenium oxide which offers an improvement in

the stability and sensitivity of voltammetric (voltage) and amperometric (current) measurements of insulin compared to the individual (CNT or RuOx) coated electrodes [62]. Serafín et al. 2014 developed an amperometric immunosensor for the determination of the hormone insulin-like growth factor 1. Multi-walled carbon nanotubes were electro-polymerized with poly-pyrrole propionic acid; this approach provided a high content of surface-confined carboxyl groups suitable for direct covalent binding of anti-IGF1 monoclonal antibodies [63].

3.2.2 Carbon nanotube as DNA sensor

Carbon nanotubes are also used in detecting and identifying the sequence of DNA, the basic building of all life. Zheng et al. 2003 did a fundamental study of wrapping a carbon nanotube and single stranded DNA and showed the binding of the carbon nanotube and the ssDNA is sequence dependent. The ssDNA self-assembles into a helical structure around individual nanotubes in such a way that the electrostatic properties of the DNA-CNT hybrid depends on tube diameter and its electronic properties [64]. Keren et al. 2003 used the self-assembly property of DNA and single-walled carbon nanotubes to realize a carbon nanotube-based electronics. Keren et al. used a self-assembly strategy to form a functional circuit on a scaffold DNA network to fabricate a single-walled carbon nanotube field effect transistor [65]. Tang et al. 2006 fabricated a single-walled carbon nanotube DNA sensor with a simple and generic protocol for label free detection of DNA hybridization. The device fabricated by Tang et al. is based on the carbon nanotube field effect device, which can be readily scalable to high density sensor arrays and amenable to integration with "lab-on-a-chip" microanalysis systems [66].

3.2.3   Application of carbon nanotube to detect biomolecules

Carbon nanotubes are also used to detect other biomolecules, with some important applications listed below:

1. Fructose: Carbon nanotubes synthesized on Platinum electrode [67].

2. Influenza virus (type A): Influenza virus type-A DNA covalently bound to amine-functionalized multi-walled carbon nanotubes [68].

3. Hepatitis C virus RNA: Single-Walled Carbon Nanotube Field Effect Transistor (FET) devices functionalized with Peptide Nucleic Acid (PNA) [69].

4. Hepatitis B virus DNA: Multi-walled carbon nanotube based screen printed graphite electrodes used for electrochemical monitoring of DNA hybridization related to specific sequences on Hepatitis B virus DNA [70].

5. Adenine, Guanine, Thymine: Multi-walled CNT and β-cyclodextrin deposited of glassy carbon electrode [71].

6. Cholesterol: Multi-walled carbon nanotube functionalized by electro-deposition of Au particles onto thiol (–SH) for the immobilization of cholesterol oxidase into a cross-linked matrix of chitosan to fabricate an amperometric biosensor [72].

7. Human Immunodeficiency Virus (HIV) type-1: Single walled carbon nanotube modified by Gold nanoparticles and deposited on a Gold electrode for pico-molar electrochemical detection of HIV type-1 [73].

CHAPTER 4: MOLECULAR DYNAMICS COMPUTATION OF PULMONARY SURFACTANT PROTEINS

4.1 Molecular Dynamics Simulation

The experiments designed to observe the interaction between protein/peptide and carbon nanotube surfaces greatly enhance the understanding of the interaction between these molecules. However, the atomic details of dynamics taking place at the molecular/atomic level are still not well understood due to the limitation of current experimental technology. The dynamics of the adsorption process, which is the most fundamental process in biological applications of carbon nanotubes, is not clearly understood. Molecular dynamics (MD) simulation is of great importance, since it gives us the understanding of the environmental and biological activity of carbon nanotubes as well as their potential applications in nanostructure fabrication [74].

In 1977, McCammon et al. reported molecular dynamics simulations for the first time. The MD simulation was performed on the bovine pancreatic trypsin inhibitor (BPTI) in vacuum with a crude molecular mechanics potential and lasted for only 9.2 ps [75]. Later Brünger et al. 1985 [76] and Frauenfelder et al. 1987 [77] showed the importance of the effect of solvent and temperature variations on protein structure and its dynamics. Brooks et al. 1983 reported the role of configurational entropy in proteins by making use of an empirical potential function including local and nonlocal (nonbonded)

interactions in the full conformational space of the molecule (1,740 degrees of freedom) [78].

With the development in computation and massive scalable computers, like the IBM Bluegene, current simulations are now possible, 1000 times longer than this, and at a much faster computation speed. Much of the gain in simulation time is re-invested into studying much larger systems ($10^4 - 10^6$ atoms instead of 500), and this includes a system with an explicit solvent and/or membrane environment. In addition to being able to perform simulations for a much longer period, another important consequence of the access to faster computers is that multiple simulation runs can be performed to obtain estimates of statistical errors.

4.2 Molecular Dynamics Softwares

Widely used programs for molecular dynamics such as CHARMM [79] and its direct descendants AMBER [80] and GROMOS [81] have a great range of capabilities These programs can do everything that users often find that they cannot do in order to reach an exact solution to their problem [82].

NAMD (NAnoscale Molecular Dynamics program) [83] is a parallel molecular dynamics code designed for high-performance simulation of large bio-molecular systems. NAMD is based on Charm++ parallel objects (parallel programming model). NAMD scales to hundreds of cores for typical simulations and beyond 200,000 cores for the largest simulations. NAMD is known for its parallel efficiency, and it is often used to simulate large systems (millions of atoms). NAMD uses the popular molecular graphics

program VMD (Visual Molecular Dynamics) for simulation setups and trajectory analysis, but it is also file-compatible with AMBER, CHARMM, and X-PLOR.

VMD software is designed for modeling, visualization, and analysis of biological systems, such as proteins, nucleic acids, lipid bilayer assemblies, etc. It can be used to view more general molecules, since VMD can read standard Protein Data Bank (PDB) files and display the contained structure in 3D. VMD provides a wide variety of methods for rendering and coloring a molecule. VMD can be used to animate and analyze the trajectory of a molecular dynamics (MD) simulation. In particular, VMD can act as a graphical front end for an external MD program by displaying and animating a molecule undergoing simulation [84].

The interaction and binding of a pulmonary surfactant protein with a carbon nanotube can be studied in detail (i) by performing molecular dynamic simulation in an aqueous medium at constant temperature and pressure, (ii) by applying appropriate force field parameters, and (iii) by providing suitable periodic boundary conditions. Selecting the right software for visualization and computation is very critical. The most up-to-date software version of Visual Molecular Dynamics (VMD) is 1.9.1 for windows OpenGL, with CUDA compatibility used for visualization and trajectory analysis. NAMD 2.8 is designed for multicore use with MPI capability used to compute atomic trajectories.

4.3 Materials and Methods

4.3.1   Pulmonary Surfactant Protein

Appropriate X-ray structures for all four pulmonary surfactant proteins (SP-A, SP-B, SP-C, and SP-D) are obtained from the Protein Data Bank (http://www.pdb.org) in pdb file format. The codes for these pdb files are:

1. Pulmonary surfactant protein A (SP-A) [85]: 1r13 (1 − 148 residues)

2. Pulmonary surfactant protein B (SP-B) [86]: 1dfw (1 − 25 residues)

3. Pulmonary surfactant protein C (SP-C) [87]: 1spf (1 − 35 residues)

4. Pulmonary surfactant protein C (SP-D) [88]: 3DBZ (1 − 160 residues)
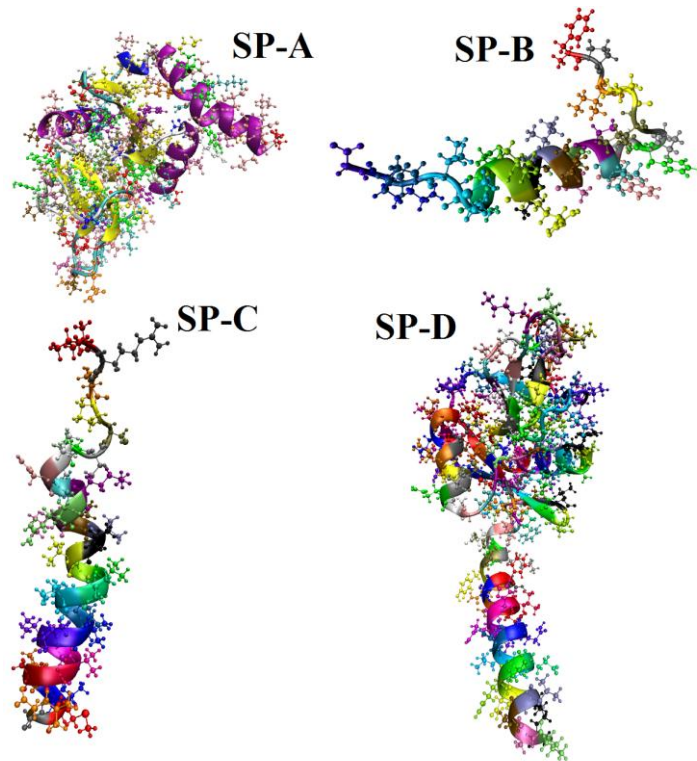
Figure 4.1: 3D structure of human pulmonary surfactant protein molecules.

Figure 4.1, shows the 3D structure of pulmonary surfactant protein molecules used in simulations. In SP-A all residues are used, and its structure shows 3 α-helixes and 3 β-sheets. SP-B and SP-C have one α-helix each. The SP-D molecule comes as a trimer, and one of the monomers is used for simulation. Like SP-A, it also has 3 α-helixes and 3 β-sheets. For protein SP-A and SP-C all of the residues are used for simulation. Given the critical in-vivo role for SP-B in lung function, it is of interest to us that numerous actions of the full-length protein on surfactant lipids are mimicked by a synthetic peptide representing the N-terminal domain of SP-, i.e. SP-B1-25. Therefore, only residues of 1–25 are considered for simulation [86, 89]. The polypeptides of protein SP-D are assembled into trimers which consist of a short non-collagenous N-terminal region, a collagen-like triple helix, followed by a helical coiled region which finally diverges into the three globular C-terminal CRDs that contain the ligand-binding sites [88]. All three monomers have similar properties and functions, and this eliminates the computational redundancy, sine only one of the three same monomers is used in simulation.

4.3.2   Carbon Nanotube

A single-walled carbon nanotube is generated using the "Nanotube Builder" plug-in from VMD software. Single-walled carbon nanotubes are cylindrical tubes of carbon atoms that can assume a wide range of atomic structures. Each structure is defined by two positive integers (n, m) called the chiral indices. The Nanotube Builder plug-in generates single-walled carbon nanotube structures of arbitrary length and chirality. Nanotube Builder can generate all three kinds of carbon nanotubes, viz. Armchair (n = m), Zigzag (m = 0), Chiral (m ≠ n). The carbon nanotube used in our simulation is Armchair (n = 6, m = 6) with length 5 nm and diameter approximately 0.8 nm, and it contains 503 carbon

atoms. All carbon atoms of a single-walled carbon nanotube are sp^2 hybridized, and they are neutral.

The coordinates of protein and a carbon nanotube have been adjusted such that distance between the geometric centers of protein and the carbon nanotube is equal to 2.5 nm, and the protein molecule is placed such that the protein-carbon nanotube contact surface is greater than or equal to 0.6 nm. This assures us that there is no initial interaction between atoms of protein and the carbon nanotube.

4.3.3   Solvating the Protein and Carbon Nanotube

The protein and carbon nanotube first need to be solvated, i.e. place them inside water to more closely resemble a cellular environment. The protein/carbon nanotube complex is placed inside a water box. The dimensions of the water box are selected such that the protein and carbon nanotube complex does not interact with its image in the next cell, in the event that periodic boundary conditions are used. The water box should be large enough so that, even if the protein is fully extended, water will immerse the protein and carbon nanotube complex. The water model selected for building the water box is TIP3P (transferable intermolecular potential 3P) [90]. Dimensions of the water box for all four proteins and carbon nanotube complexs are as follows:

Pulmonary surfactant protein with CNT	Water box Dimension in $Å^3$
SP-A	106×83×100
SP-B	58×65×67
SP-C	65×87×79
SP-D	88×111×76

Table 4.1: TIP3P water box dimensions

24

Ions are placed in the water to represent a more typical biological environment. They are especially necessary if the subject protein carries an excess charge. The ions will shield the regions of the protein that carry the charge and make the entire system more stable. Ions are placed in regions of potential minima, since they will be forced to those regions during the simulation anyway. In all cases, the protein and carbon nanotube complex is solvated in a 0.15 mol/liter sodium chloride solution.

Before starting the simulation, the X-ray structure obtained from protein database files for all four pulmonary surfactant proteins should equilibrate to the relaxed state. This is done by solvating the protein molecule alone in the water box with the 0.15 mol/L NaCl; this involves 5000 steps of energy minimization, followed by 10 ns of equilibration. After equilibration, the final coordinates of the protein molecules used to make the protein carbon nanotube complex is calculated.

4.4 Force field Parameter File

Selecting the right type of force field parameter is very important in the performance of molecular dynamics simulation. For simulation with protein and a carbon nanotube, CHARMM force field parameters are very suitable. A CHARMM force field parameter file contains all of the numerical constants needed to evaluate forces and energies, given a protein structure file and atomic coordinates. The current version of the CHARMM force field used for protein is CHARMM22.

4.5 NAMD Configuration Parameter

The exact configuration is given to NAMD on the command line, and it specifies virtually everything about the computation to be performed. The only exception is details

relating to the parallel execution environment, which varies between platforms. Therefore, the configuration file should be portable between machines, platforms, or processors in a run, as long as the referenced input files are available.

All computations are performed at a constant temperature of 300 K and constant pressure 1 atm or 101.3 kPa. Periodic boundary conditions have to be selected such that they can accommodate the complete water box even if the molecules/CNT have grown in size during the simulation. NAMD allow giving periodic boundary condition in 3D. Particle Mesh Ewald (PME) is an efficient full electrostatic method for use with periodic boundary conditions. PME also calculates the long-range electrostatic interactions with a cutoff distance of 12 Å for the separation of the direct and reciprocal space.

Molecular dynamic simulation uses the theory of Newton's laws and the laws of kinematics applied in discrete steps in order to determine the trajectories of atoms. The time step tells NAMD how to discretize the particle dynamics, and this is specified in femtoseconds (fs or 10^{-15} s). The integration time-step is normally limited to 1 fs but can be extended to 2 fs by fixing the length of all bonds in the molecule involving hydrogen atoms; this also makes water molecules completely rigid. Theoretically, a short-time step can improve the accuracy of calculations, and a long time-step can reduce calculation time and save computer resources. For any simulations involving water molecules, water should be made rigid since water molecules have been parameterized as rigid. Non-bonded forces must be calculated at least every 2 fs. Full electrostatic forces (from a particle mesh Ewald, a discussed above) are evaluated every other step.

To make computation faster, pair-list distance is specified in Angstroms (Å). By specifying this distance, NAMD will only search within this distance for atoms, which

26

may interact electrostatically or by Van der Waals forces. NAMD does not have to search the entire system of atoms in order to do its work. This distance must be greater than the cutoff distance, and the list must be updated during the simulation.

Energy minimization and equilibration in molecular dynamic simulations involve more than one minimization equilibration cycle, often fixing and releasing molecules in the system. For instance, one typically minimizes the system which then equilibrates with the atoms in the protein fixed in space, and then minimizes the system again and equilibrates again, this time with the protein free to move. In a protein carbon nanotube complex, fixed protein equilibration is performed for 40 ps, as energy minimization (5000 steps) and equilibration of the protein molecule take 10 ns. Coordinates are obtained and stored for the equilibrated protein molecule.

Fixing the protein allows the water, which typically responds much faster to forces than the protein, to complete relaxation in the first step. This saves computational effort and prevents the introduction of artifacts from an unstable starting structure. After completion of the fixed process, a protein molecule will be released and free to move, and this process will be followed by energy minimization for 5000 steps and equilibration for 100 ns.

4.6 Results and Discussion

The X-ray 3D structure of pulmonary surfactant proteins, SP-A, SP-B, SP-C and SP-D were obtained from the protein data bank (PDB code: 1r13, 1dfw, 1spf and 3DBZ, respectively). For SPD, one of the three same monomers was used. In this study, all MD simulations were performed by NAMD software with the force field CHARMM27.

Carbon nanotubes used were Armchair type with chiral vector (6, 6), generated using the Carbon Nanostructure Builder plug-in of VMD software with 0.8nm diameter and 5nm length containing 503 carbon atoms. The water box used is TIP3P model. All of the carbon atoms of carbon nanotube are neutral and defined as the SP2 hybrid form.

All molecular dynamics simulations are perform in the following manners:

1. Energy minimization and energy equilibration of four proteins is performed at constant temperature (300K) and pressure (1atm). Pulmonary surfactant proteins were solvated in 0.15 mol/L NaCl solution using the TIP3 water model. Dimensions of water boxes were ($106 \times 83 \times 100$) Å3 for SP-A, ($58 \times 65 \times 67$) Å3 for SP-B, ($65 \times 87 \times 79$) Å3 for SP-C and ($88 \times 111 \times 76$) Å3 for SP-D. All of four systems underwent 5000 steps energy minimization. Molecular dynamics simulations were run for all four systems until the Root-Mean-Square Deviation (rmsd) of all four pulmonary surfactant proteins fluctuate around a constant value. Then, coordinates are extracted and used in the final structures with the carbon nanotube to simulate a trajectory over a time of 100ns.

2. Due to the complex spatial structure of proteins, the orientation of a pulmonary surfactant protein molecule, relative to a carbon nanotube, is random. The initial distance between the geometrical center of a pulmonary surfactant protein and the nanotube is set to 2.5nm. The minimum distance between the protein and the nanotube is 0.6nm, so that there are several water layers in between to reduce the initial effect. The protein and carbon nanotube complex is solvated in a 0.15 mol/L sodium chloride solution. The water box sizes are ($104 \times 99 \times 101$)Å^3 SPA-CNT, ($82 \times 106 \times 111$)Å^3 SPB-CNT, ($95 \times 109 \times 111$)Å^3 SPC-CNT, and

$(105 \times 116 \times 101) \text{Å}^3$ SPD-CNT. Figure 4.2, shows all four proteins solvated in a water box.

3. Initially, energy minimization is performed for 5000 steps at constant temperature and pressure for all four systems. After minimization, all four systems equilibrate for 100ns until the rmsd and the system's total energy fluctuate around a constant value.

4. For all simulations, the time step was set up to 2 fs and the cutoff distance of non-bonded van der Waals force was 12 Å. Particle mesh Ewald (PME) summation was used to calculate the long-ranged electrostatic interactions, with a cutoff distance of 12 Å for the separation of the direct and reciprocal space. Periodic boundary conditions were used for setting up the initial cell. The Langevin method was applied to control the constant temperature at 300 K and the pressure at 101.3 kPa. Visualization of results and trajectories is done by the VMD (visual molecular dynamic) software package.
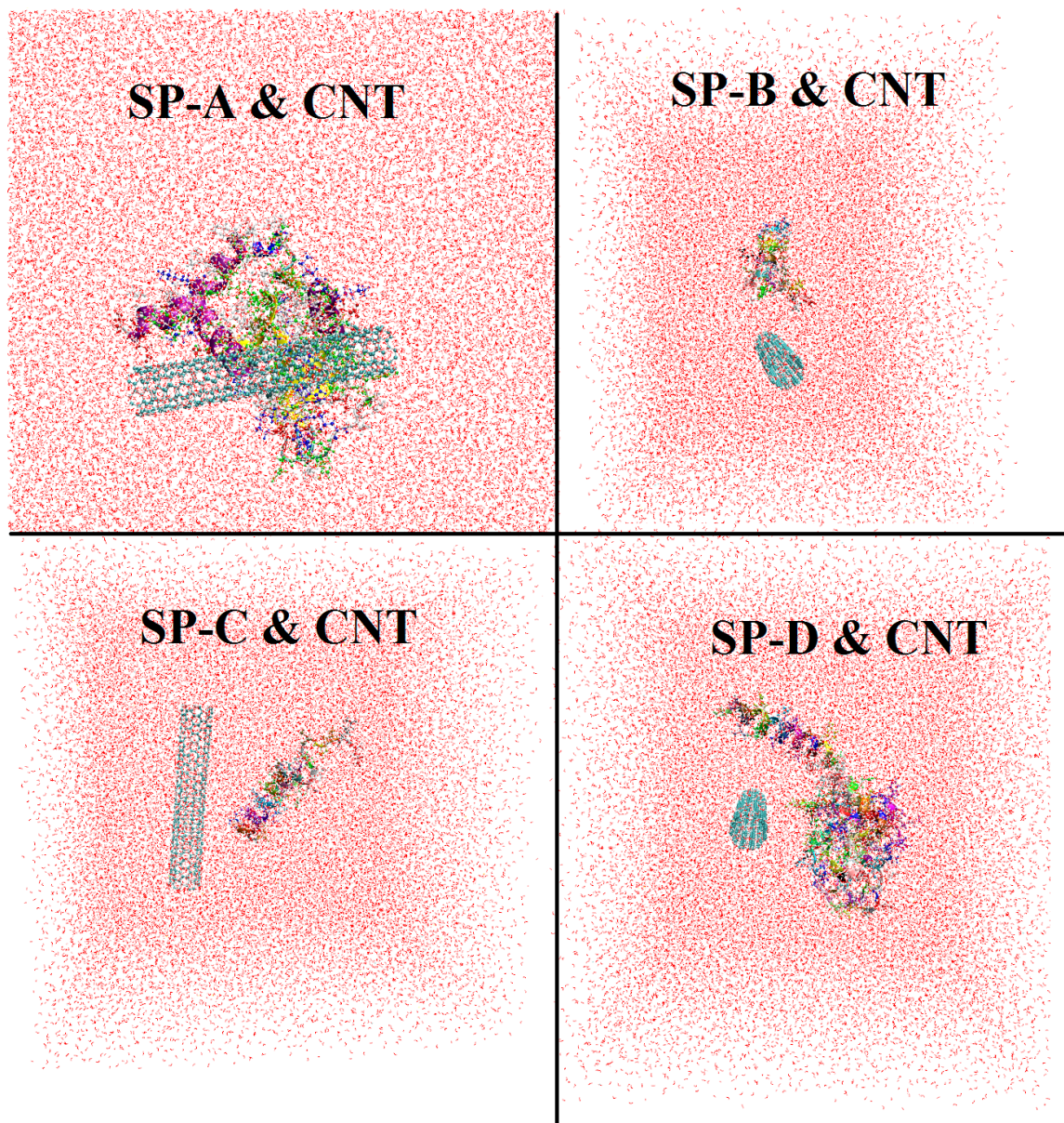
Figure 4.2: Pulmonary surfactant proteins solvated in water box and carbon nanotube.

Figure 4.2 illustrates all four pulmonary surfactant protein molecules in a water box with a carbon nanotube resting at its initial position.
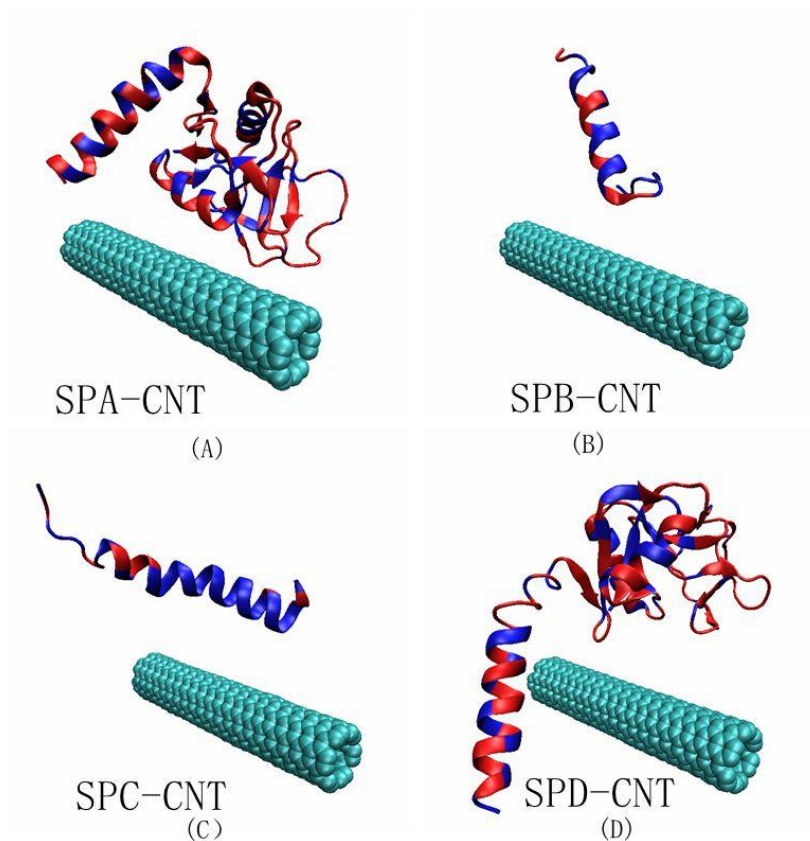
Figure 4.3: Initial conformations of the molecular systems: (A) SP-A with SWCNT, (B) SP-B with SWCNT; (C) SP-C with SWCNT, (D) is SPD with SWCNT. The hydrophobic portion of protein highlighted by blue color while hydrophilic portion highlighted by red color. For clarity, the water and ions removed.

In all of four molecular dynamic simulations, the dynamics of pulmonary surfactant proteins adsorption on the surface of a carbon nanotube is observed and demonstrated in the trajectory animation. The final conformations of four systems are shown in Figure 4.4. In Figure 4.4, the water molecules are removed for clarity. Figure 4.2, show all four pulmonary surfactant proteins solvated in a water box with the carbon nanotube at initial position. All four pulmonary surfactant protein molecules, SP-A, SP-B, SP-C, and SP-D, move close to the carbon nanotube and are adsorbed on the surface of the carbon nanotube.
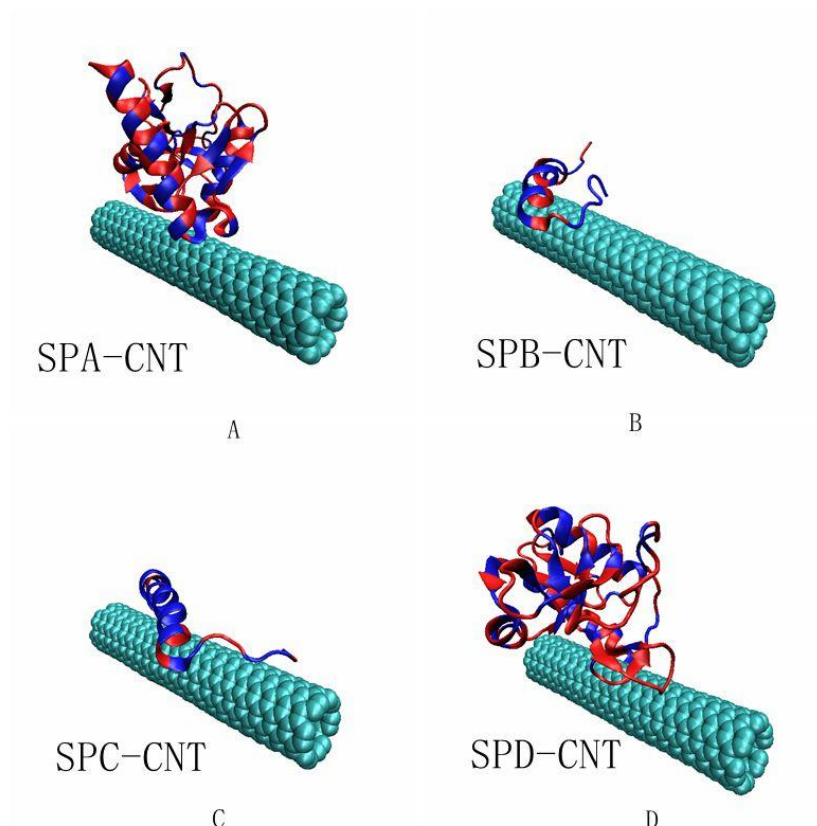
Figure 4.4: Final conformations of the molecular systems: (A) SP-A with SWCNT, B SP-B with SWCNT, (C) SP-C with SWCNT, (D) is SP-D with SWCNT.

4.7 Distance of Center of Mass

Figure 4.5, shows the distance of the center of mass for the pulmonary surfactant protein molecule to the surface of a carbon nanotube for 100ns. The distance between the center of mass for all four systems fluctuates around a constant value after 40 ns. All four proteins have attained a stable position on the surface of nanotube after 40 ns. For SP-B and SP-C, the distance decreased quickly after several nanoseconds. Since SP-A and SP-D are bigger molecules they struggle in beginning to attain their equilibrium position after 40 ns. On the other hand, SP-B and SP-C being smaller molecules their distance

from the carbon nanotube decreases rapidly and shows less fluctuation at 40 ns compared to SP-A and SP-D. This rapid fluctuation in SP-A and SP-D values also indicates proteins adjusting their conformations and rearranging their residues to reach thermodynamic equilibrium states and stable spatial configurations.
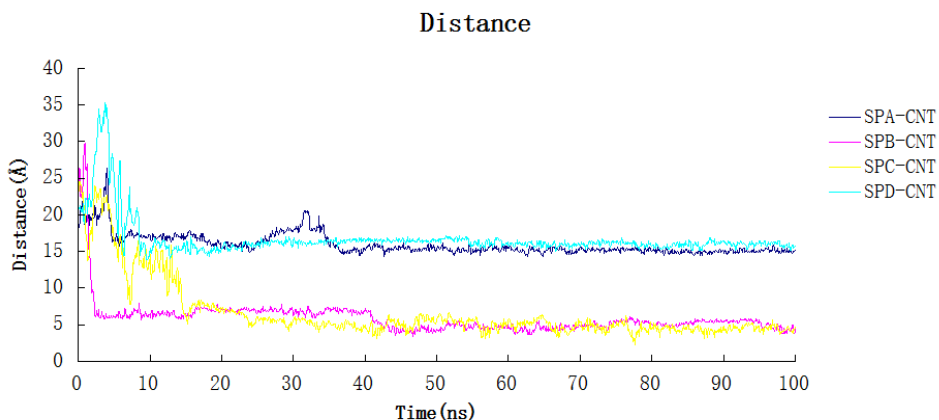
Figure 4.5: The distance of the center-of-mass for the protein to the surface of carbon nanotube in100ns simulations

SP-A and SP-D are typical hydrophilic proteins that mostly contain several α-helixes and extended conformations. They bury their hydrophobic groups inside themselves and spread hydrophilic residues on the surface to maintain a stable configuration. Distance as a function of time reveals that SP-B quickly moves (5 ns) closer to the surface of SWCNT and stays there for 100 ns. On the other hand, SP-C takes almost 15 ns and smoothly moves closer to surface of the SWCNT and stays adsorbed on the surface for the rest of the time. From Figure 4.5, it can be seen that for a very short duration of time, SP-B moves away from the carbon nanotube and then quickly moves closer; this is because the protein adjusts and readjusts its spatial orientation toward the surface of the carbon nanotube in order to achieve optimal conformation. The final value for the center of mass for SP-B is 4.034 Å, and for SP-C it is 4.7151 Å. The decrease in

33

the center of mass distance of both proteins shows the adsorption of protein on the surface of carbon nanotube. During the adsorption process, it appears that at the time when the hydrophobic surfaces of the protein and the carbon nanotube come closest, the adsorption process seems to stabilize.

4.8 Root Mean Square Deviation

The root mean square deviation (rmsd) between corresponding atoms of two protein chains is commonly used to measure the similarity between two protein structures. The smaller the rmsd is between two structures, the similar these two structures appear. Since the dynamics of interacting forces between a carbon nanotube and protein continuously influences the protein's structure to change, run time for a successful simulation should be long enough that rmds attains equilibrium and fluctuates between a stable value. Typically, the rmsd is considered stable if the fluctuations are less than or equal to 3 Å [91].

The Root Mean Square Deviation (rmsd) of a pulmonary surfactant's protein backbone is shown in Figure 4.6, and this is used to study the monolithic displacement of proteins over 100ns. During the last 15ns of all simulations, the rmsds of all four systems fluctuate around a constant values. The distance curve shown in Figure 4.5 indicates that proteins first move closer to the surface of a carbon nanotube, and then they walk along the carbon nanotube surface looking for suitable binding site until the protein finds the most stable conformation. In Figure 4.6, SP-A and SP-D rmsd values stabilize more quickly than SP-B and SP-C. This is because SP-A and SP-D have large complex spatial structure, and they bury their hydrophobic groups inside. SP-B and SP-C proteins have

one α-helix respectively and they expose all their residues to the aqueous surrounding. This leads to the instability of SP-B and SP-C when they interact with a carbon nanotube, and they need longer time to adjust their structures to reach stable configuration. We observe that the RMSD of SP-B is very stable and fluctuates between 2 Å and 4 Å, with a steady pattern throughout the 100 ns time of simulation. By contrast, SP-C shows a higher RMSD value at the beginning, where the protein stabilizes its fluctuations to within 4 Å and 6 Å throughout the remaining100ns.
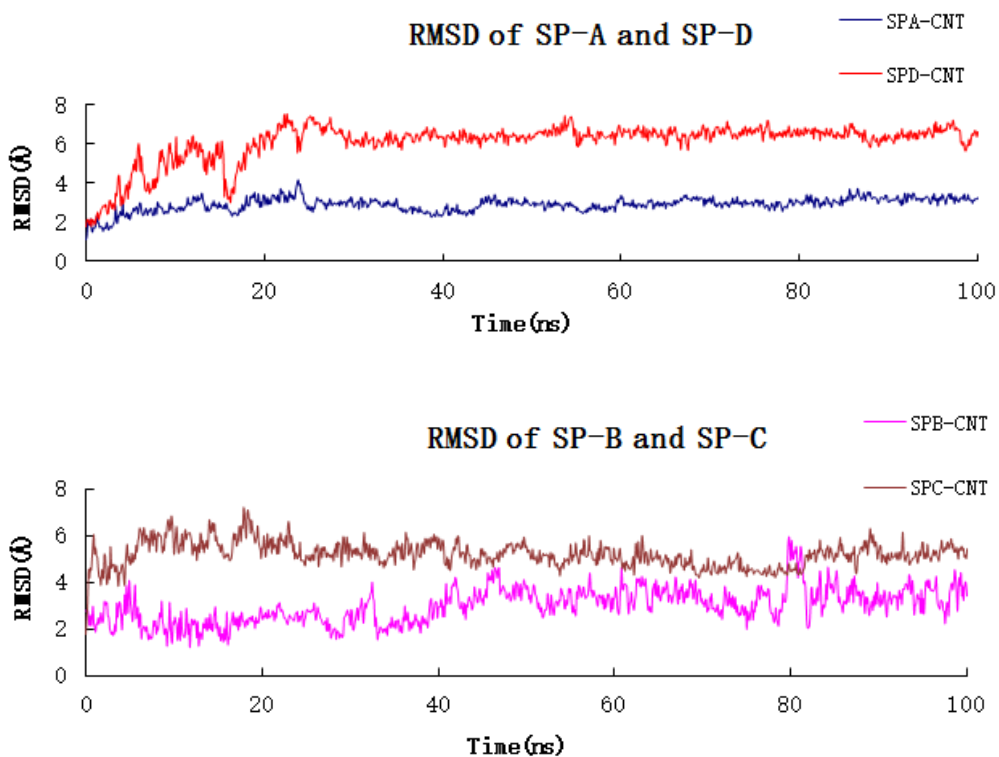
Figure 4.6: RMSD of proteins backbone for 100ns simulations

The tendency of hydrophilic residues escaping from water prevents proteins from adsorbing on to the surface of a nanotube, which is hydrophobic. α-helixes in the N-terminal of SPA and SPD consist of both hydrophilic and hydrophobic residues. They

moved quickly during the simulation process due to the coil and turn that link SPA and SPD to the remaining residues. This can explain why these two α-helixes can turn freely.

4.9 Root Mean Square Fluctuation

The root mean square fluctuation (rmsf) calculates the deviation of position of the residues. Comparing the rmsf of the protein structure over its trajectory gives the flexibilities of parts of the protein. The rmsf is useful for characterizing local changes along the protein chain. On an rmsf plot, peaks indicate areas of the protein that fluctuate the most during the simulation. Typically, the tails N-terminal and C-terminal fluctuate more than any other part of the protein. Secondary structure elements, like alpha helices and beta strands, are usually more rigid than the unstructured parts of the protein, and they fluctuate less than the loop regions.

From their root mean square fluctuation (RMSF) curve (Figure 4.7), SP-B and SP-C consist of an α-helix structure. For SP-B, the RMSF of the C-terminal is significantly higher than the rest of the residues, while for SP-C, both the C-terminal and N-terminal of RMSF are higher than rest of the residues because in the C-terminal of SP-B and in the C and N-terminals of SP-C, there are several hydrophilic residues that prevent them from adsorbing on the surface of a carbon nanotube.
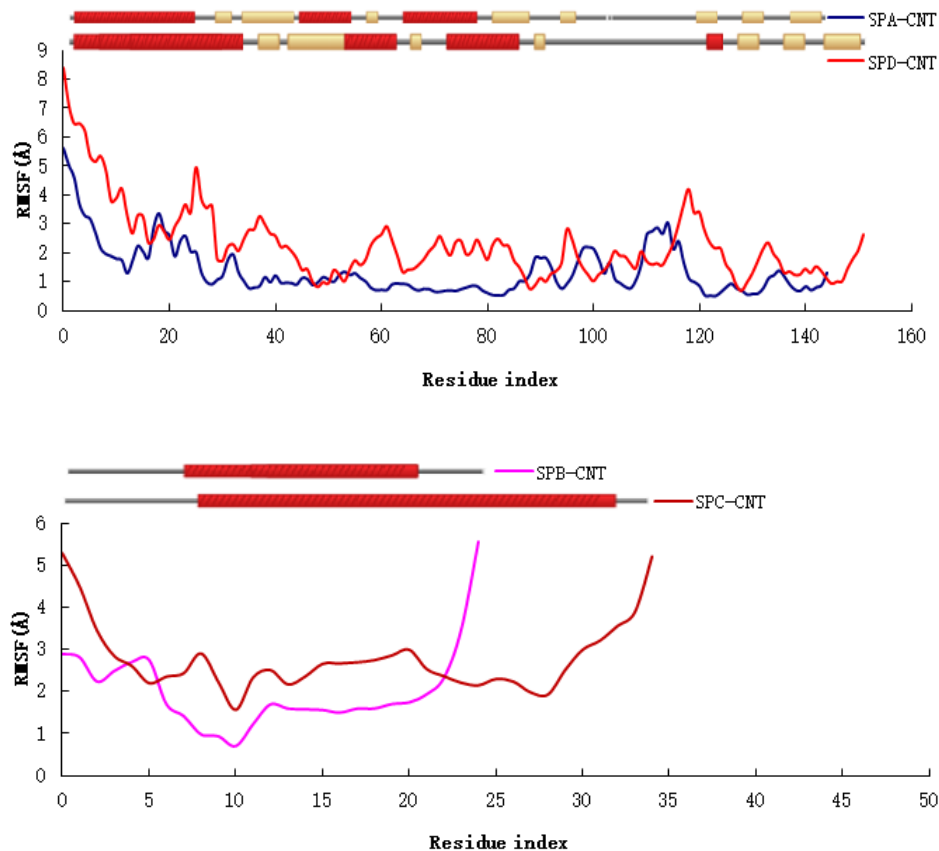
Figure 4.7: Root mean square fluctuation of backbone carbon atoms of proteins for 100ns simulations

In SP-C both the N-terminal and C-terminal residues (side chains, turns, and loops) show more fluctuations than the middle part of the α-helix. In SP-B the N-terminal residues show less fluctuations then the C-terminal residues, since the residues in the α-helix of SP-B are stable. Residues in the C-terminal of SP-C are mostly made up of loops and turns, and they show more fluctuations. It is observed that the residues of the α-helix of SP-B are more stable than the residues of SP-C while interacting with the surface of SWCNT. This is perhaps because of the hydrophilic residues of the C-terminals of SP-B and both the N and C-terminals of SP-C that prevent them from their adsorption on the SWCNT surface.

4.10 Number of Protein Atoms Within 5 Å of Carbon Nanotube Surface
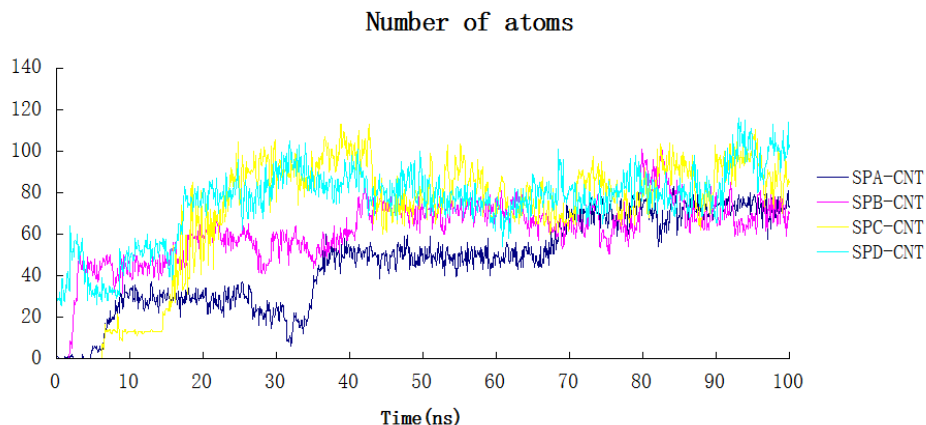
Figure 4.8: Number of pulmonary surfactant protein atoms (SP-A, SP-B, SP-C, and SP-D) within 5Å from the surface of carbon nanotube in 100ns simulations

Figure 4.8, shows the number of protein atoms absorbed on the surface of a carbon nanotube. Adsorption of atoms can be defined as the distance between protein atoms and the surface of a nanotube that is less than 5 Å. At the beginning of the timeline, few atoms are adsorbed, but after 10ns the number of adsorbed atoms increases quickly and around 65ns the number of protein atoms within 5 Å of a carbon nanotube surface for all four systems fluctuates around a constant value. This indicates that absorption of all four proteins on the surface of a carbon nanotube has come close to its stable state. While a protein molecule gets closer to the carbon nanotube surface, it starts rearranging its structure until a stable configuration is achieved. Over time, more and more protein atoms come closer to the SWCNT surface, and at the end, the number fluctuates around a constant: 70 atoms of SP-B and 85 atoms of SP-C are adsorbed on the SWCNT surface. This indicates that the adsorption process of protein on a SWCNT is complete in 100 ns, and both the protein and the SWCNT have reached their stable state.

Figure 4.9, shows the 3D representation of atoms within 5Å of a carbon nanotube's surface at 100 ns. In Figure 4.9, atoms are represented by color code: blue are nitrogen atoms, green are carbon atoms, red are oxygen atoms, and white are hydrogen atoms
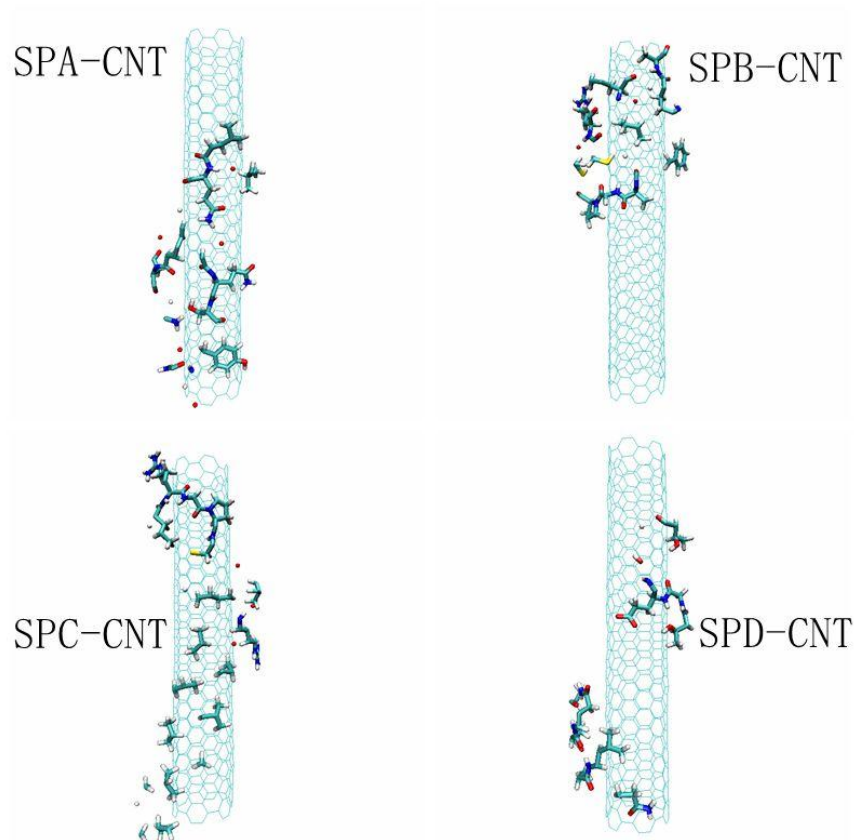
Figure 4.9: The atoms of pulmonary surfactant proteins SP-A, SP-B, SP-C and SP- D within 5Å around the surface of carbon nanotube in final conformations at 100 ns 3d representation.

4.11 Interaction Energy

NAMD computes all internal energies of interactions and summarizes this in an output log file. The standard units used by NAMD are Angstroms for length, kcal/mol for energy, Kelvin for temperature, and bar for pressure. Interacting energies are:

BOUNDARY -- energy is restrained by spherical boundary conditions and harmonic restraints.

MISC -- energy is from external electric fields and various steering forces.

TOTAL – this is the sum of the various potential energies and the KINETIC energy.

TOTAL2 – this uses a slightly different kinetic energy that is better conserved during equilibration in a constant energy ensemble.

TOTAL3 -- this is another variation of TOTAL with much smaller short-time fluctuations that is adjusted to have the same running average as TOTAL2.

NAMD also calculates electrostatic energy, various kinetic and potential energies, bonding and non-bonding energies like van der Waals energy, cross-term energies in dihedral, angles and hydrogen bonding.

Interacting energies will give information about the stability of the protein-CNT structure, and it also tells the different kinds of forces involved in the interaction. If protein and carbon nanotube atoms are forming bonds, then in the beginning interacting energies are high, and as more and more bonds are formed between protein and the carbon nanotube atoms, a more stable and lower energy situation is produced. Energy

change is also associated with change in pressure and temperature. NAMD computes the corresponding fluctuations in pressure and temperature.

4.11.1 Van Der Waals Energy of Interaction

As atoms of a protein molecule get close to surface of a carbon nanotube, the van der Waals (VDW) energy of interaction increases. Figure 4.10 shows that the van der Waals energy is negative which indicates an attractive force between the pulmonary surfactant protein molecule and the carbon nanotube. Generally, the van der Waals interaction is a non-bonding interaction, and it is due to the presence of polar residues in the pulmonary surfactant protein molecule.
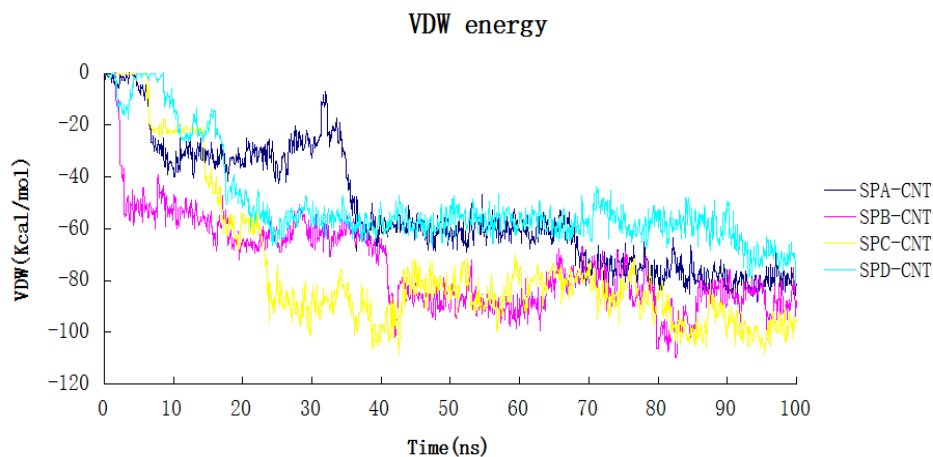
Figure 4.10: Interaction of the VDW energy between a protein molecule and a carbon nanotube for a 100ns simulation.

VDW energy for SP-B decreases sharply and in a short period of time compare to SP-C, and both energies fluctuates around a constant value for most of the time of simulation. Throughout the simulation, the VDW energy remains negative, indicating VDW bonding between protein atoms and carbon atoms of the carbon nanotube [92].

4.12   Adsorbed Residues of Pulmonary Surfactant Proteins on a

Carbon Nanotube Surface

Adsorbed residues, which are observed after a system achieves equilibrium, can be hydrophobic, hydrophilic, or a combination of both. Adsorbed residues demonstrated by a 3D model of the protein fragments align with the carbon nanotube. These fragments of protein may contain aromatic rings, which align with the hexagonal rings of the carbon nanotube, indicating $\pi - \pi$ stacking.

Adsorbed residues of pulmonary surfactant proteins on the surface of a carbon nanotube are shown in Table 4.2. For SP-A, 14 residues are adsorbed on the surface of a carbon nanotube, including 9 hydrophilic residues and 5 hydrophobic residues. For SP-B, 11 residues are adsorbed on the carbon nanotube surface, 5 hydrophilic and 6 hydrophobic. For SP-C, 18 residues are adsorb on the carbon nanotube surface, and most of them are hydrophobic. For SP-D, 13 residues are adsorbed on the carbon nanotube surface, of them are hydrophobic. This indicates that the combination of hydrophobicity and hydrophilicity of proteins determines the adsorption process of a pulmonary surfactant protein on the surface of a carbon nanotube. The main driving force responsible for adsorption is the non-bonding Van der Waals' force of attraction, since all of the atoms of the carbon nanotube are neutral for this simulation.
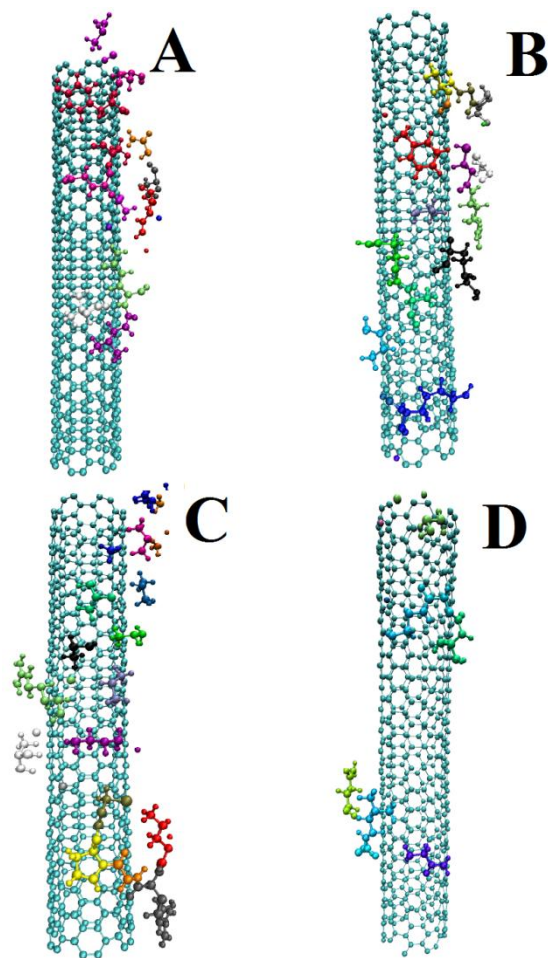
Figure 4.11: Functional groups of pulmonary surfactant proteins within 5Å of the surface of the carbon nanotube in their final conformations at 100ns. (A) SP-A & CNT, (B) SP-B & CNT, (C) SP-C & CNT (D) SP-D & CNT.

System	Adsorbed residues
SPA-CNT	VAL LEU GLN ASN GLY GLN SER LYS TYR ASN ASN LEU GLN TYR
SPB-CNT	PHE ILE PRO LEU CYS CYS ARG ILE LYS GLN ALA
SPC-CNT	LEU ARG ILE PRO CYS VAL LYS ARG VAL VAL VAL VAL VAL LEU LEU LEU LEU LEU
SPD-CNT	SER GLN GLN ALA LEU GLN HES THR GLU THR GLY GLU SER

Table 4.2: The adsorbed residues of pulmonary surfactant proteins on carbon nanotube surface after 100 ns.

Figure 4.11, shows the 3D illustration of absorbed functional groups of pulmonary surfactant proteins SP-A, SP-B, SP-C, and SP-D at final conformation after 100ns. All the absorbed groups are within 5Å of the surface of the carbon nanotube. Most of the adsorption atoms and functional groups of the four proteins include backbones of proteins, hydrophobic parts of side chains, and conjugate rings. The common functional groups of the four proteins were methyl (CH_3) and alkylene ($[-(CH2)_n-]$).This indicates that hydrophobic effects also play an important role in the adsorption process. In addition, several polar atoms and functional groups were observed in the final adsorption structures, such as carboxyl, amide bond, and amidogen. For SP-A & CNT, SP-B & CNT and SP-C & CNT, systems conjugate aromatic rings are observed. Alignment of aromatic rings of pulmonary surfactant protein and the carbon nanotube constitute the key factor that drives protein adsorbed on the surface of a nanotube due to π–π stacking.

4.13   Radius of Gyration

The radius of gyration R_g describes the equilibrium conformation of a total system and is computed by first finding the coordinates of the center of mass R_C, disregarding the hydrogen atoms. The radius of gyration determines the protein structure compactness. For instance, α proteins have the highest radius of gyration throughout the protein size range considered, suggesting a less tight packing when compared with β and (α + β)-proteins. A change in the radius of gyration will help determine any changes in protein structure during the adsorption process on the surface of carbon nanotube. Rg values indicate folded chain conformation of both types of proteins. This also shows that when folded chain proteins come to the carbon nanotube surface, this process will increase the

stiffness of the nanocomposite structure of the combination carbon nanotube-protein [93, 94].

The radius of gyration (R_g) determines any structural change during the adsorption process of protein on the surface of a carbon nanotube. Figure 4.12, shows the variation in Rg for all four pulmonary surfactant proteins for a time of 100 ns. SP-A and SP-D, being large protein molecules with multiple α-helixes and β-sheets, undergo noticeable structural changes, and this is reflected in the timeline illustration of their secondary structure in Figure 4.13.
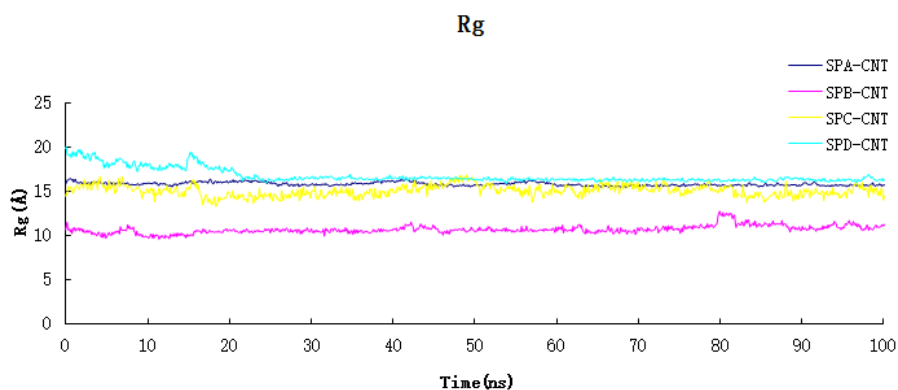
Figure 4.12: Radius of gyration of pulmonary surfactant proteins in 100ns simulations

4.14   Time Evolution of the Secondary Structure of Protein

Depending on their secondary structures, proteins are arranged in four classes:

1. All α–proteins have only α–helix secondary structures.

2. All β–proteins have mainly β–sheet secondary structures.

3. α+ β proteins have α-helix and β-strand secondary structure segments that do not mix but tend to segregate along the polypeptide chain.

45

4. α/β proteins have a mixture or approximately alternating segments of α–helix and β–strand secondary structures.

The relationship between a protein amino acid sequence and a secondary structure is complex and reflects the intricate thermodynamic and kinetic process of protein folding. This knowledge of structural changes in protein is applied in numerous important predictive tasks that address structural and functional features of proteins, and this knowledge can identify protein binding sites with the carbon nanotube surface.

From Figure 4.12, radius of gyration, and Figure 4.13, the time evolution of secondary structures, it can be clearly seen that SP-B and SP-C have one α-helix each, and their structure remains more compact when compared to SP-A and SP-D. SP-B and SP-C show a more stable radius of gyration, with very little variation, and they keep their structures intact most of the time. SP-D has highest radius of gyration, and after 20 ns one of its α-helix changes it structure permanently. On the other hand, SP-A shows less variation in its radius of gyration; initially SP-A also changes the structure of one α-helix, but it regains this structure in the last 10 ns.
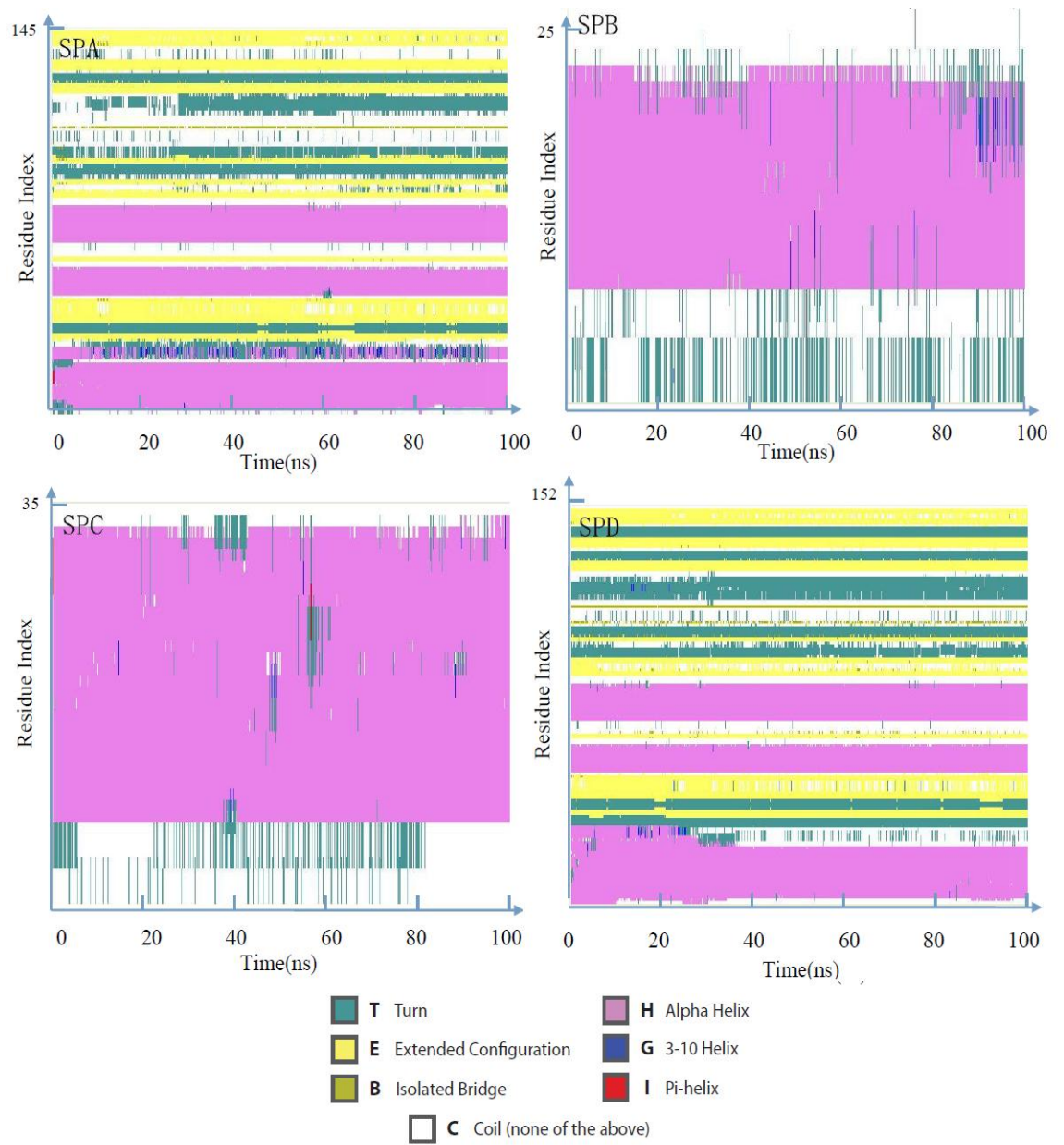
Figure 4.13: Time evolution of the secondary structure for all four pulmonary surfactant proteins for 100 ns. Top left: SP-A, top right: SP-B, bottom left: SP-C, bottom right SP-D.

4.15 Solvent Accessible Surface Area (SASA)

The surface topology of a protein molecule is closely related to its functions, which tell the parts of the surface that are directly involved in the interaction with other molecules (in our case SWCNT). The solvent-protein interface is almost certainly related to the structure of the native molecule [95]. An atom, or group of atoms, is defined as accessible if a solvent molecule of specified size can be brought into van der Waal's contact. The surface topology of protein is closely related to its functions; parts of the surface are directly involved in the interaction with other molecules. The solvent – protein interface is almost certainly related to the structure of the native molecule. For the purpose of calculation, the solvent accessible surface area (SASA) of the solvent molecule has been assumed to be a sphere of radius 1.4 Å. Figure 4.14, shows the variation in SASA for all four pulmonary surfactant protein molecules over 100 ns. Both SP-B and SP-C proteins are hydrophobic, and the majority of their structures are α-helix. Nevertheless, SP-C undergoes noticeable SASA changes for the first 30 ns, and this suggests that SP-C is going through structural changes in order to achieve its meta-stable state. This shows that even in the beginning of our simulation, SP-C goes through small structural changes, but after 40 ns SP-C regains its structural and functional characteristics. SP-B, within the first 10 ns, moves closer to the SWCNT surface, and therefore SP-B shows considerably less change in SASA value as the majority of SP-B is in contact with SWCNT. SP-A and SP-D are bigger molecules compared to SP-B and SP-C, and they show more variation for the first 20 ns, after which they achieve almost stable values. This is also confirmed by changes in the secondary structures of SP-A and SP-D from Figure 4.13.
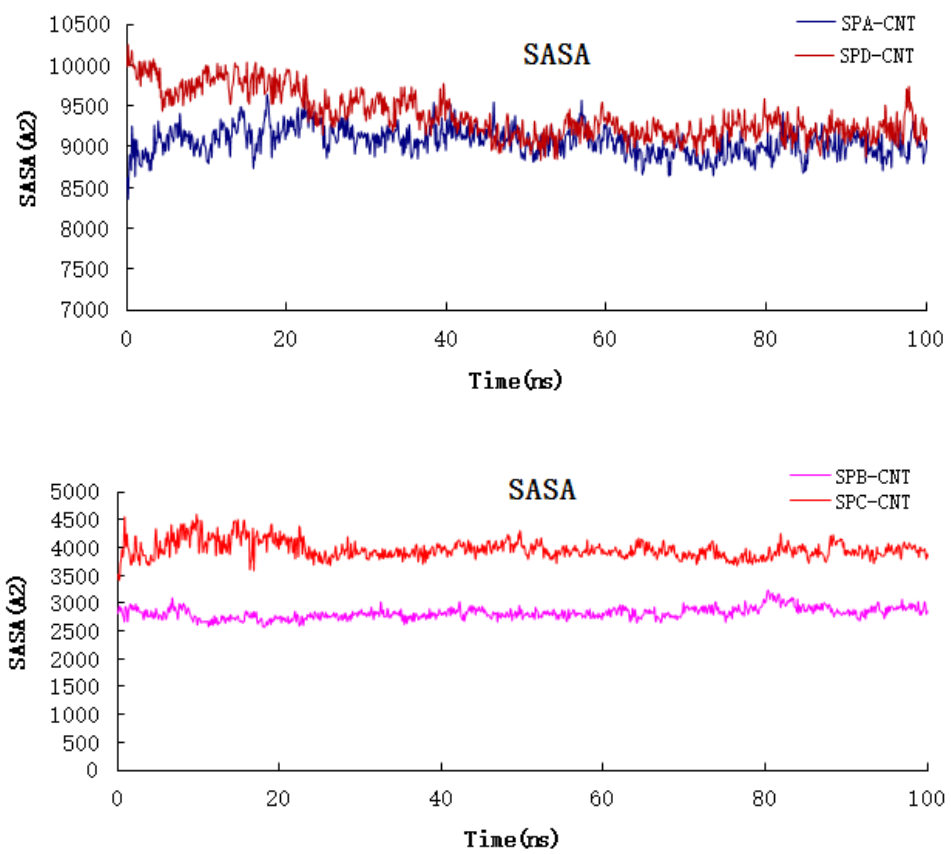
Figure 4.14: Solvent accessible surface area for pulmonary surfactant proteins in 100ns simulations

4.16   Trajectory of SP-A and Carbon Nanotube for 100 ns
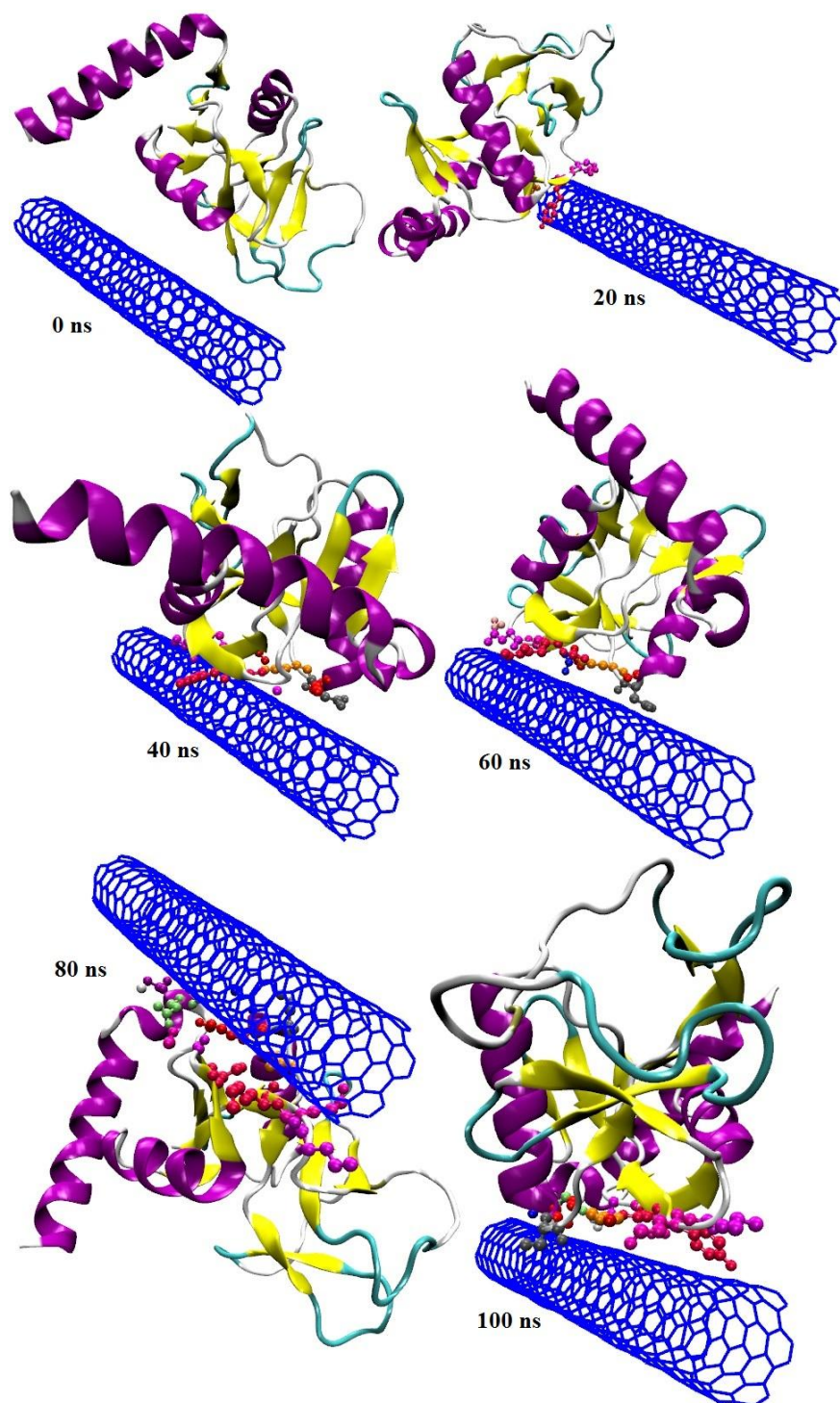
Figure 4.15: Molecular Dynamic model of pulmonary surfactant protein SP-A and a carbon nanotube over 100ns. SP-A illustrates its secondary structure and its atomic model.

4.17   Trajectory of SP-B and Carbon Nanotube for 100 ns
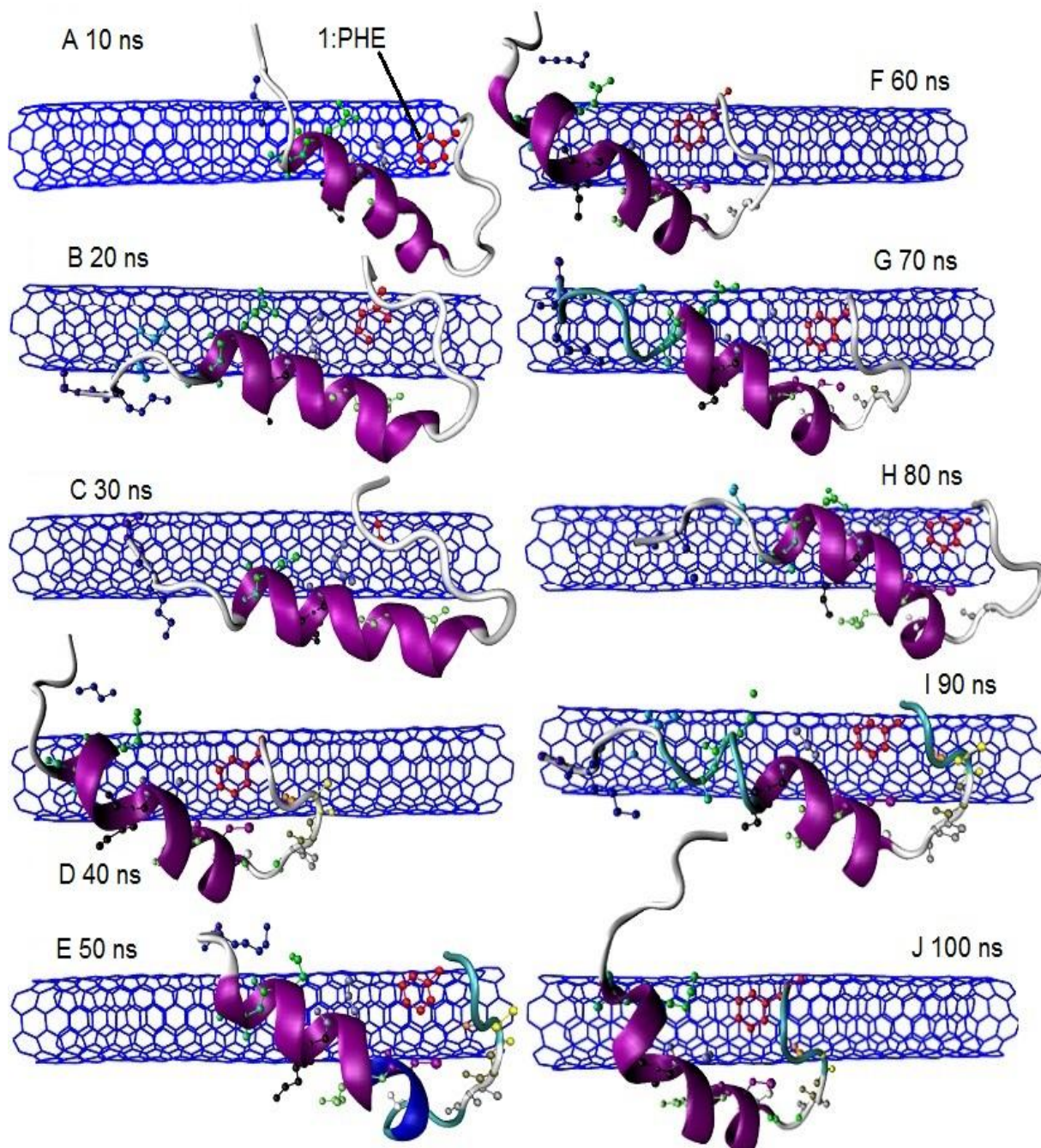
Figure 4.16: Molecular Dynamic model for pulmonary surfactant protein SP-B and a carbon nanotube for 100ns. SP-B illustrates its secondary structure and its atomic model.

4.18   Trajectory of SP-C and Carbon Nanotube for 100 ns
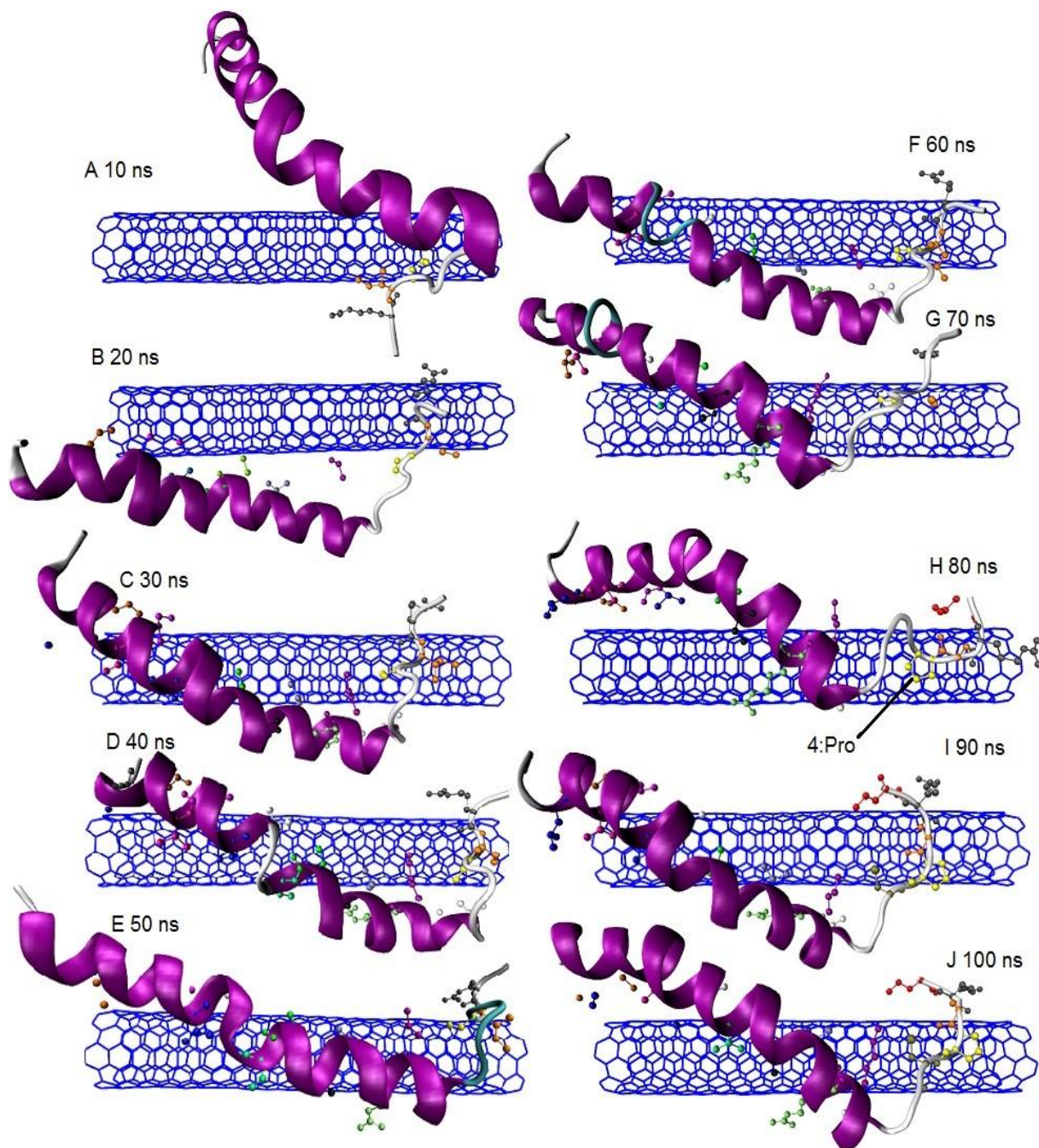
Figure 4.17: Molecular Dynamic model for pulmonary surfactant protein SP-C and a carbon nanotube for 100ns. SP-C illustrates its secondary structure and its atomic model.

4.19   Trajectory of SP-D and Carbon Nanotube for 100 ns
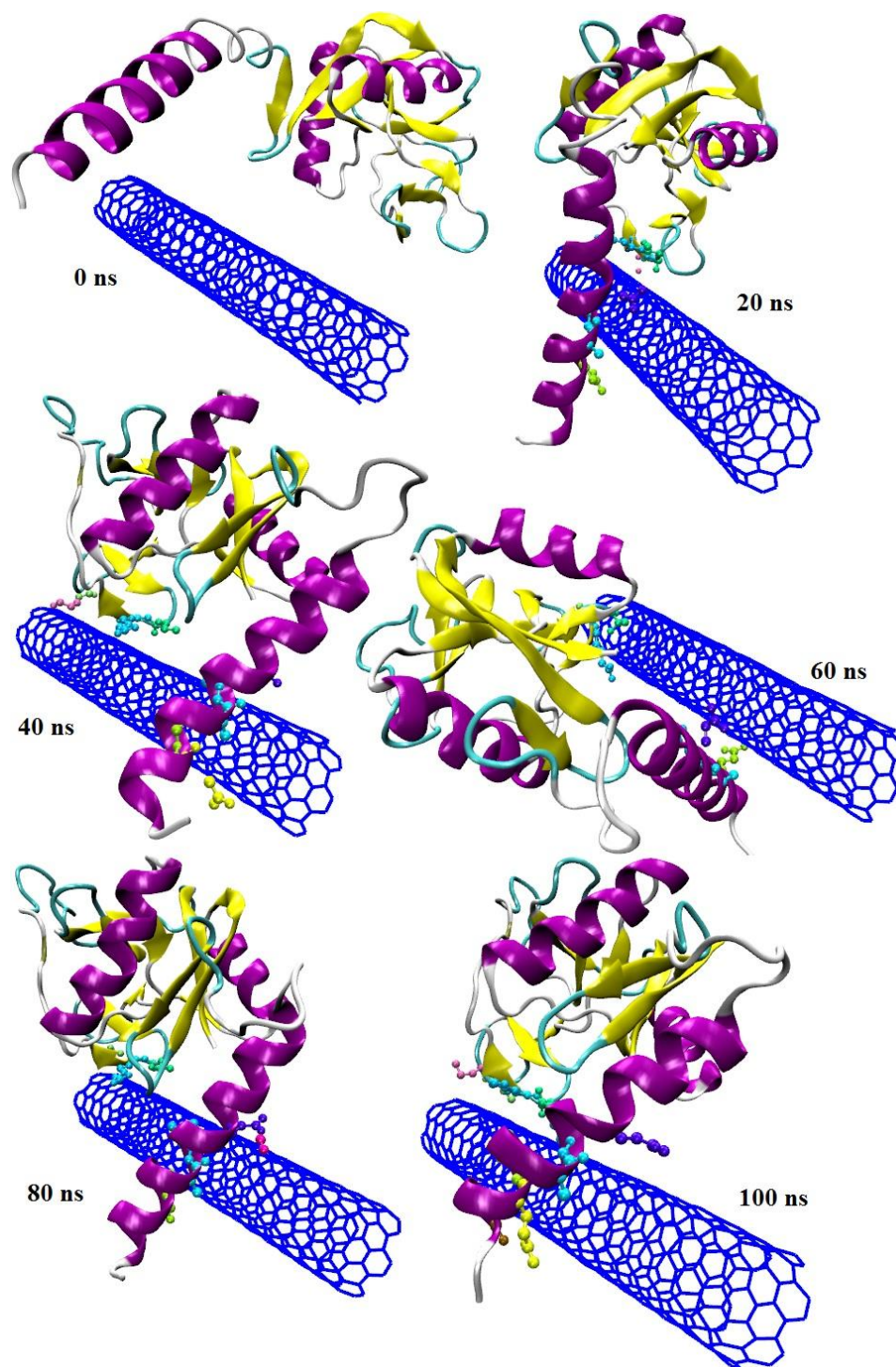
Figure 4.18: Molecular Dynamic model for pulmonary surfactant protein SP-D and a carbon nanotube for 100ns. SP-D illustrates its secondary structure and its atomic model.

Results show that all four human pulmonary surfactant proteins SP-A, SP-B, SP-C, and SP-D are adsorbed on the surface of a carbon nanotube. Root mean square deviation and van der Waals energy graphs indicate that all four pulmonary surfactant protein molecules achieve equilibrium positions after 40 ns. Hydrophilic and hydrophobic residues of all four proteins play equal roles in adsorption dynamics on the surface of a carbon nanotube, even though the carbon nanotube surface is hydrophobic in nature. Since the carbon nanotube surface is neutral, the protein adsorption process on the surface of a carbon nanotube results from the non-bonding van der Waals interaction (attraction type). Pulmonary surfactant proteins SP-A and SP-D are big molecules with multiple α helixes and β sheets, and they change their secondary structure in the process of adsorption. SP-B and SP-C are small molecules with one α helix, and they are hydrophobic in nature; they are adsorbed on the surface of a carbon nanotube more quickly. After finding absorbed residues of SP-A, SP-B, and SP-C on the carbon nanotube surface, the alignment of aromatic rings of protein residues with the carbon nanotube is observed, and this suggests $\pi - \pi$ stacking. After 70 ns, the number of atoms within 5 Å remains almost constant suggesting that the adsorption process is complete, and the protein has found its optimal position on the surface of carbon nanotube.

CHAPTER 5: MOLECULAR DYNAMICS COMPUTATION OF PULMONARY SURFACTANT PROTEINS B ADSORBED ON CHARGED CARBON NANOTUBE

The electrical properties of a carbon nanotube change when it is bonded to a biomolecule such as protein. Understanding the molecular mechanism of the conformational change of SP-B affected by a charged carbon nanotube allows us to find suitable ways to use a carbon nanotube in bio-systems, such as bio-scaffolds, biosensors, and drug-delivery systems. We set up three different charged carbon nanotubes with SP-B and water box models using the VMD software package. The trajectories for all three systems are computed by molecular dynamics using NAMD for 100ns. The conformational changes of SP-B are found from trajectory analysis parameters such as RMSD, RMSF, radius of gyration (Rg) and the interaction energy in the form of VDW and electrostatic energies. The simulation results shown that positive charge can prevent SP-B from being adsorbed on the carbon nanotube, and the conformational change is slight. In Negative and neutral charge systems, SP-B gets adsorbed on the surface of a carbon nanotube, and conformational changes are significantly larger than a positively charged carbon nanotube interacting with SP-B. Results show that using a negatively charged or neutral carbon nanotube is a good choice for charged carbon nanotube based SP-B biosensors. In most protein and carbon

nanotube solutions, protein can be adsorbed on the carbon nanotube spontaneously [96] due to the charge interaction between protein residues with the carbon nanotube [97]. Cheng et al. calculated the binding free energy between a single walled carbon nanotube and polypeptide, and they showed that the main driving force of their binding is a van der Waals' force, with $\pi - \pi$ stacking between aromatic rings of protein and carbon nanotube and hydrophobic effects also playing important roles [98]. Research by Kang et al describe the process of protein passing through the carbon nanotube, and they found the protein was adjusting its structure when it interacted with the carbon nanotube to maintain its spatial configuration [99].

5.1 Materials and methods

Molecular dynamics simulations were carried out for the pulmonary surfactant protein SP-B with a charged carbon nanotube performed by NAMD with CHARMM27 force field parameters. Lennard–Jones potential parameters were set for a cross interaction between non-bonded atoms of a carbon nanotube–protein and carbon nanotube –water and protein–water. The X-ray structure of SP-B (ID code: 1dfw) was acquired from the protein data bank. SP-B contains 1 to 25 residues (FPIPLPYCWLCRALIKRIQAMIPKG) with side chains and one α-helix. Sequences 1 to 25 of Human surfactant protein SP-B are used for surfactant protein SP-B that demonstrates the same surface and biophysical properties of the full human surfactant protein SP-B1-78, based on the N-terminal. The carbon nanotube generated by the "Carbon Nanostructure Builder" plug-in of the VMD software is an armchair nanotube with chiral vectors of (6, 6), length of 5nm made up of 503 sp2 hybridized carbon atoms and diameter of 0.8 nm.

All atoms, including hydrogen, were defined explicitly in all simulations. The time step of 2 fs was set, and the cutoff of the non-bonding van der Waals force was set to a switching start distance of 10 Å, and this reached to zero at 12 Å. Particle mesh Ewald (PME) summation was used for full system periodic electrostatic calculations, with PME grid spacing of 1 Å. Langevin dynamics parameters were set to control the temperature and pressure. The Langevin parameter for hydrogen coupling was kept off. All MD simulations were performed at 300 K temperature and 1 atm pressure. Simulations were performed in the following manner:

1. The energy minimization and energy equilibration of SP-B (1-25) and a single walled carbon nanotube was performed. SP-B(1-25) was solvated in 0.15 mol/L sodium chloride solution using TIP3 [100]. The water box is $61 \times 48 \times 71 Å^3$ in dimension. The protein and carbon nanotube systems underwent 5000 steps toward energy minimization. The molecular dynamics was running the Root-Mean-Square Deviation (RMSD) of proteins fluctuating around a constant value. The final structure was used for setting up the initial structure for SPB and a carbon nanotube interaction simulation.

2. A carbon nanotube with three different charge configurations (neutral (0.00e), negative (-0.01e) and positive (+0.01e) charges) interacting with protein SP-B (1-25) was built. Positional constraints are applied to the carbon nanotube. The minimum distance between the protein and the nanotube is 1.2nm so that there are several ordered water layers to reduce the effects by initial status. The protein and carbon nanotube

complex was then solvated with a 0.15 mol/L sodium chloride solution. The water box size was $61 \times 48 \times 71 \text{Å}^3$. In all three charge configurations, the initial position and orientation of protein are same. Figure 5.1, show the initial position for SP-B and the carbon nanotube.

3.   A fixed protein process with the carbon nanotube was performed at constant temperature (300 K) and pressure (1 atm) for 5000 energy minimizations, and molecular dynamics for a fixed protein with a carbon nanotube was performed for 40 ps. After this, the protein and the carbon nanotube were re-set and used for further molecular dynamics runs.

4.   Initially, energy minimization for 5000 steps at constant temperature and pressure was performed for all systems (containing protein molecule, a carbon nanotube, water molecules, and Na Cl ions). After minimization, all systems underwent equilibration for 100ns until the RMSD and system's total energy fluctuate around a constant value. This indicates that the system has achieved a stable state. The focus of this simulation is (i) on the protein residues' adsorption on the surface of the carbon nanotube, (ii) on the study of the changes in energy interaction, and (iii) on the protein folding-unfolding events over a period of 100 ns.
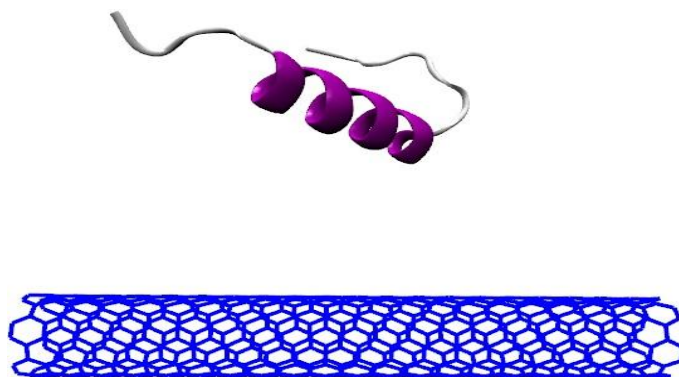
Figure 5.1: Initial position of pulmonary surfactant protein SP-B and the carbon nanotube. All three systems have the same initial position.

5.2 Results and Discussion

5.2.1 Distance between the Center of Mass of Protein and the Carbon nanotube
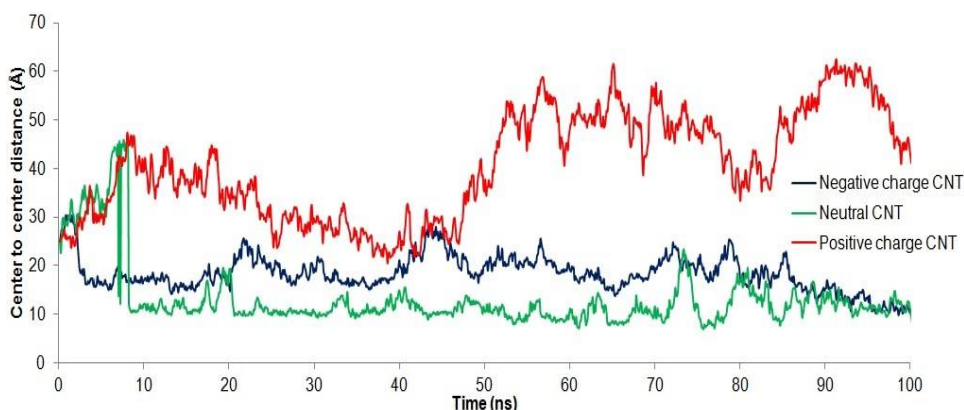
Figure 5.2: Distance between the center of mass of pulmonary surfactant protein SP-B and a carbon nanotube for 100 ns

Figure 5.2, shows the distance between the center of mass of pulmonary surfactant protein and a carbon nanotube. Over time, SP-B gets closer to the neutral and negatively charged carbon nanotube. For a neutral carbon nanotube, SP-B moves swiftly

toward the surface of the carbon nanotube within 10 ns and stays there for the remaining time of the computation. SP-B with a negatively charged carbon nanotube shows a stronger center-to-center of mass distance as compare to that observed for a neutral carbon nanotube; this is caused by polar residues trying to re-orientate in order to find their equilibrium position on the surface of the carbon nanotube. During the last 10 ns of computation time, the neutral and negatively charged carbon nanotubes follow similar patterns, and by end 100 ns, the fluctuation becomes smaller and smaller, and the two values stabilize at 10.41 Å and 10.8 Å respectively.

Pulmonary surfactant protein SP-B has a +4e positive charge. During the interaction with a positively charged carbon nanotube, SP-B moves away from the positively charged carbon nanotube surface. Around 40 ns, the SP-B center of mass moves closer to the positively charged carbon nanotube because of the non-polar residual interaction but quickly moves away from surface of the carbon nanotube and maintains its equilibrium position at 42.39 Å from the carbon nanotube without making contact with the carbon nanotube surface.

5.2.2 Number of Protein Heavy Atoms within 5 Å of Carbon nanotube
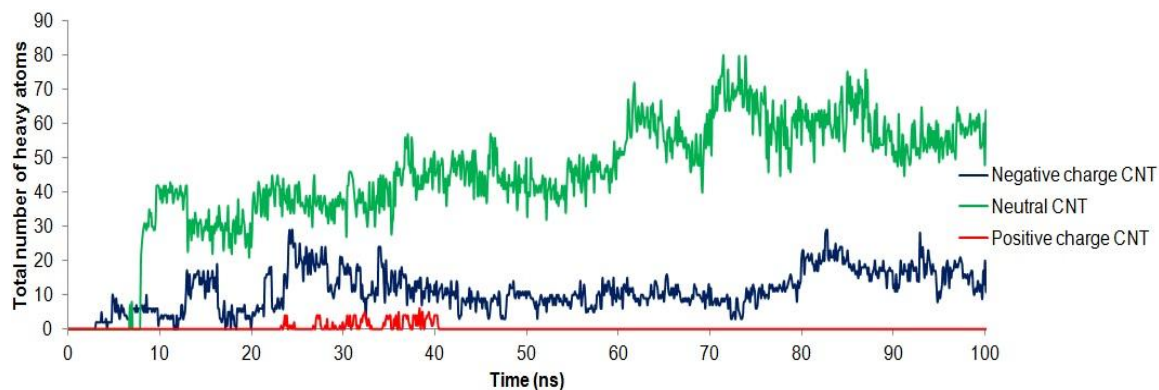
Figure 5.3: The number of protein's heavy atoms coming within 5 Å of the surface of a carbon nanotube: Red is number of heavy atoms of SP-B within 5 Å of positively charged carbon nanotube, blue is number of heavy atoms of SP-B within 5 Å of negatively charged carbon nanotube and green is number of heavy atoms of SP-B within 5 Å of neutral carbon nanotube for 100 ns.

As SP-B moves closer to the surface of a neutral carbon nanotube, the number of heavy atoms within 5 Å grows rapidly and fluctuates around a constant value until 60 ns. After 60 ns the number of heavy atoms again increases, and between 90 to 100 ns it stabilizes and fluctuates around a constant value. This behavior is almost step-like. At the end of 100 ns, a total of 60 atoms are adsorbed on the surface of a carbon nanotube. SP-B shows a lower number of adsorbed atoms on the surface of a negatively charged carbon nanotube. Since SP-B has a net positive charge, it stays away from the positively charged carbon nanotube surface for most of the time. Between 25 ns and 40 ns, 4 to 5 heavy atoms of Lysin (resid 24) and Glycine (resid 25) come within 5 Å of the surface of the carbon nanotube.

5.2.3 Root Mean Square Deviation (RMSD)
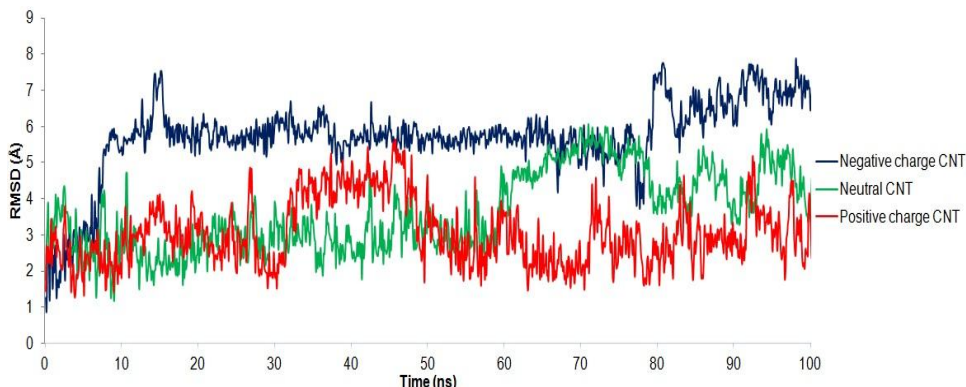
Figure 5.4: Root Mean Square Deviation (RMSD) of pulmonary surfactant protein SP-B with charged carbon nanotube over 100 ns

Figure 5.4 shows the root mean square deviation of SP-B during its interaction with a charged carbon nanotube. SP-B shows the highest value of RMSD with a negatively charged carbon nanotube; this may be due to the fact that most of the SP-B residues carry positive charge and the force of attraction of opposite charges is greater, and this would tend to exhibit a stronger deviation in protein structure. The RMSD of SP-B with a positively charged carbon nanotube shows a higher value when a few heavy atoms of SP-B come close to the carbon nanotube surface. After the protein moves away from the surface of a positively charged carbon nanotube, the RMSD returns back to its original value and fluctuates around that value. The same result occurs in the case of a neutral carbon nanotube, as the number of heavy atoms of SP-B near the carbon nanotube increases; the RMSD tends to increase as the protein molecule is stabilized on the surface of the neutral carbon nanotube, and the RMSD approaches its original value.

5.2.4 Contact Probability of Protein Residues with a Carbon Nanotube
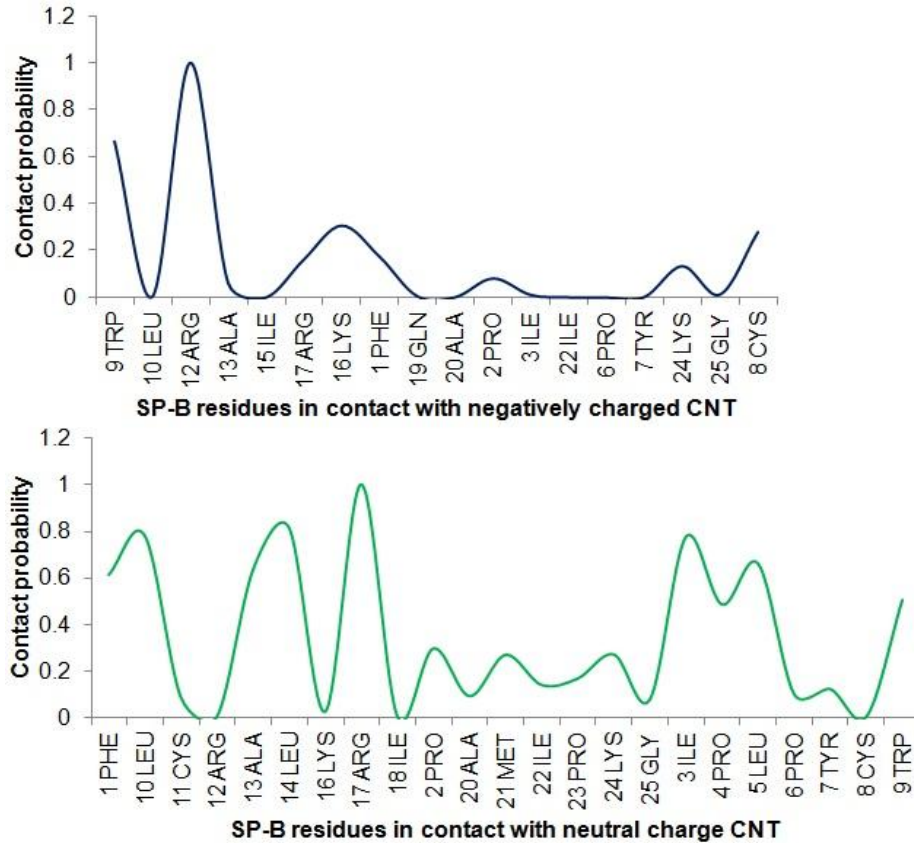
Figure 5.5: Contact probability of pulmonary surfactant protein SP-B residues with a carbon nanotube over 100 ns

Figure 5.5 shows the contact probability of all residues of SP-B proteins coming in contact with the surface of a neutral or negatively charged carbon nanotube for a time of 100 ns. The cutoff distance for contact of the residue to the surface of the carbon nanotube is kept at 5 Å, not counting the hydrogen atoms in the residue. During the 100 ns, 18 residues of SP-B come in contact with the negatively charged carbon nanotube surface, and 23 residues come in contace the neutral carbon nanotube surface. Residues

which have a contact probability of 1 are in closest contact with the carbon nanotube surface. In both cases of negatively charged and neutral carbon nanotube surfaces, the residue arginine (ARG) is makes the strongest contact with the carbon nanotubem i.e. SP-B resid 12:ARG for a negatively charged carbon nanotube and SP-B resid 17:ARG for a neutral carbon nanotube. The strong attraction of arginine to the SWCNT (6,6) is attributed to it's guanidinium group, which interacts with the SWCNT through the formation of multiple salt bridges [101].

5.2.5 Interaction Energy

The interaction energy is calculated between a pulmonary surfactant protein and a carbon nanotube, and the system shows two forms of energy:

1. Van der Waals (VDW) energy in all three-charge systems of a carbon nanotube (positive, neutral, and negative).

2. Electrostatic energy for positively and negatively charged carbon nanotube systems

Figure 5.6, shows the interaction energy, i.e. VDW energy, for all three-charge systems of a carbon nanotube and SP-B for a time of 100 ns. All three curves for a positive, neutral, and negatively charged carbon nanotube surface remain negative, indicating the VDW bonding between the protein atoms and the carbon atoms of the carbon nanotube, and this is due to the strong attraction of the VDW forces [92].
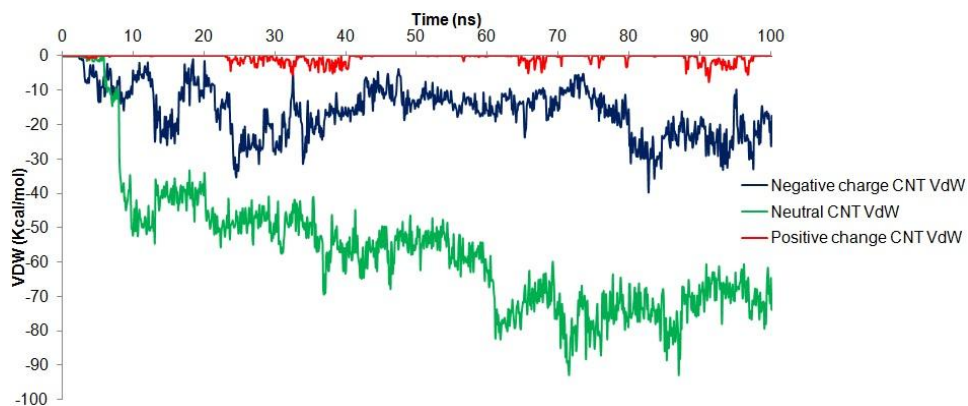
Figure 5.6: Van der Waals energy between pulmonary surfactant protein SP-B and the carbon nanotube.

SP-B shows minimal contact with the positively charged carbon nanotube; it has the least interaction energy. This is because SP-B has a net positive charge on its surface and repels the positively charged carbon nanotube. For a charged carbon nanotube system, the interaction energy is the sum of the VDW and electrostatic energies. On other hand, a neutral carbon nanotube has the interaction energy equal to the VDW energy, since there is no external charge on the carbon nanotube or protein. When SP-B interacts with a neutral carbon nanotube, it has a stronger attractive VDW force, when compared to negatively charged or positively charged carbon nanotube. Figure 5.3 shows that as more heavy atoms come close to the surface of a carbon nanotube, the VDW energy curve decreases and stabilizes, and this suggests that the system has achieved a meta-stable state.

Figure 5.7 shows the energy curve for electrostatic energy for SP-B with a positively charged carbon nanotube and SP-B with a negatively charged carbon nanotube. As SP-B comes in contact with the negatively charged carbon nanotube, there is more

electrostatic energy, and the energy curve stays negative for the entire 100 ns, and this
shows an attractive type of electrostatic force.
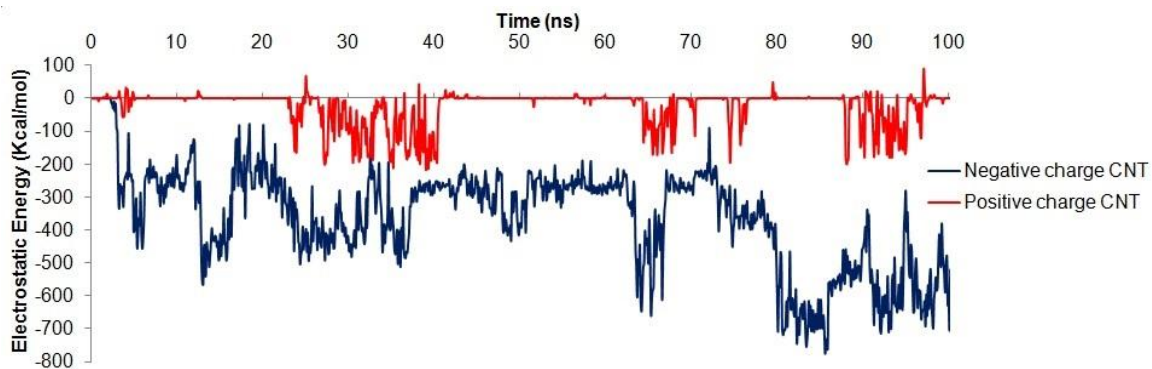
Figure 5.7: Electrostatic energy of interaction between SP-B with positively charged carbon
nanotube and SP-B with negatively charged carbon nanotube

Figure 5.3 and Figure 5.7 show that as more heavy atoms come in contact with a
negatively charged carbon nanotube, the energy curve becomes more negative. SP-B and
a positively charged carbon nanotube show positive and negative values of electrostatic
energy, though the energy curve remains more negative than positive. SP-B makes
minimal contact with a positively charged carbon nanotube, hence it shows the smallest
value of electrostatic energy. As heavy atoms come within the cutoff distance of the
positively charged carbon nanotube, we determine the electrostatic energy for SP-B and
the carbon nanotube.

5.2.6   Adsorbed Residues and Secondary structure

Adsorbed residues are observed after each system achieves equilibrium at 100 ns.
Adsorbed residues could be hydrophobic, hydrophilic, polar, non-polar or a combination
of all of these. Adsorbed residues are demonstrated by a 3D model of protein fragments
aligning with a carbon nanotube. These fragments of protein may contain aromatic rings,

which are align with hexagonal rings of the carbon nanotube indicating $\pi - \pi$ stacking. The criterion for adsorption of residues on the surface of a carbon nanotube is for the residue atoms to come within 5 Å of the surface of a carbon nanotube with hydrogen atoms omitted from the adsorption process. Figure 5.8, shows residues of SP-B adsorbed on the surface of a neutral and negatively charged carbon nanotube.
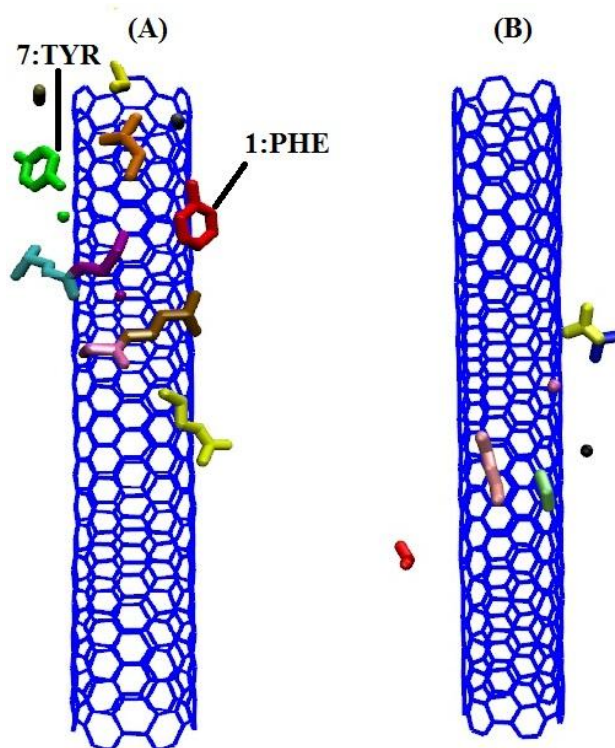
Figure 5.8: Adsorbed residues of pulmonary surfactant protein SP-B on a charged carbon nanotube: (A) SP-B residues adsorbed on the surface of a neutral carbon nanotube after 100 ns and (B) SP-B residues adsorbed on the surface of a negatively carbon nanotube after 100 ns

Figure 5.8 (A), a neutral charged carbon nanotube shows more adsorption of SP-B residues (including two hexagonal rings of Phenylalanine (residue ID 1:PHE) and Tyrosine (residue ID 7:TYR)). Adsorption of hexagonal aromatic rings indicates $\pi - \pi$ stacking; after 100 ns all 11 residues of SP-B are adsorbed on the surface of a neutral carbon nanotube; this is detailed in Table 5.1. When compared to a neutral carbon nanotube, there is a smaller number of residues adsorbed on the surface of a negatively

charged carbon nanotube. In the case of a negatively charged carbon nanotube, the majority of residues adsorbed are positively charged and hydrophobic residues. By the end of 100 ns, seven residues of SP-B are adsorbed on the surface of a negatively charged carbon nanotube. In the case of a positively charged carbon nanotube, residues Lysine (residue ID 24) and Glycine (residue ID 25) make brief contact with the surface of a carbon nanotube during ≈40 ns before moving away from the positively charged carbon nanotube.

Charge on Carbon nanotube	SP-B adsorbed residues
Neutral	1:PHE, 2:PRO, 3:ILE, 4:PRO, 5:LEU, 7:TYR, 10:LEU, 11:CYS, 13:ALA, 14:LEU, 17:ARG
Negative	1:PHE, 9:TRP, 12: ARG, 16:LYS, 13:ALA, 17:ARG, 24:LYS

Table 5.1: Adsorbed residues of the pulmonary surfactant protein SP-B on a charged nanotube surface for 100 ns

Figure 5.9, shows the trajectory of SP-B and a neutral carbon nanotube after 100 ns at intervals of 25 ns. At 25 ns a pentagonal ring of 2: Proline comes in contact with the carbon nanotube surface and tries to match itself with the hexagonal ring of the carbon nanotube.
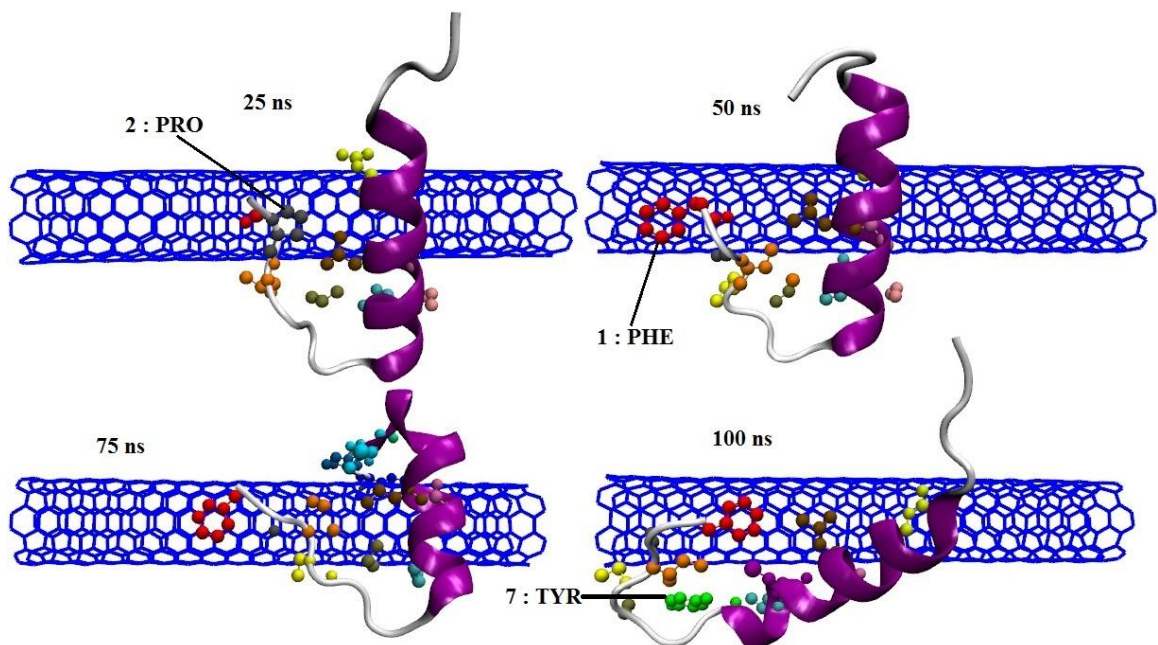
Figure 5.9: Time line of SP-B residues adsorbed on the surface of a neutral carbon nanotube for 100 ns. Top left at 25 ns, top right at 50 ns, bottom left at 75 ns and bottom right at 100ns. The carbon nanotube is represented by a horizontal line, the protein structure is represented in purple, and adsorbed residues are represented in CPK by colored residue ID.

At 50 ns the hexagonal ring of Phenylalanine (residue ID 1:PHE) comes in contact with the carbon nanotube and maintains contact throughout the remaining time period up to 100 ns. During the last section of the trajectory at 100 ns, the hexagonal ring of Tyrosine (residue ID 7:TYR) also comes in contact with the surface of the carbon nanotube.
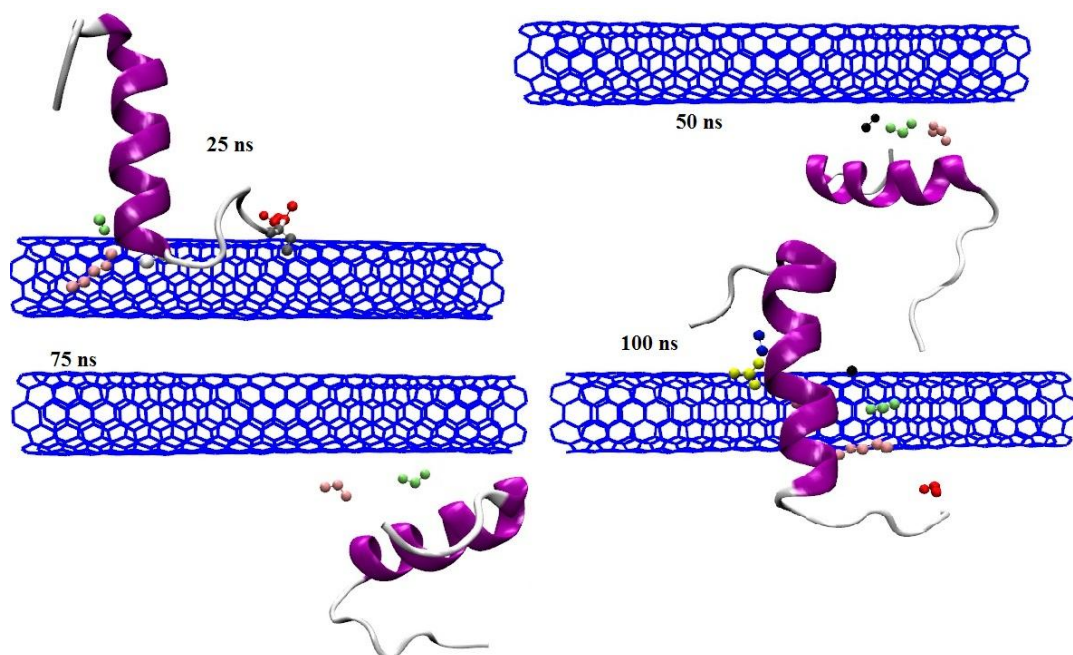
Figure 5.10: Time line of SP-B residues adsorbed on the surface of a negatively charged carbon nanotube for 100 ns: top left at 25 ns, top right at 50 ns, bottom left at 75 ns and bottom right at 100ns. The carbon nanotube is represented as a horizontal line, the protein structure is represented in purple with secondary structure color scheme, and adsorbed residues are represented in CPK and colored by residue ID.

Figure 5.10 shows the trajectory of SP-B with a negatively charged carbon nanotube for 100 ns. Adsorbed residues are described in detail in Table 5.1.
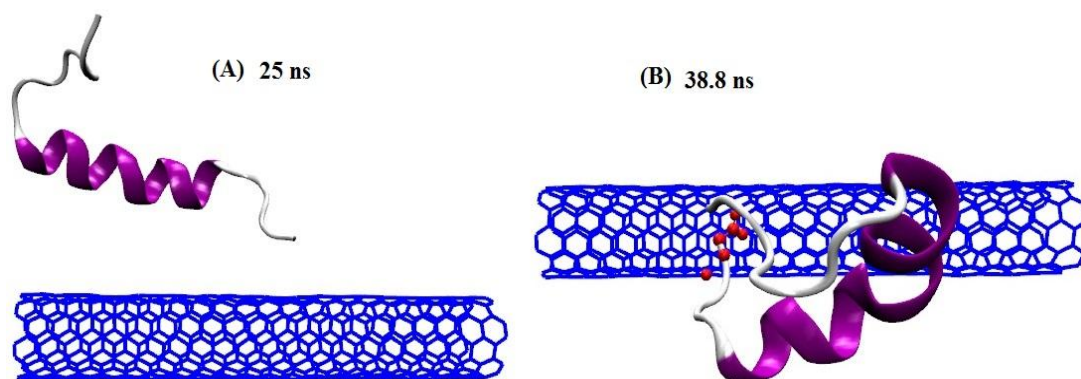
Figure 5.11: Time line of SP-B residues adsorbed on surface of positively carbon nanotube for 100 ns. (A) 25 ns, (B) 38.8 ns. The carbon nanotube is represented a as a horizontal line, the protein structure is represented in purple with secondary structure color scheme, and the adsorbed residues are represented in CPK and colored by residue ID.

Figure 5.11 shows the time line for SP-B as it interacts with a positively charged carbon nanotube. For a short time (about 38.8 ns) few atoms of residues 24: LYS and 25:GLY of SP-B come within 5 Å of carbon nanotube surface.
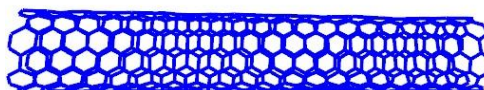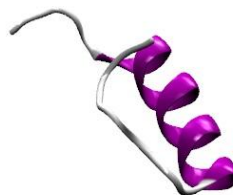
Figure 5.12: Final position of pulmonary surfactant protein SP-B with respect to a positively charged carbon nanotube after 100 ns. The carbon nanotube horizontal and the protein structure is represented in purple and secondary structure color scheme.

Figure 5.12 shows the final position of SP-B with respect to a positively charged carbon nanotube. At the end of 100 ns, SP-B shows no adsorption to the carbon nanotube surface and maintains an equilibrium position of 42.3931 Å from the center of the positively charged carbon nanotube.

Figure 5.13 shows the evolution of the secondary structure of SP-B with a charged carbon nanotube. As SP-B makes closer contact with the surface of a neutral carbon nanotube, its secondary structure changes, especially when compared to a similar contact with a negatively charged nanotube. At the end of 100 ns, the SP-B with the neutral carbon nanotube changes its structure from a helix to 3-10 helix and back; all of

these changes are temporary, and the α-helix regains its structure in case of a neutral carbon nanotube.
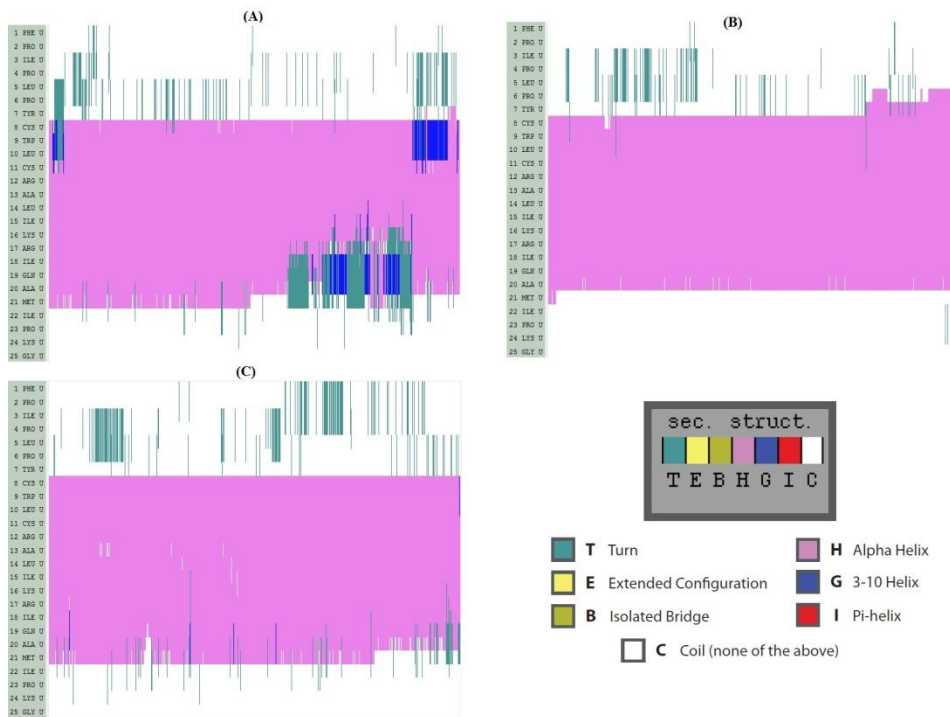
Figure 5.13: Time evolution of the secondary structure for pulmonary surfactant proteins SP-B for 100 ns with a charged carbon nanotube. (A): SP-B with neutral carbon nanotube, (B): SP-B with negatively charged carbon nanotube, (C): SP-B with positively charged carbon nanotube

The pulmonary surfactant protein SP-B is made of one α-helix represented by the pink area in Figure 5.13, which shows the secondary structure evolution of protein SP-B with a charged carbon nanotube for 100 ns. Figure 5.13 C shows the changes in secondary structure of SP-B with a positively charged carbon nanotube. SP-B shows minimal to no interaction with a positively charged carbon nanotube, and this is especially manifest by the very small changes in the secondary structure. A negatively charged carbon nanotube shows an interaction with SP-B and few residues of α-helix are

adsorbed on the carbon nanotube surface. After 80 ns, the α-helix at the C-terminal shows an extended conformation, and some turns of resID7 get changed to an α-helix. During this time, many heavy atoms come in contact with the negatively charged carbon nanotube.

A neutral carbon nanotube (Figure 5.13 A) has the maximum interaction with SP-B, and more residues are adsorbed on the surface of a neutral carbon nanotube surface shown by more changes in the secondary structure of the SP-B. After about 70 ns, more changes in the α-helix are observed. Near the N-terminal of the SP-B, the α-helix converts to turns and a 3-10 helix, but by the end of the simulation, it regains its original secondary structure.

From these results, the adsorption of pulmonary surfactant protein SP-B is more pronounced in a neutral or negatively charged carbon nanotube. A positively charged carbon nanotube shows very little interaction with SP-B, and the protein moves away from the surface of the carbon nanotube. A negatively charged carbon nanotube shows more variation in its interaction with the protein molecule, and it also generates a stronger value of RMSD. In order to develop a carbon nanotube based biosensor for pulmonary surfactant protein SP-B, a neutral or negative charged carbon nanotube surfaces is best.

CHAPTER 6: ELECTROPHORETIC ALIGNMENT OF CARBON NANOTUBE IN POLY VINYL ALCOHOL SLIME

We studied the electro-phoretic alignment of the multi-walled carbon nanotube in the PVA slime matrix, when exposed to a DC field, by the Gel Electrophoresis technique. Electrochemical analysis of the gel was done using cyclic voltammetry to evaluate the effect of PVA slime on the alignment of carbon nanotubes.

Carbon nanotubes are typically considered as tubes of graphitic carbon. Depending on the number of carbon layers, they are categorized as single-walled and multi-walled nanotubes. The unique structure provides nanotubes with extraordinary mechanical and electrical properties. They have been extensively investigated and proposed for various applications in the fields of chemistry, physics, and engineering. Alignment of carbon nanotubes (CNT) in a polymer matrix is a highly desirable feature for the fabrication of nanostructure devices with tailored properties. Mechanical and magnetic techniques have been recently investigated for manipulating CNTs in polymers. Although mechanical [102, 103] and magnetic [104] techniques have shown promising results for CNT alignment, structural damage of nanotubes was caused by mechanical processing. Therefore, the application of electric fields emerges as a suitable option for tailoring the CNT in a polymer matrix and improving its physical properties by making electric field-aligned CNT/polymer composites in the alignment direction [105]. Based

74

on reports of the orientation and purification of CNTs using the electrophoresis technique [106, 107], it is known that CNTs are able to migrate in polymer matrices when an electric field is applied. This study investigates the electrophoretic alignment of multi-walled carbon nanotubes (MWNTs) in polymer gels of different concentrations using the Gel Electrophoresis technique.

6.1 Gel Electrophoresis

Electrophoresis refers to the electromotive force (EMF) that is used to move molecules through a gel matrix. By placing molecules in wells approximately one cm deep and filled with a gel and by applying an electric field, the molecules will move through the matrix at different rates determined largely by their mass when the charge to mass ratio (Z) of all species is uniform. However, when charges are not all uniform, the electric field used by the electrophoresis process will affect the species that have different charges; the odd species with different charges will be attracted. Species that are positively charged (cations) will migrate towards the cathode, which is negatively charged, and species that are negatively charged (anions) will migrate towards the positively charged anode.

6.1.1   Principle of Gel Electrophoresis

If a mixture of electrically charged molecules is placed in an electric field of strength E, they will move freely toward the electrode of opposite charge. However, different molecules will move at different and unique rates of speed, depending on the physical characteristics of the molecule and on the experimental system used. The velocity of movement, v, of a charged molecule in an electric field is

75

$$v = \frac{E \times q}{f} \tag{6.1}$$

Where f is the frictional coefficient and q is the net charge on the molecule. The frictional coefficient describes frictional resistance to mobility and depends on a number of factors: mass of the molecule, its degree of compactness (individual density), buffer viscosity, and the porosity of the matrix in which the experiment is performed. The number of positive and negative charges in the molecule determines the net charge.

Equation 6.1 means that molecules will move faster as their net charge increases, as the electric field increases, and as f decreases (which is a function of molecular mass/shape). Molecules of similar net charge separate due to differences in frictional coefficient while molecules of similar mass/shape may differ widely from each other in net charge. Consequently, it is often possible to achieve very high resolution in separation by electrophoresis [108-111].

A gel is used as an anti-convective medium and/or sieving medium during electrophoresis for the movement of a charged particle in an electrical field. It suppresses the thermal convection caused by the application of the electric field, and it can also act as a sieving medium, retarding the passage of molecules; gels can also simply serve to maintain the finished separation, so that a post electrophoresis stain can be observed.

If several samples have been loaded into adjacent wells in the gel, they will run parallel in individual lanes. Depending on the number of different molecules, each lane shows separation of the components from the original mixture as one or more distinct bands, one band per component. Incomplete separation of the components can lead to

overlapping bands or to indistinguishable smears representing multiple unresolved components. Bands in different lanes that end up at the same distance from the top contain molecules that passed through the gel with the same speed, which usually means they are approximately the same size. The distance a band travels is approximately inversely proportional to the logarithm of the size of the molecule [112].

The migration of particles through different concentrations is studied through the Ferguson Plot, and the migration of particles is measured as the mobility, where

$$\text{Mobility} = \text{Migration Velocity (cm/s)} \Big/ \text{Field Strength (V/cm)} \qquad (6.2)$$

6.2 Poly Vinyl Alcohol (PVA)

Poly vinyl alcohol (PVA) is a polymer of great interest because of its many desirable characteristics for pharmaceutical and biomedical applications. The crystalline nature of PVA has been of specific interest for physically cross-linked hydrogels.

6.2.1 Structure of PVA

Poly Vinyl alcohol (PVA) has a simple chemical structure with a hydroxyl group. The monomer vinyl does not exist in a stable form and seeks to rearrange itself to its tautomer, acetaldehyde. Therefore, PVA is produced by polymerization when vinyl acetate goes to poly vinyl acetate, followed by hydrolysis of PVAc to PVA. The hydrolysis reaction does not go to completion, and this results in polymers with a certain degree of hydrolysis that depends on the extent of the reaction.

poly(vinyl alcohol-*co*-vinyl acetate)
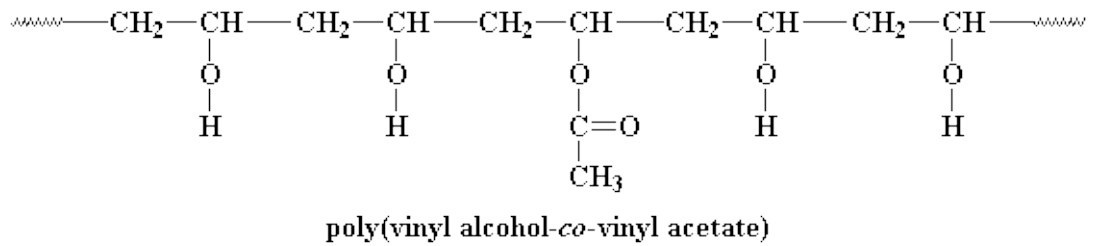
Figure 6.1: Structure of poly vinyl alcohol

PVA is always a copolymer of PVA and PVAc. The degree of hydrolysis and polymerization affect the solubility of PVA in water. It has been shown that PVA with high degrees of hydrolysis have low solubility in water [113].

6.2.2 Properties of PVA

1. Polyvinyl has excellent film forming, emulsifying and adhesive properties. It is also resistant to oil, grease, and solvents. It is odorless and nontoxic.

2. It has high tensile strength and flexibility, as well as high oxygen and aroma barrier properties. However, these properties are dependent on humidity. In other words, with higher humidity more water is absorbed.

3. PVA is fully degradable and dissolves quickly.

4. PVA has a melting point of 230°C and 180–190°C (356-374 degrees Fahrenheit) for the fully hydrolyzed and partially hydrolyzed grades, respectively. It decomposes rapidly above 200°C as it can undergo pyrolysis at high temperatures [12].

5. PVA exhibits crystallinity as the hydroxyl groups are small enough to fit into the lattice without disrupting it.

6.2.3 Slime

Slime is a unique material composed of a cross-linked polymer. It is classified as a liquid and is typically made by combining polyvinyl alcohol solutions with borate ions in a large mixer. It often has an unpleasant odor and a green color, and it is cold and slimy to the touch. In scientific terms, slime is classified as a non-Newtonian fluid. These are thick liquids that have a variable viscosity. Viscosity is the measurement of the resistance to flow when a shearing force is applied. Newtonian fluids have a constant viscosity depending on their composition. Non-Newtonian fluids like slime have different viscosities based on the amount of force put on them. If a small amount of force is applied, such as stirring them slowly with your fingers, they feel thin and water-like. If a high force is applied, like throwing it against a wall, the resistance is very strong. They are called non-Newtonian fluids because they do not behave as predicted by Newton's laws. The most abundant material in slime is water, typically making up over 90% of the whole. Slime contains specially treated de-ionized water. Water is a diluent that gives the slime its liquid consistency.

While polymeric materials give slime its substance, a gelling agent is needed to give it its non-Newtonian liquid behavior. In classic slime formulations, sodium borate (Borax) or sodium tetraborate is used. When dissolved in water, sodium borate dissociates into sodium ions and borate ions. If a polymer is present like PVA, the borate ions interact with the polymer chains and form weak ionic bonds that make the solution thicker. These bonds also have the ability to stretch when a force is applied. Typically, sodium borate makes up about 2% of the final product. The ratio of the polymer to the gelling agent is one factor in determining the consistency of the slime.
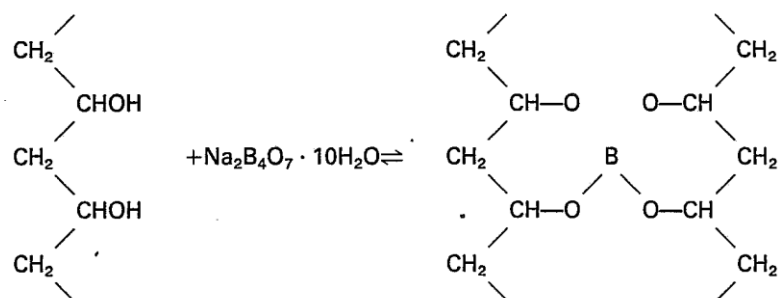
Figure 6.2: PVA and Borax reaction of gel formation

6.3 Experimental Methods

6.3.1 Preparation of PVA Solution

Materials required:

1. Beaker, stirring rod.

2. Polyvinyl alcohol (99-100% fully hydrolyzed), 4% solution in water.

3. Borax (sodium tetraborate decahydrate), Na2B4O7 10H2O, 4% solution, weight in water.

4. Heat source Hot plate or Microwave oven.

5. Zip-lock bag to store.

Procedure I:

This procedure uses water bath to maintain a constant temperature. A measured amount of PVA granules are put into a measured amount of hot double distilled water of temperature more than 30ºC. The temperature range of 70 - 80ºC was maintained, to avoid boiling the solution. Continuous stirring of the mixture is required. This procedure has many limitations—it takes a long time and about 10ml of solution gets evaporated during preparation. The final solution obtained is not clear.

Figure 6.3: Experimental set up for PVA solution preparation

Procedure II:

A measured amount of PVA was put into a measured amount of double distilled water in a beaker. The mixture was heated in a microwave oven for 20 seconds. It was then stirred and heated for another 20 seconds. This continued for 20 seconds intervals until a clear solution is obtained. Avoid boiling the solution. This is a very simple procedure, and the solution is prepared in 15min. But the actual time to complete this process depends on the amount of PVA granules used.

6.3.2 PVA and Borax Gel Preparation

The hot PVA solution was poured in the clean gel-casting tray for gel electrophoresis. One part of Borax solution is added to the PVA solution drop-by-drop. This mixture is kept undisturbed for 24hrs to from a gel. Avoid the formation of air bubbles while mixing the PVA and Borax solution.

81

6.3.3   Dispersion of Multi Walled Carbon Nanotube

Materials required:

1. Multi-walled nanotubes(MWNTs) 0.001 wt%

2. 1% PVA solution.

3. 0.0001g of Sodium Dodecyl Sulfate (SDS) as surfactant.

4. Ultra Sonication chamber

Multi-walled carbon nanotube surfactant dispersion in a 1% PVA solution was done using the Ultra sonication chamber at 55Hz for 1hr 15mins. The addition of the surfactant increases the dispersion of carbon nanotubes and avoids the coagulation of the nanotubes.

6.3.4   Electrophoresis of Multi Walled Carbon Nanotubes

Materials required:

1. Dispersed solution of Multi-walled carbon nanotube.
2. Micropipettes
3. 1x Tris acetic EDTA (TAE) buffer solution.
4. Power supply EC-454

A multi-walled carbon nanotube solution of volume 10-20µliters was loaded into the wells of PVA gel. The samples were loaded at the cathode end of the electrophoresis unit. The required amount of 1x Tris Acetic EDTA (TAE) buffer solution was poured to fill the unit. The power supply EC-454 was connected to the unit and initially 50V was applied. The voltage was gradually increased every 20-30mins depending on the

movement of carbon nanotubes. The voltage was gradually increased for every 20-30mins of time interval depending on the movement of carbon nanotubes.

6.4   Results and Discussion

The migration of multi-walled carbon nanotubes toward the negative electrode when a DC electric field is applied can be explained in terms of the theory of electrophoresis. Electrophoresis is a strong, polarity dependent phenomenon related to a double-layer formation at the surface of certain particles suspended in aqueous media. This double-layer formation consists on ions of one sign that collect at the particles' surface while a surrounding counter-ion cloud shields this net charge from the bulk of the fluid. When a DC electric field is applied, the mobile counter-ion charge is set in motion, creating a flow parallel to the surface, so that the particles move in response to the shear stresses exerted upon the particle by this fluid convection.
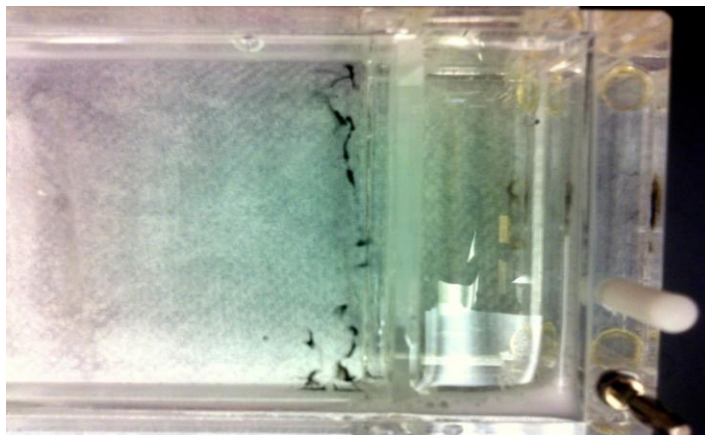
Figure 6.4: Migration of multi-walled carbon nanotubes in 4% PVA & borax gel at 150V after 30mins

Figure 6.5: Migration multi walled carbon nanotube in 4% PVA & borax gel at 200V after 25mins

Figure 6.6: Migration multi walled carbon nanotube in 4% PVA & borax gel at 250V after 10mins

Figure 6.7: Migration multi walled carbon nanotube in 6% PVA & borax gel at 200V after 30mins
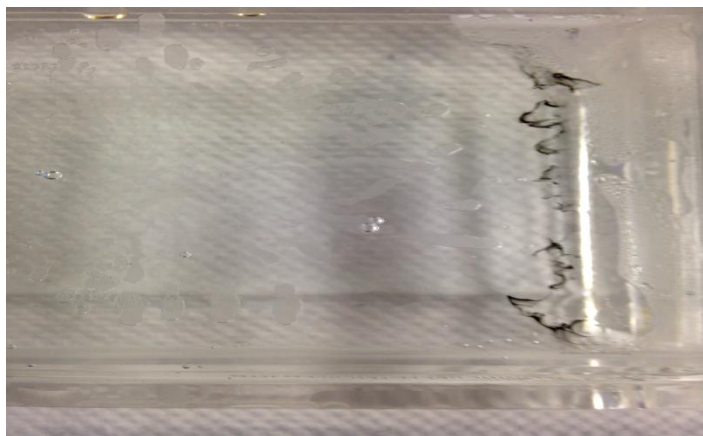
Figure 6.8: Migration multi walled carbon nanotube in 8% PVA & borax gel at 250V after 25mins

From Figure 6.4 to Figure 6.8 it can be seen that the alignment and movement of carbon nanotubes toward the negative terminal depends on the concentration of the gel and the characteristics of the applied electric field.

Gel Concentration	Voltage (V)	Time (min)	Movement
4%	100	30	No
	150	30	Yes
	200	25	Yes
	250	10	Yes
6%	100	30	No
	150	30	No
	200	25	Yes
	250	20	Yes
8%	100	30	No
	150	30	No
	200	25	No
	250	25	Yes

Table 6.1: Displacement of carbon nanotube with different PVA & borax gel concentrations and voltages

Table 6.1 shows us that carbon nanotubes move at voltages ranging from 150V to 200V. In this voltage range, the electric field drives the nanotubes toward the anode. The variation in the concentration of the PVA and borax gel also has an effect on the migration of the nanotubes. A lower concentration of gel increases the speed of the movement of the multi-walled carbon nanotubes.

In a 4% gel concentration, the multi-walled carbon nanotubes migrate at 150V and move quickly through the gel matrix. At 250V, the nanotubes are completely swept from the wells. The gel consistency is very soft and the cross-linking of the polymer with the borate ions is good enough to form the gel at 4% concentration of PVA. In this concentration, the porosity is moderate and because of this, the nanotubes require less time to pass through the gel matrix; hence the nanotubes move very fast through the matrix.

In a 6% PVA gel concentration, the multi-walled carbon nanotubes where able to migrate at 200V for 25 mins and move with a speed less than that of the 4% concentration. Due to the increase in the concentration of the PVA, the cross-linking of the gel matrix is increased, and the 6% PVA gel is stiffer than the 4% gel. Therefore, the nanotubes require more time to penetrate the matrix.

In the case of the 8% PVA gel concentration, the multi-walled carbon nanotubes were not able appear at 200V, even after 30mins. This is due to the increased concentration which makes the cross-linking very high and this, in turn, makes the nanotubes move slow through the gel matrix. The nanotubes showed a slight movement at 250V after 25mins, and this shows that the cross- linking of the gel is very high. In an 8% gel concentration, the nanotubes require more force and time to penetrate and pass

through the gel matrix. The polymer PVA binds very well around the multi-walled carbon nanotubes, and this obstructs the movement of the nanotubes.
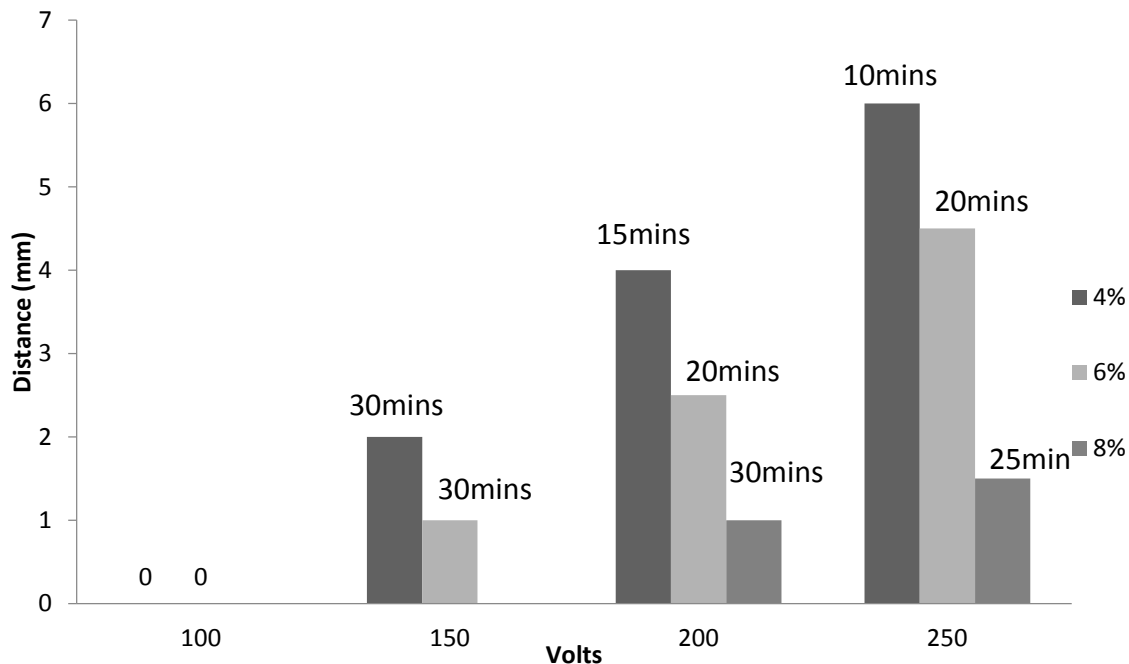
Figure 6.9: Migration of multi-walled carbon nanotubes, distances travelled from their initial position (mm) and applied voltage (V)

Carbon nanotubes are able to move at voltages ranging from 150V to 200V. In this voltage range, the electric field drives the nanotubes towards the anode. The variation in the concentration of the PVA gel also effects the migration of the nanotubes. A lower concentration of gel means faster movement for the multi-walled carbon nanotubes.

6.5 Cyclic Voltammetry Electrochemical Study

Cyclic Voltammetry (CV) is an electrochemical technique, which measures the current that develops in an electrochemical cell under conditions where voltage is in

excess of that predicted by the Nernst equation. CV is performed by cycling the potential of a working electrode and measuring the resulting current.

A CV system consists of an electrolysis cell, a potentiostat, a current-to-voltage converter, and a data acquisition system. The electrolysis cell consists of a working electrode, counter electrode, reference electrode, and electrolytic solution. The working electrode's potential is varied linearly with time, while the reference electrode maintains a constant potential. The counter electrode conducts electricity from the signal source to the working electrode. The purpose of the electrolytic solution is to provide ions to the electrodes during oxidation and reduction. A potentiostat is an electronic device which uses a dc power source to produce a potential which can be maintained and accurately determined while allowing small currents to be drawn into the system without changing the voltage. The current-to-voltage converter measures the resulting current, and the data acquisition system produces the resulting voltammogram.
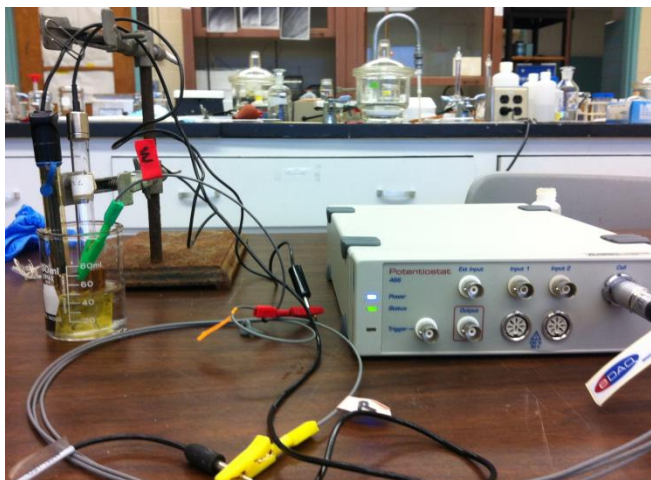
Figure 6.10: Cyclic voltammetry setup

Materials required:

1. Potentiostat eDAQ-486

2. 1M KCL solution (electrolyte).

3. Reference electrode(RE)- Silver

4. Working electrode(WE)- Gold

5. Counter electrode(CE)- Platinum

We used 30ml of 1M KCL electrolyte in a 50ml beaker. The three electrodes are fixed to the beaker. The sample (PVA film) was dipped into the electrolyte with a string attached to it.

Figure 6.11: The PVA films of 2cm x 2cm used for electrochemical analysis

Figure 6.12: The PVA impregnated with MWNTs of 2cm x 2cm for electrochemical

The PVA gel after electrophoresis was dried, and this produces a film of PVA and PVA impregnated with carbon nanotube films. These films are used to show the results of the electrochemical study using cyclic voltammetry.

6.5.1 Electrochemical Response of PVA Film

Figure 6.13, shows that the PVA film did not exhibit any electrochemical response. From this result, we can say that the polymer PVA is not conductive and it cannot show electro-activity.
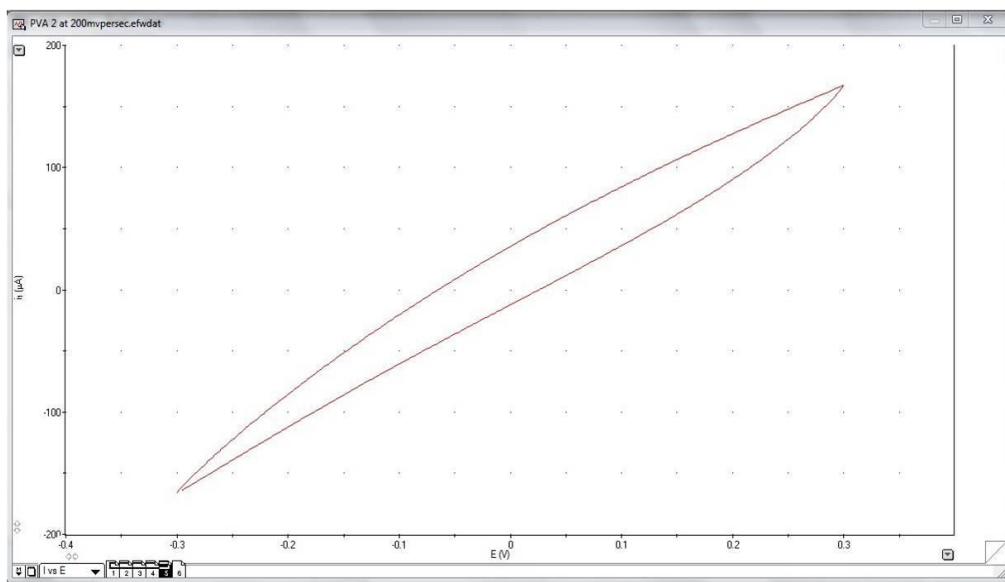
Figure 6.13: Cyclic voltammogram of first five potential cycles of PVA films in 1M KCL

6.5.2 Electrochemical response of PVA impregnated with Multi Walled Carbon Nanotube

Figure 6.14 shows clearly defined peaks, and this indicates that there is an electron transfer taking place in the polymer when it is impregnated with the MWNTs. The MWNT/PVA composite films demonstrate sharply defined peaks, which indicate

higher electro-activity over neat PVA. It was shown earlier that the electro-chemical activities of poly vinyl alcohol films coincide with the degree of protonation; hence, a promotion in the protonation with a doping effect of MWNTs on poly vinyl alcohol may be expected.
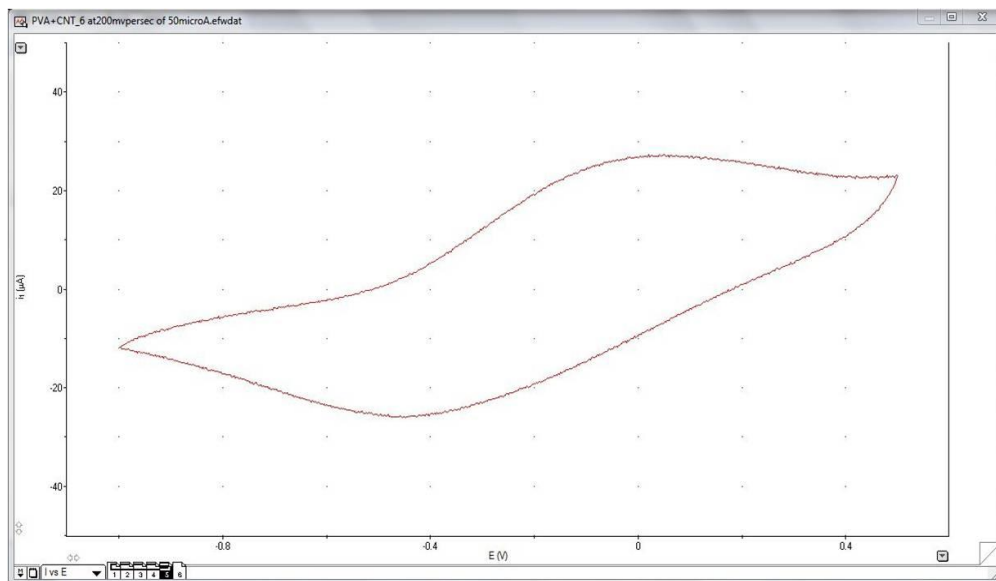
Figure 6.14: Cyclic voltammogram of first five potential cycles of MWNTs 0.001wt% impregnated PVA films in 1M KCL

A possible explanation is the electrophoretic alignment of multi-walled carbon nanotubes; also, because large π-bonds on the surface of multi-walled carbon nanotubes interact strongly with the conjugated structure of poly vinyl alcohol via π-stacking, and the resulting highly conjugated π-system would promote electron delocalization [114, 115]

The variation of voltage applied over time was associated with the migration of the multi- walled carbon nanotube in the gel matrix. The influence of the electric field magnitude and concentration of the polymer gel on the multi-walled carbon nanotube

alignment was studied. Multi-walled carbon nanotubes migrate toward the negative electrode, and this was observed when a direct current electric field was applied. A higher concentration of the gel yields slower multi-walled carbon nanotube movement, evidenced by the time taken by the nanotubes to migrate. An electrochemical study on the PVA and multi-walled carbon nanotube/PVA was performed to evaluate the alignment of the multi-walled carbon nanotube in the polymer. The multi-walled carbon nanotube/PVA composite films demonstrate sharply defined peaks, which indicate higher electro-activity over neat PVA [116].

6.6 A Simple Electric Circuit Model to Explain the Impedance of Polymers Doped with Carbon Nanotubes
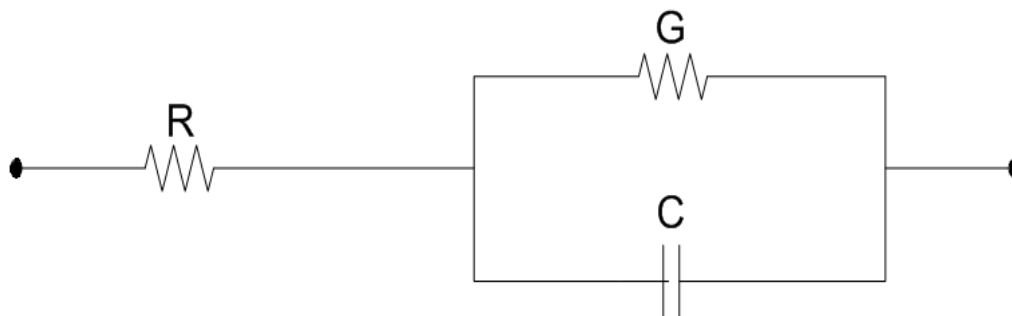
Figure 6.15: Electronic model of polymer-carbon nanotube composite, where R represents the contact resistance, C represents the material dielectric and G is the conductance of the conductive mesh within the composite.

The value of R is the contact resistance. It depends on the points where contact is made and what type of contact is made. Typically, silver paste or gold-deposition is the contact material of choice. G is the conductance of a resistor, which represents the effective conductance of the carbon nanotube structure within the polymer matrix. C is

the capacitance of the bulk composite. Given that the electric contacts are silver paste at each end, and assuming we can neglect contact effects, R= 0 and we have a simple parallel plate capacitor with capacitance give as

$$C = \frac{K \, \varepsilon_0 \, A}{L} \qquad (6.3)$$

This capacitor is shunted by a leakage resistor of resistance 1/G. The value of ε_0 is the value of the dielectric of air or vacuum. K represents the added dielectric strength due to the dipole nature of the material dielectric (i.e. the polymer/carbon nanotube composite).

If we plot the data that fits the model of Figure 6.15, we would get graphs that appear in Figure 6.16. Note: these graphs are not to scale. The x-axis is the logarithm of the frequency of measurement. The y-axis is the log of the impedance or admittance of the material under investigation. Graphs made in this fashion are Bode plots of the electronic device under investigation.
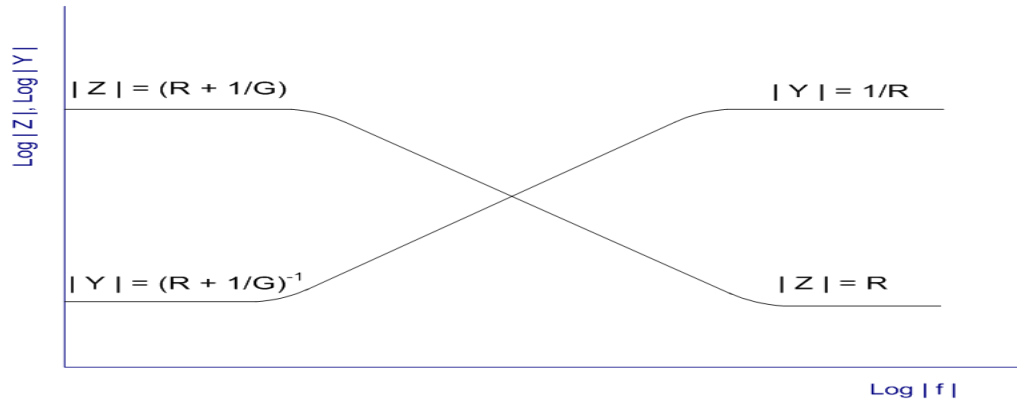
Figure 6.16: Plot of Log |Z| and Log |Y| vs. Log |f| in the fashion of the Bode plot. Y is the admittance (1/Z)

93

Data at low frequency shows the value of (R+1/G) or (G+1/R). The contact resistance for a polymer/conductive composite is usually around one or two ohms and no more than 10 [117-119]. By contrast, the resistance of the sample can be 100 to many hundreds of thousands of ohms, even when the material is highly conducting. For this reason we can approximate (1/G) >> R, and the resistance (or conductance) at low measuring frequency is taken to be equal to 1/G (or G).

CHAPTER 7: MOLECULAR DYNAMICS COMPUTATION OF MULTIPLE SP-B MOLECULES WITH A SINGLE CARBON NANOTUBE

In a real life scenario, it is difficult to isolate a single molecule of protein around a carbon nanotube. In addition, if the carbon nanotube is used as a sensor, then multiple molecules of SP-B will surround each carbon nanotube. This is the case if one has to find out the amount of SP-B present in a sample. Therefore, the focus of this chapter is on the effect of multiple molecules of protein SP-B surrounding a carbon nanotube.

In this computation, four molecules of the pulmonary surfactant protein SP-B surround one carbon nanotube. In this case, the interaction between protein and the carbon nanotube is not only influenced by the protein-carbon-nanotube interaction but also by protein-protein interactions. The length of a carbon nanotube plays a critical role in the number of SP-B protein molecules adsorbed on the surface of a carbon nanotube. Consider three cases:

1. Four molecules of SP-B protein with a 5 nm (6, 6) carbon nanotube

2. Four molecules of SP-B protein with a 7 nm (6, 6) carbon nanotube

3. Four molecules of SP-B protein with a 10 nm (6, 6) carbon nanotube

Varying the length of a carbon nanotube changes the surface area for protein adsorption on the carbon nanotube.

7.1 Materials and Methods

Molecular dynamics computation of multiple pulmonary surfactant proteins SP-B with a carbon nanotubes are done by NAMD with CHARMM27 force field parameters. Lennard–Jones potential parameters were set for interactions between non-bonded atoms of the carbon-nanotube–protein, carbon-nanotube –water, and protein–water and protein –protein. The X-ray structure of SP-B (ID code: 1dfw) was acquired from the protein data bank. SP-B contains 1 to 25 residues (FPIPLPYCWLCRALIKRIQAMIPKG) with side chains and one α-helix. The sequence 1 to 25 of Human surfactant protein SP-B is used for surfactant protein SP-B that demonstrates the same surface and biophysical properties of the full human surfactant protein SP-B1-78 that is based on the N-terminal. A carbon nanotube generated by the "Carbon Nanostructure Builder" plug-in of the VMD software is an armchair nanotube with chiral vectors of (6, 6), length of 5nm, 7nm, and 10nm sp2 hybridized carbon atoms and diameter of 0.8 nm.

All atoms including hydrogen were defined explicitly in all simulations. A time step of 2 fs was set and the cutoff of non-bonding Van der Waals force was set to a switching start distance of 10 Å, with a reach to zero at 12 Å. Particle mesh Ewald (PME) summation was used for full system periodic electrostatic calculations with grid spacing of 1 Å. Langevin dynamics parameter were set to control the temperature and pressure. The Langevin parameter for hydrogen coupling was set to off. All MD simulations were

performed at 300 K temperature and 1 atm pressure. Simulations were performed as follows:

1. The energy minimization and energy equilibration of SP-B(1-25) and a single walled-carbon nanotube was performed. SP-B(1-25) was solvated in 0.15 mol/L sodium chloride solution using TIP3 [100]. Then, the protein and carbon nanotube systems underwent 5000 steps toward energy minimization. Then, molecular dynamics ran the Root-Mean-Square Deviation (RMSD) of proteins fluctuating around a constant value. The final structure was used for setting up the initial structure for the simulation of the SPB-carbon-nanotube interaction.

2. A carbon nanotube with different lengths 5nm, 7nm, and 10nm and with four molecules of protein SP-B (1-25) were built. Positional constraints are applied to the carbon nanotube. The minimum distance between protein and the nanotube is 1.2nm, so that there are several ordered water layers to reduce the effects of initial conditions. The protein and carbon nanotube complex was solvated with a 0.15 mol/L sodium chloride solution.

3. The fixed protein process with a carbon nanotube was performed at constant temperature (300 K) and pressure (1 atm) for 5000 energy minimization steps, and the molecular dynamics to affix protein to the carbon nanotube was performed for 40 ps. After this protein reached equilibrium, the carbon nanotube was relaxed and used in another molecular dynamics run.

4. Energy minimization for 5000 steps at constant temperature and pressure performed for both systems (containing protein molecule, carbon nanotube, water molecules and Na Cl ions) was done. After minimization, all systems underwent

equilibration for 100ns until the RMSD and the system's total energy and distance between the protein and the carbon nanotube fluctuated around constant value. This indicates that system has achieved stable, dynamic equilibrium, i.e. a stable state.

The initial position of the protein molecules and the carbon nanotube used for computation are shown in Figure 7.1:
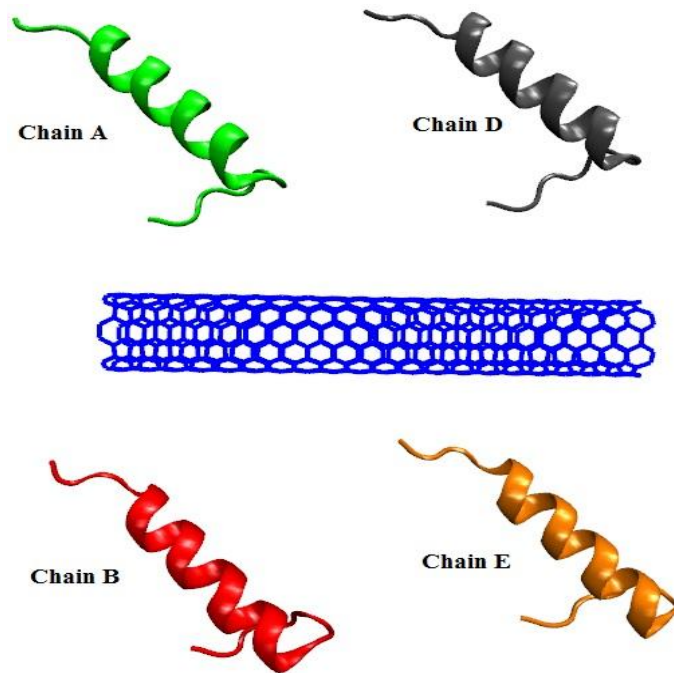
Figure 7.1: Initial position of a 5 nm carbon nanotube with four pulmonary surfactant protein SP-B molecules

Details of this model are:

1.   Length of carbon nanotube is 5 nm.

2.   Chiral vectors are (6, 6).

3.   The distance between the center of each protein molecule and the center of the nanotube is 25 Å.

4. The distance between protein molecules which are on the same side of a CNT is 34.05 Å.

5. Protein molecules and the carbon nanotube are solvated in a water box of 31.24 Å × 84 Å × 71.89 Å, with 0.15 mol/L Na Cl ions.

6. For simplicity, four molecules of SP-B are labeled as Chain A, Chain B, Chain D and Chain E
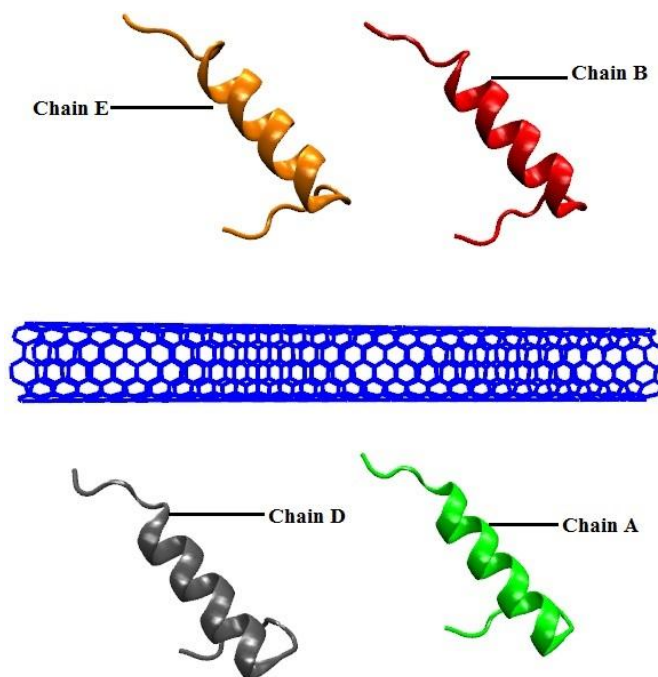
Figure 7.2: Initial position of 7 nm carbon nanotube with four pulmonary surfactant protein SP-B molecules

Details of the model shown in Figure 7.2 are:

1. The length of the carbon nanotube is 7 nm.

2. The chiral vectors are (6, 6).

3. Positional constrains are applied to the carbon nanotube to reduce the computation time.

4. The distance between the center of each protein and the center of the nanotube is 25 Å.

5. The distance between protein molecules which are on the same side of the CNT is 33.48 Å.

6. Protein molecules and carbon nanotube are solvated in a water box of 45.43 Å × 100.907 Å ×91 Å, with 0.15 mol/L Na Cl ions.
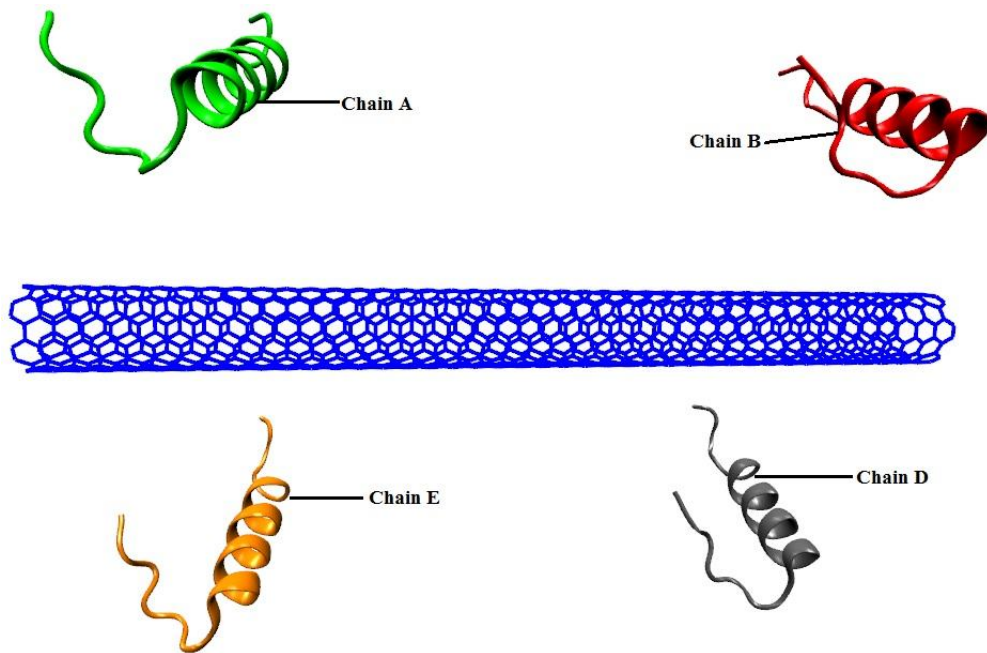
Figure 7.3: Initial position of a 10 nm carbon nanotube with four pulmonary surfactant protein SP-B molecules

Details of model shown in Figure 7.3 are:

1. The length of the carbon nanotube is 10 nm.

2. The chiral vectors are (6, 6).

3. Positional constrains are applied to the carbon nanotube to reduce the computation time.

4. In this simulation, the carbon nanotube has positional constraints at its initial position and for the entire length of this simulation. Consider if there is enough space for proteins to move and how to optimize dimension of the water box for computation in order to save computing time and memory.

5. The distance between the center of each protein and center of the nanotube is 25 Å.

6. The distance between protein molecules which are in the same side of CNT is 63.10 Å.

7. Protein molecules and the carbon nanotube are solvated in a water box of 86 Å × 110 Å × 178 Å with 0.15 mol/L Na Cl ions.

7.2 Result and Discussion

7.2.1   Four SP-B molecules with the 5 nm carbon nanotube

The variation in distance between the centers of all four SP-B molecules to the surface of the carbon nanotube is plotted versus time (ns) in Figure 7.4. Two out of four SP-B molecules are adsorbed on the surface of the carbon nanotube.
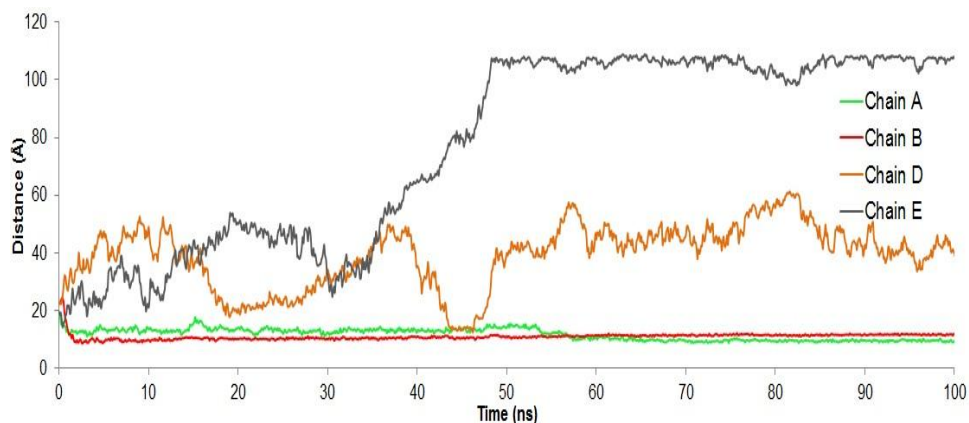
Figure 7.4: Distance between centers of protein molecules to 5 nm carbon nanotube for 100 ns. Four molecules of SP-B are named as Chain A, B, D and E.

Chain A and Chain B of SP-B move swiftly to the surface of the 5 nm carbon nanotube and stay close to the surface for the remaining time of simulation. Chain D of SP-B tries to come close to the surface of the 5 nm carbon nanotube, and after about 45 ns, some atoms of chain D come within 5 Å of the surface. Initially, chain E also tries to come close to the surface of the carbon nanotube but is pushed away after about 30 ns. The reason for this might be due to the fact that there is not enough surface area on a 5 nm carbon nanotube for adsorption of all four SP-B protein molecules. Since SP-B is hydrophobic and since it carries a positive charge on its surface, after most of the surface area of the 5 nm carbon nanotube is consumed by the adsorption of two SP-B protein molecules, the force of repulsion by the positive charges between protein-and-protein is stronger than the hydrophobic-hydrophobic forces between the 5 nm carbon nanotube surface and an SP-B protein molecule. After adsorption of chain A and chain B, there is still some free surface area remaining on the 5 nm carbon nanotube, and chain D maintains its distance from surface of the 5 nm carbon nanotube until the hydrophobic forces between the protein and the carbon nanotube come to equilibrium.

102
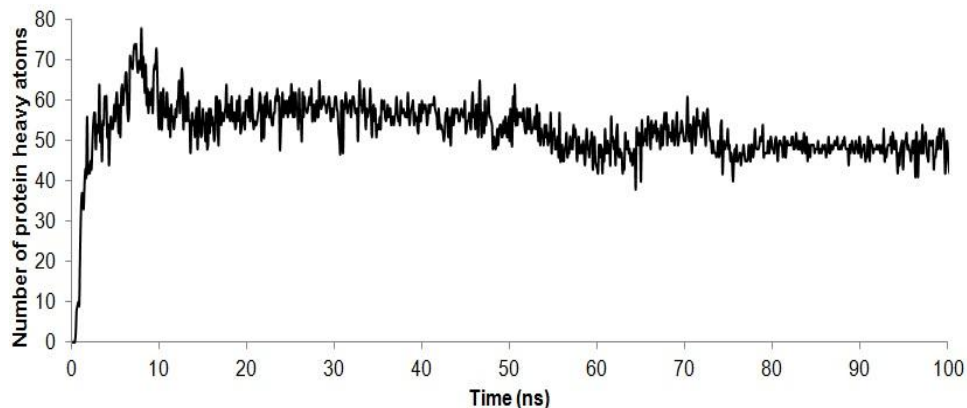
Figure 7.5: The number of heavy atoms within 5 A of a 5 nm carbon nanotube over 100 ns.
Hydrogen atoms are not counted in this number

Figure 7.5 shows the number of heavy atoms (not counting hydrogen atoms) coming within 5 Å of the surface of the 5 nm carbon nanotube over 100 ns. This includes the total number of atoms from all four SP-B molecules. Adsorption criteria are the same as they were before the first protein atom coming within 5 Å is considered adsorbed.

Figure 7.6 shows the RMSD for all four SP-B molecules over 100 ns in the presence of a carbon nanotube. At the end of 100 ns, chains A, B, and E have approximately the same RMSD. At about 40 ns, the RMSD value for chain E increases rapidly as chain E is moving away from the surface of the 5 nm carbon nanotube. In the beginning, chain B and chain D follow a similar RMSD pattern, but when chain D is at its equilibrium position, the RMSD of chain D decreases and stabilizes.

Figure 7.6: Root mean square deviation of all 4 SP-B molecules during their interaction with a 5 nm carbon nanotube over 100 ns

Figure 7.7 shows the time line in pictorial form for the four SP-B molecules as they interact with the 5 nm carbon nanotube. In (A) at 25 ns, chain A and chain B are coming into contact with the carbon nanotube surface. Also, the hexagonal ring of 1: PHE and the pentagonal ring 2: PRO of chain B make contact with the carbon nanotube, and they remain in contact until the end of the simulation. This indicates a π-π interaction. Figure 7.7 shows a protein-protein interaction. Chain A and chain B interact with each other while interacting with the carbon nanotube. This shows that most of the surface of the 5 nm carbon nanotube is reacts with only two SP-B molecule and only weakly with the remaining two.

Figure 7.7: Time line of SP-B residues adsorbed on the surface of the 5 nm carbon nanotube over 100 ns. (A) Top left at 25 ns, (B) top right at 50 ns, (C) bottom left at 75 ns, and (D) bottom right at 100ns. The carbon nanotube is represented as horizontal, the protein structure is represented as a color picture, and adsorbed residues SP-B are represented in CPK

Figure 7.8 shows adsorbed residues of chain A and chain B of pulmonary surfactant protein SP-B on the surface of the 5 nm carbon nanotube. An aromatic ring of residue 1 Phenylalanine and a pentagonal ring of residue 2 Proline of chain A are adsorbed on the surface of the 5 nm carbon nanotube.
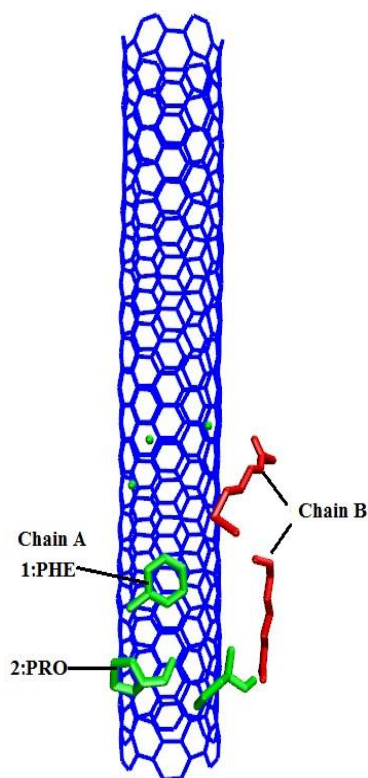
Figure 7.8: Residues adsorbed on the surface of 5 nm carbon nanotube after 100 ns. The carbon nanotube is represented as vertical, and adsorbed residues of chain A and chain B of SP-B are represented by using a "licorice" representation

7.2.2 Four SP-B molecules with the 7 nm carbon nanotube

Figure 7.9 shows that three molecules of SP-B remain close to the surface of the 7 nm carbon nanotube. It takes about 20 ns for chain A, chain D, and chain E to move to the surface of the 7 nm carbon nanotube, and they remain close to the surface for the remaining time. On the other hand, chain B moves away from the surface of the carbon nanotube and maintains this as its equilibrium position. With the increase in length of the carbon nanotube, it increases the surface area, and thus it increases the adsorption of the protein molecules on the surface of the carbon nanotube.
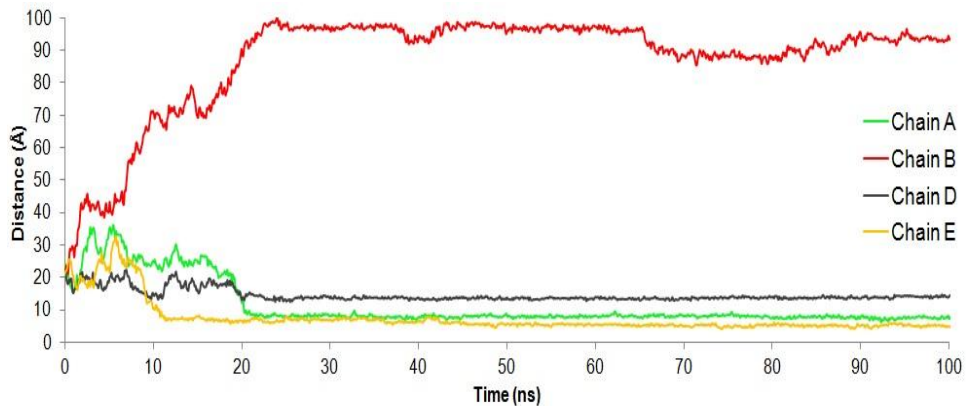
Figure 7.9: The distance between the centers of protein molecules to the 7 nm carbon nanotube over 100 ns
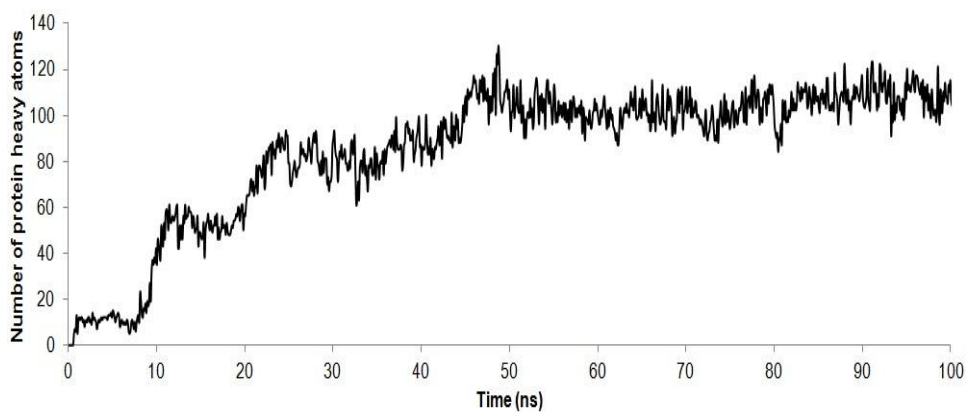
Figure 7.10: The number of heavy atoms within 5 A of the 7 nm carbon nanotube over 100 ns. Hydrogen atoms are not counted in this number

Figure 7.10 shows the total number of protein heavy atoms within 5 Å of the 7 nm carbon nanotube for all four SP-B molecules, with hydrogen atoms not counted. The increased length of the carbon nanotube increases the surface area, and this causes more protein atoms to be adsorbed on the surface.
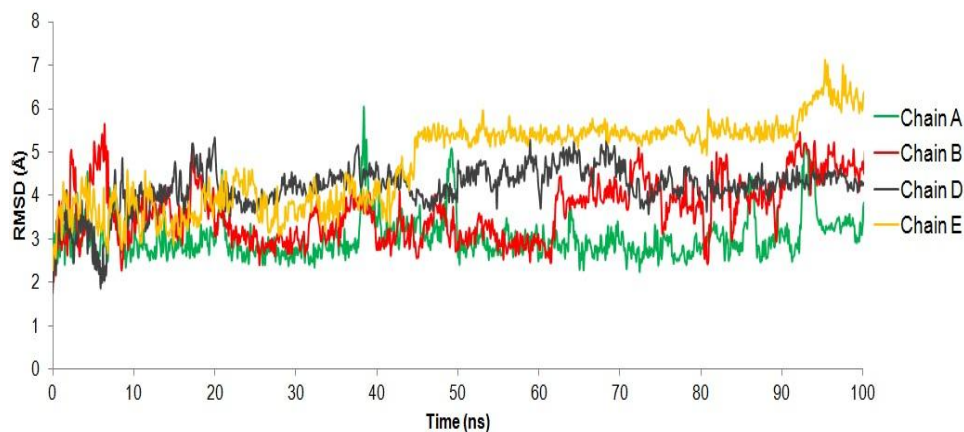
Figure 7.11: Root mean square deviation of all 4 SP-B molecules during interaction with the 7 nm carbon nanotube over a time of 100 ns

Figure 7.11 shows the RMSD for all four SP-B protein molecules with the 7 nm carbon nanotube. Chain A shows the minimum RMSD value, and chain E shows the maximum. A change in RMSD is easier to see in Figure 7.12, which shows the time line of the four SP-B molecules with the 7 nm carbon nanotube. Chain A, chain D, and chain E are adsorbed on the surface of the 7 nm carbon nanotube, and chain B moves away from the surface and stays at a constant distance at equilibrium. As more residues of chain E are adsorbed on the surface, the RMSD increases.
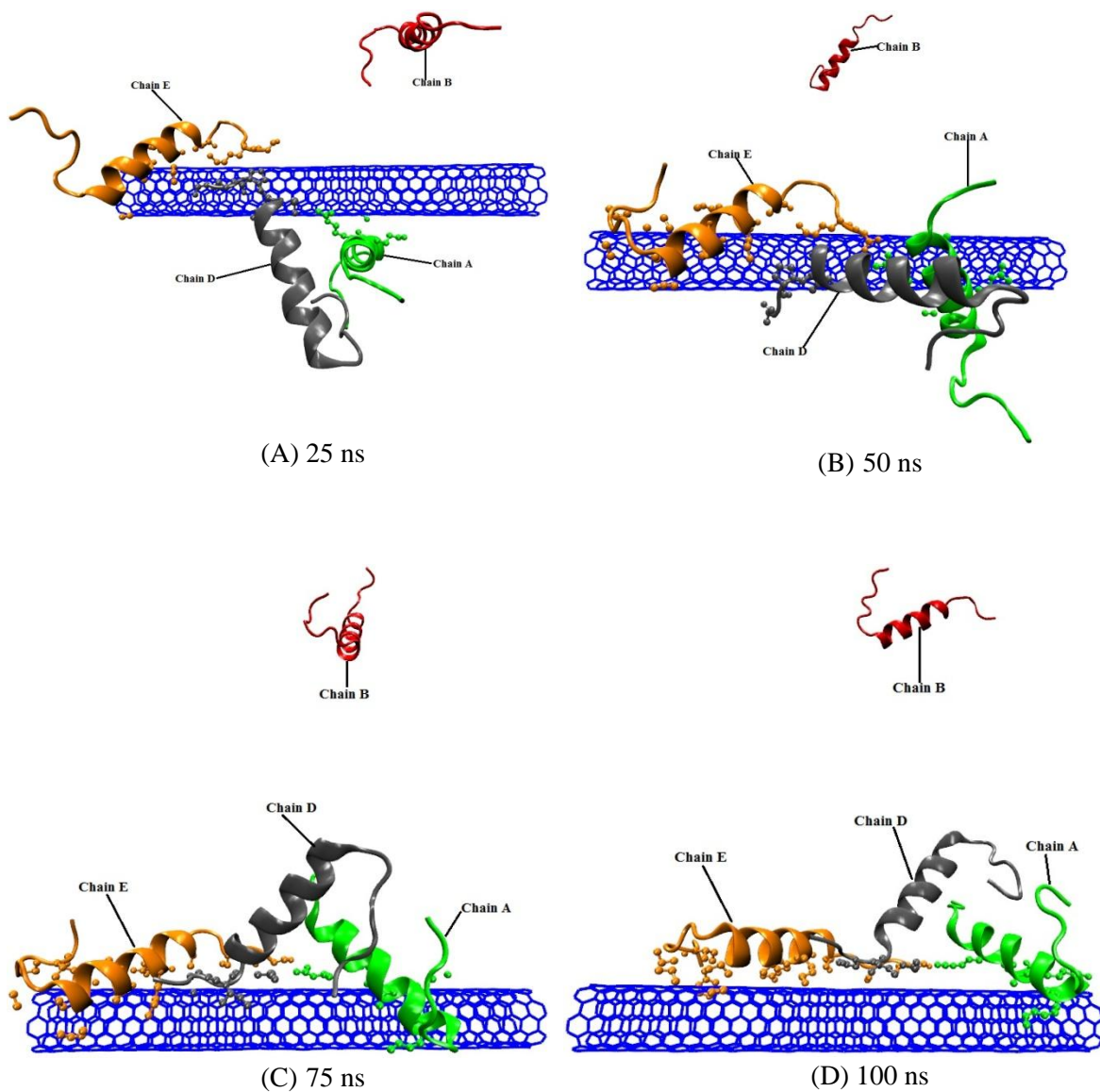
Figure 7.12: Time line of the SP-B residues adsorbed on the surface of a 7 nm carbon nanotube over 100 ns. (A) Top left at 25 ns, (B) top right at 50 ns, (C) bottom left at 75 ns, and (D) bottom right at 100ns. Carbon nanotube is represented in a horizontal line, the protein structure is represented in color spirals, and the adsorbed residues SP-B are represented in CPK

Figure 7.13 shows the adsorbed residues of SP-B on the surface of the 7 nm carbon nanotube. It shows that residues of chain A, chain D, and chain E are adsorbed on the surface. A molecule is considered adsorbed if any of its residue comes within 5 Å of the surface.
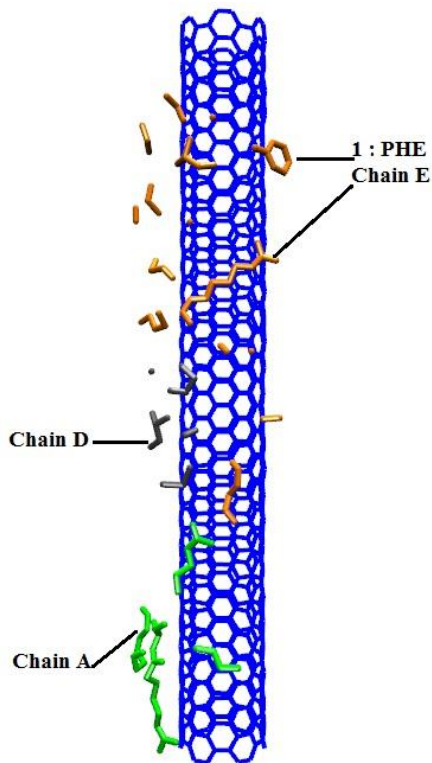
Figure 7.13: Residues adsorbed on the surface of the 7 nm carbon nanotube after 100 ns. The carbon nanotube is represented by the vertical line, and adsorbed residues of chain A and chain B of SP-B are shown by a "licorice" representation

7.2.3   Four SP-B molecules with the 10 nm carbon nanotube

Figure 7.14 shows the distance between four SP-B protein molecules and the surface of the carbon nanotube. Initially, all four molecules are at the same distance from surface. The distance between protein molecules to the surface of carbon nanotube is kept more than 1.2 nm, which makes sure that there are enough water layers between protein and the carbon nanotube to insure an un-biased result. The length of an SP-B molecule is about 30 Å, a carbon nanotube is about 10 nm, and the chiral is (6, 6); this should provide enough area for adsorption of four protein molecules. Chain E moves swiftly toward the surface of the carbon nanotube and maintains this a constant

distance for the remaining time of the simulation. After approximately 60 ns, the centers of chains A, D, and E are at same distance from the surface of the carbon nanotube.
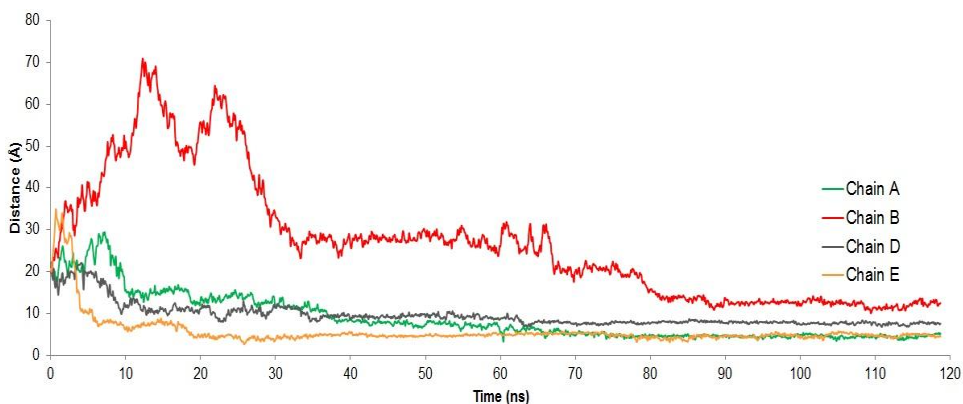
Figure 7.14: The distance between the centers of protein molecules to the 10 nm carbon nanotube over 120 ns.

In the beginning chain B moves away from the surface of the carbon nanotube, and after changing its conformation many time finds a suitable spot near chain D and the carbon nanotube's surface.

Figure 7.15 shows the total number of protein heavy atoms for all four protein molecules combined, coming to within 5 Å of the carbon nanotube surface. Atoms which are coming within 5 Å of the carbon nanotube are considered as adsorbed on the surface of the carbon nanotube. Since the 10 nm carbon nanotube provides more area for adsorption, more protein atoms are adsorbed as compare to the 5 nm and 7 nm carbon nanotubes.

111
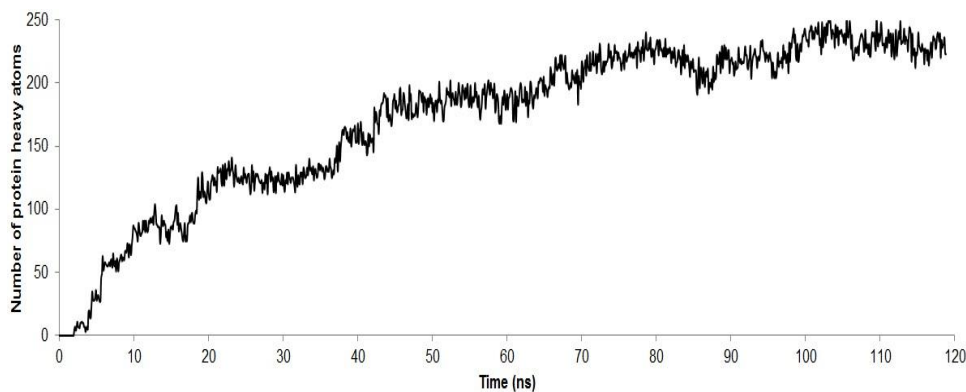
Figure 7.15: The number of heavy atoms within 5 A of the 10 nm carbon nanotube over a time of 120 ns. Hydrogen atoms are not counted
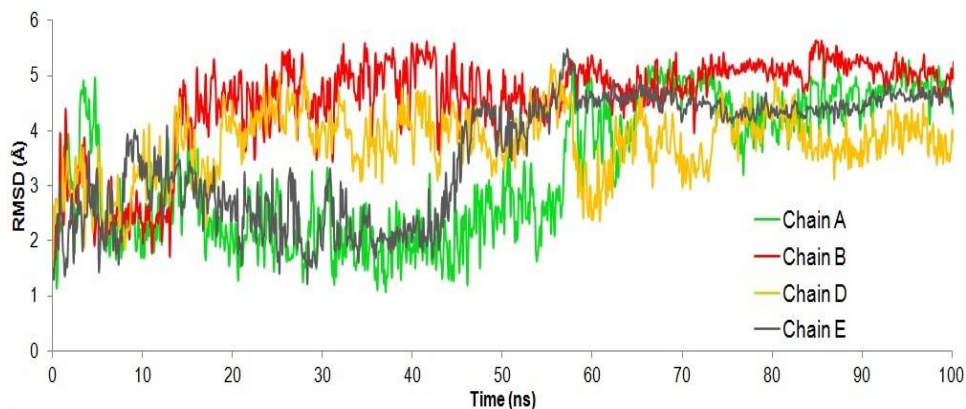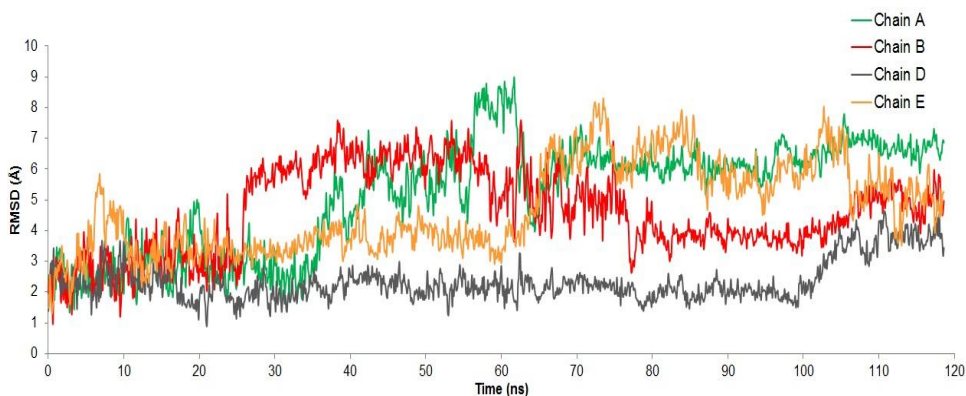

Figure 7.16: Root mean square deviation of all 4 SP-B molecules during their interaction with the 10 nm carbon nanotube for 120 ns

Figure 7.17 shows the time line pictorial for the four molecules of SP-B protein with a carbon nanotube for 100 ns. After 25 ns, chain A, chain D, and chain E are partially adsorbed on the 10 nm carbon nanotube surface. During this time aromatic hexagonal rings of chain A residues make contact with the carbon nanotube surface resulting in π-π interactions, and chain A stays in contact with the carbon nanotube until the end of the simulation. Chain B initially moves away from the surface of the carbon

112

nanotube and other SP-B molecules, but after finding a suitable conformation, chain B moves closer to chain D.
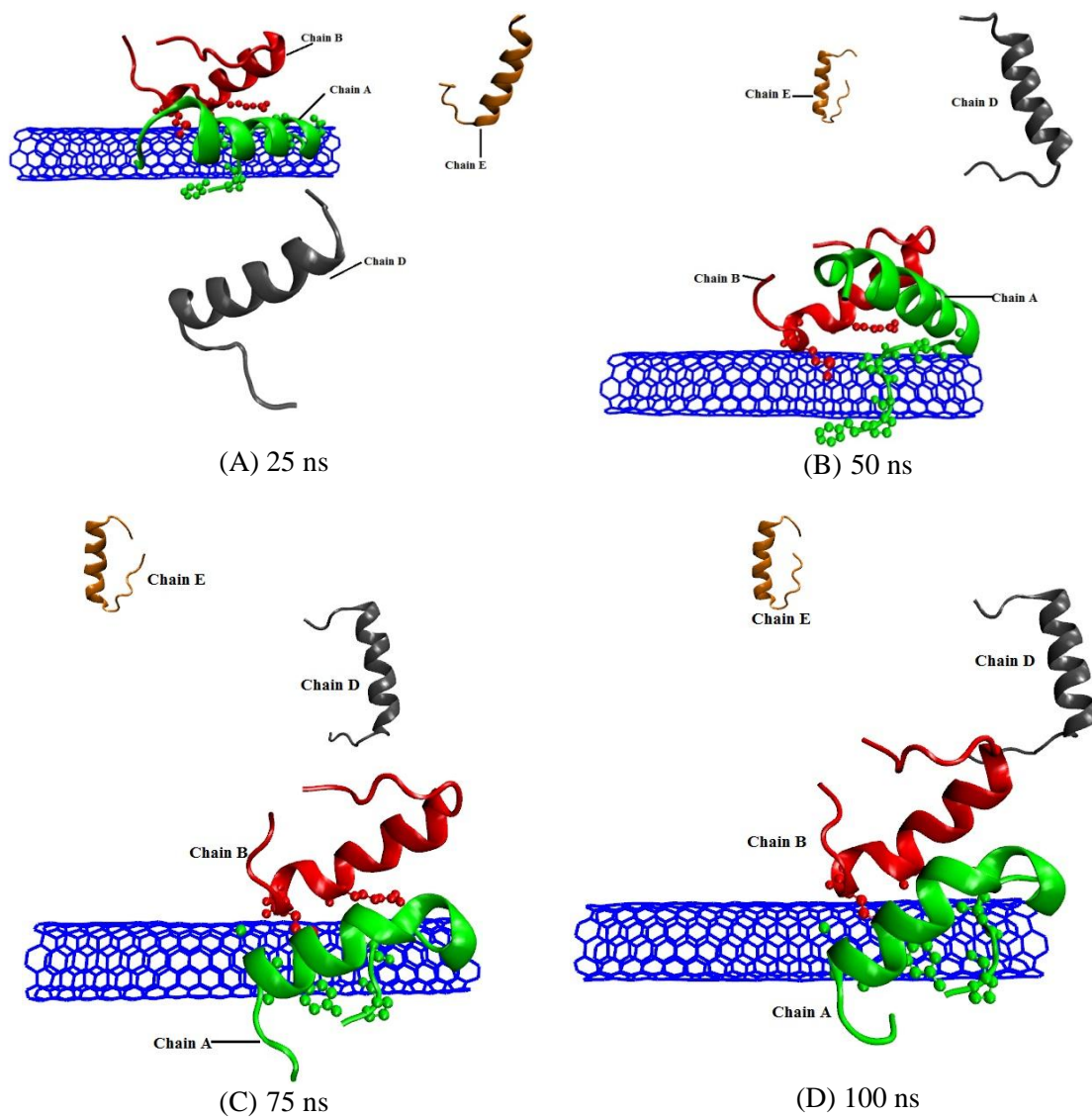

(A) 25 ns

(B) 50 ns

(C) 75 ns
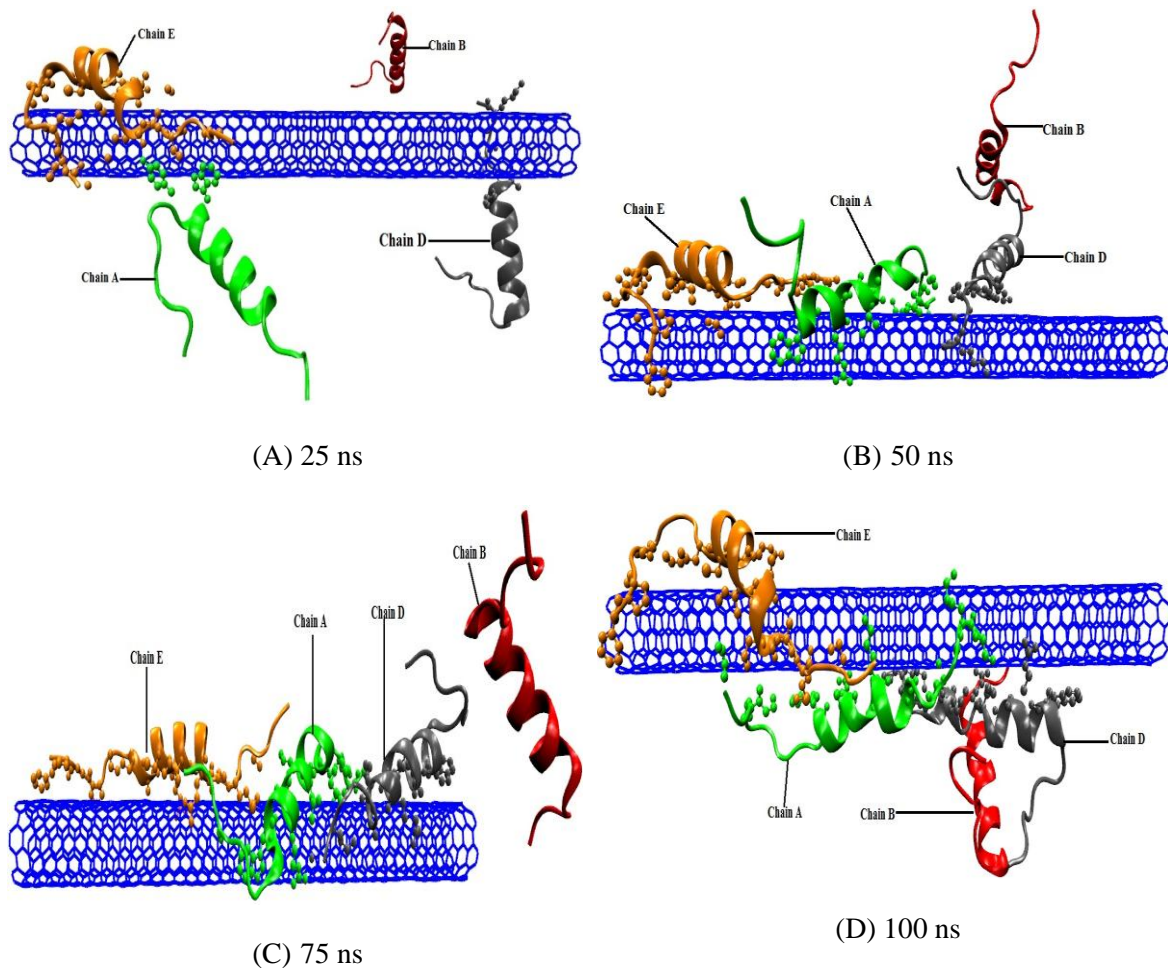
(D) 100 ns

Figure 7.17: Time line of SP-B residues adsorbed on the surface of the,10 nm carbon nanotube for 100 ns. (A) Top left at 25 ns, (B) top right at 50 ns, (C) bottom left at 75 ns, and (D) bottom right at 100ns. The carbon nanotube is represented as horizontal, the protein structure is represented in color spirals, and the adsorbed residues SP-B are represented in CPK

For four SP-B molecules interacting with a 10 nm carbon nanotube, the adsorption of protein is not only governed by the protein and the carbon nanotube interaction but also by protein – protein interactions. This is especially true in the case of chain B and chain D; chain B interacts very little with a carbon nanotube surface and

113

shows a stronger interaction with chain D of SP-B. By increasing the length of the carbon

nanotube, more stable adsorption of pulmonary surfactant protein SP-B can be achieved.
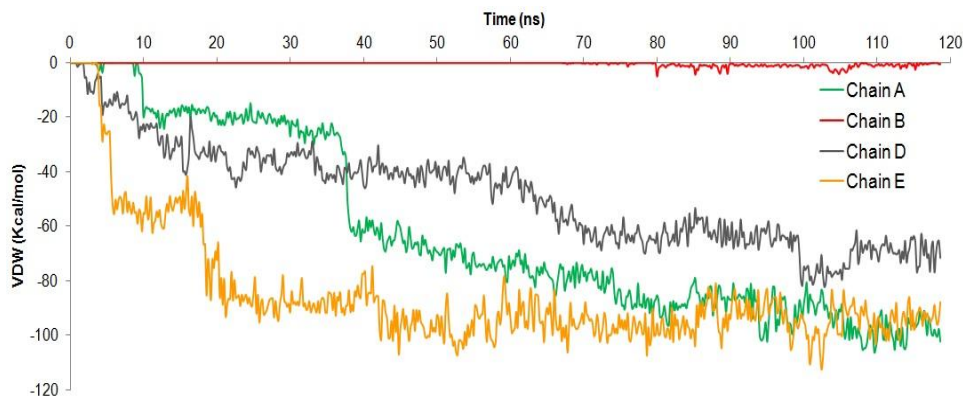
Figure 7.18: Van der Waals energy between four pulmonary surfactant protein SP-B molecules
and the 10 nm carbon nanotube

Interaction energy between the four SP-B molecules and the 10 nm carbon

nanotube is in the form of van der Waals (VDW) energy. In Figure 7.18, all values of

VDW for the four molecules are negative, and this is an indication of the attractive nature

of VDW forces between proteins and carbon nanotubes. Chain B shows a minimum

VDW, and this is because it interacts with chain D at about 80ns, as chain B makes

contact with the surface of the carbon nanotube. As the number of protein heavy atoms

within 5 Å of the surface of a carbon nanotube increases, the VDW forces also increase,

and this is a key feature to non-covalent adsorption of protein on a carbon nanotube

surface.

As the length of the carbon nanotube increases, the adsorption rate of protein also

increases. For the 5 nm carbon nanotube, two protein molecules of SP-B are adsorbed,

and in case of the 7 nm carbon nanotube 3 SP-B molecules are adsorbed. The protein

114

molecules that are not adsorbed move away from the carbon nanotube because of less of the hydrophobic area of the carbon nanotube is available, and repulsive forces between the SP-B protein molecules are high. In the case of the 10 nm carbon nanotube, all protein molecules show some level of adsorption. Chain D shows a maximum interaction force with the carbon nanotube as it occupies the maximum area on the carbon nanotube, which also interacts with chain A. chain A shows the second highest interacting force. As it interacts with the surface of the carbon nanotube, chain A also interacts with chains D and E. At first, chain B moves away from the surface of the carbon nanotube, but later, while moving closer to the surface of the carbon nanotube, chain B shows a stronger interaction with chain D, as a few residues of chain B are adsorbed on the carbon nanotube surface. In the case of a 10 nm carbon nanotube, adsorption of the protein on the surface is influenced by protein-protein and protein-carbon-nanotube interactions.

CONCLUSION

Preliminary results show that all four human pulmonary surfactant proteins SP-A, SP-B, SP-C, and SP-D adsorbed on the surface of a carbon nanotube. Root mean square deviation and Van der Waals energy graphs indicate that all four pulmonary surfactant protein molecules achieve equilibrium positions after 40 ns. Hydrophilic and hydrophobic residues of all four proteins play equal roles in adsorption dynamics on the surface of a carbon nanotube, even though the carbon nanotube surface is hydrophobic in nature. Since the carbon nanotube surface is neutral, the protein adsorption process is the result of a non-bonding Van der Waals interaction (attraction). Pulmonary surfactant proteins SP-A and SP-D are big molecules with multiple α helixes and β sheets, and they lose their secondary structure in the process of adsorption. SP-B and SP-C are the small molecules with one α helix. They are hydrophobic and are adsorbed on the surface of the carbon nanotube more quickly. After finding absorbed residues of SP-A, SP-B, and SP-C on the carbon nanotube surface, we observed the alignment of aromatic rings of protein residues with the carbon nanotube, and this suggests $\pi - \pi$ stacking. After 70 ns the number of atoms within 5 Å of the nanotube surface remains almost constant. This suggests that the adsorption process is complete, and protein has found its optimal position on the surface of the carbon nanotube.

Pulmonary surfactant protein SP-B plays an important role in homeostasis in the pulmonary system. Its deficiency leads to IRDS or even death of a newborn.

Carbon nanotube based sensors use electrical signals for detection of protein. Different proteins carry different charges on their surface. Some are polar; some are non-polar. Molecular dynamics computation of different charge configurations on carbon nanotube gives more insight as to which system is more suitable for pulmonary surfactant protein SP-B. From these results, adsorption of pulmonary surfactant protein SP-B is more often observed for a neutral and negatively charged carbon nanotube. Positively charged carbon nanotubes show very little interaction with SP-B, as the protein moves away from the nanotube's surface. Negatively charged carbon nanotubes show a greater variation in protein structure, and this generates a stronger signal of RMSD for the SP-B protein molecule. To develop carbon nanotube based biosensors for the pulmonary surfactant protein SP-B, one should use neutral or negative charged carbon nanotube surfaces.

To observe the movement and alignment of a carbon nanotube in a protein matrix gel, electrophoresis of a carbon nanotube in a PVA-borax gel was performed. A PVA-borax gel is considered analogous to a protein matrix, and carbon nanotubes were suspended in a surfactant of sodium dodecyl sulfate (SDS). An electrochemical study on the PVA and carbon nanotube/PVA shows the alignment of the carbon nanotubes in the polymer. The carbon nanotube/PVA composite films demonstrate sharply defined peaks, which indicate higher electro-activity over the PVA. It was shown earlier that the electro-chemical activities of poly-vinyl alcohol films coincide with the degree of protonation; hence, a promotion in the protonation with a doping effect of MWNTs on poly-vinyl

alcohol may be expected. An explanation for this is based on the fact that the electrophoretic alignment of carbon nanotubes plus the large π-bond on the surface of a carbon nanotube can interact strongly with the conjugated structure of poly-vinyl alcohol via π-stacking, with the result that the resulting highly conjugated π-system would promote a high degree of electron delocalization. Aligned carbon nanotube/PVA solid composites were fabricated. The electrical properties of the carbon nanotubes and the surrounding medium and the characteristics of the applied electric field play important roles in the carbon nanotube's response.

Molecular dynamics computation for the multiple molecules of SP-B surrounding the carbon nanotube were performed with different positions and different lengths of the carbon nanotube. Results show that number of protein molecules adsorbed on the surface of a carbon nanotube depends on the length of the carbon nanotube. In all, lengths of 5 nm, 7 nm and 10 nm, were studied, with the adsorption rate of protein increasing for an increase in the length of the carbon nanotube.

The carbon nanotube provides a new generation of nano-bio-sensors with fast and specific adsorption rates. Computational studies of the interaction between nano-bio-interfaces are useful in developing nano-electrochemical biosensors in the future, for identifying and quantifying pulmonary surfactant proteins.

REFERENCES

[1]   S. R. Walker, M. C. Williams, and B. Benson, "Immunocytochemical localization of the major surfactant apoproteins in type II cells, Clara cells, and alveolar macrophages of rat lung," *J Histochem Cytochem,* vol. 34, pp. 1137-48, Sep 1986.

[2]   M. E. Avery, "Surfactant Deficiency in Hyaline Membrane Disease," *American Journal of Respiratory and Critical Care Medicine,* vol. 161, pp. 1074-1075, 2000/04/01 2000.

[3]   W. H. Northway, Jr., R. C. Rosan, and D. Y. Porter, "Pulmonary disease following respirator therapy of hyaline-membrane disease. Bronchopulmonary dysplasia," *N Engl J Med,* vol. 276, pp. 357-68, Feb 16 1967.

[4]   K. Von Neergaard, "New opinions about the fundamentals of respiratory mechanics. The retraction force of the lung in relationship to the surface tension within the alveoles," *Z ges exp Med,* vol. 66, pp. 373-394, 1929.

[5]   K. Von Neergaard, "New notions on a fundamental principle of respiratory mechanics: the retractile force of the lung, dependent on the surface tension in the alveoli," *Z. Gesamte Exp. Med,* vol. 66, pp. 373-394, 1929.

[6]   K. Von Neergaard and K. Wirz, "Die Messung der Strömungswiderstände in den Atemwegen des Menschen, insbesondere bei Asthma und Emphysem," *Z Klin Med,* vol. 105, 1927.

[7]   M. Avery and J. Mead, "Surface properties in relation to atelectasis and hyaline membrane disease," *A.M.A. Journal of Diseases of Children,* vol. 97, pp. 517-523, 1959.

[8]   R. E. Pattle, "Properties, Function and Origin of the Alveolar Lining Layer," *Nature,* vol. 175, p. 2, 1955.

[9]   J. A. Clements, "Surface tension of lung extracts," *Proc Soc Exp Biol Med,* vol. 95, pp. 170-2, May 1957.

[10]   M. Amrein, A. von Nahmen, and M. Sieber, "A scanning force- and fluorescence light microscopy study of the structure and function of a model pulmonary surfactant," *Eur Biophys J,* vol. 26, pp. 349-57, 1997.

[11]   D. Moses, B. A. Holm, P. Spitale, M. Y. Liu, and G. Enhorning, "Inhibition of pulmonary surfactant function by meconium," *Am J Obstet Gynecol,* vol. 164, pp. 477-81, Feb 1991.

[12]   R. Veldhuizen, K. Nag, S. Orgeig, and F. Possmayer, "The role of lipids in pulmonary surfactant," *Biochim Biophys Acta,* vol. 1408, pp. 90-108, Nov 19 1998.

[13]   B. A. Holm, Z. Wang, E. A. Egan, and R. H. Notter, "Content of dipalmitoyl phosphatidylcholine in lung surfactant: ramifications for surface activity," *Pediatr Res,* vol. 39, pp. 805-11, May 1996.

[14]   J. Goerke, "Pulmonary surfactant: functions and molecular composition," *Biochimica et Biophysica Acta (BBA) - Molecular Basis of Disease,* vol. 1408, pp. 79-89, 11/19/ 1998.

[15]   J. Pérez-Gil, "Structure of pulmonary surfactant membranes and films: The role of proteins and lipid–protein interactions," *Biochimica et Biophysica Acta (BBA) - Biomembranes,* vol. 1778, pp. 1676-1695, 7// 2008.

[16]   B. A. Hills, *An alternative view of the role(s) of surfactant and the alveolar model* vol. 87, 1999.

[17]   E. C. Crouch, "Collectins and pulmonary host defense," *Am J Respir Cell Mol Biol,* vol. 19, pp. 177-201, Aug 1998.

[18]   T. E. Weaver and J. A. Whitsett, "Function and regulation of expression of pulmonary surfactant-associated proteins," *Biochem J,* vol. 273(Pt 2), pp. 249-64, Jan 15 1991.

[19]   B. Robertson and H. L. Halliday, "Principles of surfactant replacement," *Biochimica et Biophysica Acta (BBA) - Molecular Basis of Disease,* vol. 1408, pp. 346-361, 11/19/ 1998.

[20]   F. X. McCormack, "Structure, processing and properties of surfactant protein A," *Biochimica et Biophysica Acta (BBA) - Molecular Basis of Disease,* vol. 1408, pp. 109-131, 11/19/ 1998.

[21]   R. T. White, D. Damm, J. Miller, K. Spratt, J. Schilling, S. Hawgood*, et al.*, "Isolation and characterization of the human pulmonary surfactant apoprotein gene," *Nature,* vol. 317, pp. 361-363, 09/26/print 1985.

[22]   T. R. Korfhagen, M. D. Bruno, G. F. Ross, K. M. Huelsman, M. Ikegami, A. H. Jobe*, et al.*, "Altered surfactant function and structure in SP-A gene targeted mice," *Proceedings of the National Academy of Sciences,* vol. 93, pp. 9594-9599, September 3, 1996 1996.

[23] S. Hawgood, M. Derrick, and F. Poulain, "Structure and properties of surfactant protein B," *Biochimica et Biophysica Acta (BBA) - Molecular Basis of Disease,* vol. 1408, pp. 150-160, 11/19/ 1998.

[24] J. C. Clark, S. E. Wert, C. J. Bachurski, M. T. Stahlman, B. R. Stripp, T. E. Weaver*, et al.*, "Targeted disruption of the surfactant protein B gene disrupts surfactant homeostasis, causing respiratory failure in newborn mice," *Proc Natl Acad Sci U S A,* vol. 92, pp. 7794-8, Aug 15 1995.

[25] X. Yin, Y. Wang, L. Xie, X. Kong, C. Wang, W. Qu*, et al.*, "Expression of Pulmonary Surfactant-Associated Protein B in Neonatal Respiratory Distress Syndrome," *Journal of Medical Biochemistry,* vol. 32, pp. 146-151, 2013.

[26] A. Hamvas, L. M. Nogee, G. B. Mallory, Jr., T. L. Spray, C. B. Huddleston, A. August*, et al.*, "Lung transplantation for treatment of infants with surfactant protein B deficiency," *J Pediatr,* vol. 130, pp. 231-9, Feb 1997.

[27] L. M. Nogee, S. E. Wert, S. A. Proffit, W. M. Hull, and J. A. Whitsett, "Allelic Heterogeneity in Hereditary Surfactant Protein B (SP-B) Deficiency," *American Journal of Respiratory and Critical Care Medicine,* vol. 161, pp. 973-981, 2000/03/01 2000.

[28] P. A. Chetcuti and R. J. Ball, "Surfactant apoprotein B deficiency," *Arch Dis Child Fetal Neonatal Ed,* vol. 73, pp. F125-7, Nov 1995.

[29] R. J. King and J. A. Clements, "Surface active materials from dog lung. II. Composition and physiological correlations," *The American journal of physiology,* vol. 223, pp. 715-726, 1972.

[30]   J. Johansson, "Structure and properties of surfactant protein C," *Biochimica et Biophysica Acta (BBA) - Molecular Basis of Disease,* vol. 1408, pp. 161-172, 11/19/ 1998.

[31]   P. Elisa, H. M. Lara , L. M. Ivan, C. Antonio, M. Francisco, and P.-G. Jesus, "A combined action of pulmonary surfactant proteins SP-B and SP-C modulates permeability and dynamics of phospholipid membranes," *Biochemical Journal,* vol. 438, pp. 555-564, 2011.

[32]   J. Johansson, T. Szyperski, T. Curstedt, and K. Wuthrich, "The NMR structure of the pulmonary surfactant-associated polypeptide SP-C in an apolar solvent contains a valyl-rich α-helix," *Biochemistry®,* vol. 33, pp. 6015-6023, 1994.

[33]   A. Clercx, G. Vandenbussche, T. Curstedt, J. Johansson, H. Jornvall, and J. M. Ruysschaert, "Structural and functional importance of the C-terminal part of the pulmonary surfactant polypeptide SP-C," *European Journal of Biochemistry,* vol. 229, pp. 465-472, 1995.

[34]   S. W. Glasser, M. S. Burhans, T. R. Korfhagen, C. L. Na, P. D. Sly, G. F. Ross*, et al.*, "Altered stability of pulmonary surfactant in SP-C-deficient mice," *Proc Natl Acad Sci U S A,* vol. 98, pp. 6366-71, May 22 2001.

[35]   W. E. Lawson, V. V. Polosukhin, G. T. Stathopoulos, O. Zoia, W. Han, K. B. Lane*, et al.*, "Increased and prolonged pulmonary fibrosis in surfactant protein C-deficient mice following intratracheal bleomycin," *Am J Pathol,* vol. 167, pp. 1267-77, Nov 2005.

[36]   S. W. Glasser, A. P. Senft, M. D. Maxfield, T. L. Ruetschilling, J. E. Baatz, K. Page*, et al.*, "Genetic replacement of surfactant protein-C reduces respiratory syncytial virus induced lung injury," *Respir Res,* vol. 14, p. 19, 2013.

[37]   H. Sano and Y. Kuroki, "The lung collectins, SP-A and SP-D, modulate pulmonary innate immunity," *Molecular Immunology,* vol. 42, pp. 279-287, 2// 2005.

[38]   E. C. Crouch, "Structure, biologic properties, and expression of surfactant protein D (SP-D)," *Biochimica et Biophysica Acta (BBA) - Molecular Basis of Disease,* vol. 1408, pp. 278-289, 11/19/ 1998.

[39]   C. Botas, F. Poulain, J. Akiyama, C. Brown, L. Allen, J. Goerke*, et al.*, "Altered surfactant homeostasis and alveolar type II cell morphology in mice lacking surfactant protein D," *Proceedings of the National Academy of Sciences,* vol. 95, pp. 11869-11874, September 29, 1998 1998.

[40]   T. R. Korfhagen, V. Sheftelyevich, M. S. Burhans, M. D. Bruno, G. F. Ross, S. E. Wert*, et al.*, "Surfactant protein-D regulates surfactant phospholipid homeostasis in vivo," *J Biol Chem,* vol. 273, pp. 28438-43, Oct 23 1998.

[41]   T. Fukuzawa, J. Ishida, A. Kato, T. Ichinose, D. M. Ariestanti, T. Takahashi*, et al.*, "Lung Surfactant Levels are Regulated by Ig-Hepta/GPR116 by Monitoring Surfactant Protein D," *PLoS ONE,* vol. 8, pp. 1-12, 2013.

[42]   S. Iijima, "Helical microtubules of graphitic carbon," *Nature,* vol. 354, pp. 56-58, 11/07/print 1991.

[43]   Y. Zhang, Y. Bai, and B. Yan, "Functionalized carbon nanotubes for potential medicinal applications," *Drug Discovery Today,* vol. 15, pp. 428-435, 2010.

[44]   L. R. Inc, "The Nanotech Report - Investment Overview and Market Research for Nanotechnology," vol. 4th Edn, 2006.

[45]   D. W. H. Fam, A. Palaniappan, A. I. Y. Tok, B. Liedberg, and S. M. Moochhala, "A review on technological aspects influencing commercialization of carbon nanotube sensors," *Sensors and Actuators B: Chemical,* vol. 157, pp. 1-7, 9/20/ 2011.

[46]   M. F. L. De Volder, S. H. Tawfick, R. H. Baughman, and A. J. Hart, "Carbon Nanotubes: Present and Future Commercial Applications," *Science,* vol. 339, pp. 535-539, February 1, 2013 2013.

[47]   B. Yakobson and P. Avouris, "Mechanical Properties of Carbon Nanotubes," in *Carbon Nanotubes*. vol. 80, M. Dresselhaus, G. Dresselhaus, and P. Avouris, Eds., ed: Springer Berlin Heidelberg, 2001, pp. 287-327.

[48]   T. Dürkop, S. A. Getty, E. Cobas, and M. S. Fuhrer, "Extraordinary Mobility in Semiconducting Carbon Nanotubes," *Nano Letters,* vol. 4, pp. 35-39, 2004/01/01 2003.

[49]   J. Hone, M. Whitney, C. Piskoti, and A. Zettl, "Thermal conductivity of single-walled carbon nanotubes," *Physical Review B,* vol. 59, pp. R2514-R2516, 01/15/ 1999.

[50]   P. M. Ajayan, "Nanotubes from Carbon," *Chemical Reviews,* vol. 99, pp. 1787-1800, 1999/07/01 1999.

[51]   P. J. Britto, K. S. V. Santhanam, A. Rubio, J. A. Alonso, and P. M. Ajayan, "Improved Charge Transfer at Carbon Nanotube Electrodes," *Advanced Materials,* vol. 11, pp. 154-157, 1999.

[52]   U. Yogeswaran and S.-M. Chen, "A Review on the Electrochemical Sensors and Biosensors Composed of Nanowires as Sensing Material," *Sensors,* vol. 8, pp. 290-313, 2008.

[53]   X. W. Sun, J. X. Wang, and A. Wei, "Zinc oxide nanostructured biosensor for glucose detection," *Journal of Materials Science and Technology,* vol. 24, pp. 649-656, 2008.

[54]   Z.-G. Zhao, C.-Y. Niu, Y.-P. Zhang, R. Han, Y.-L. Hou, B.-l. Li*, et al.*, "The mechanism of myocardium and pancreas injury in rabbits with acute renal failure might be related to myeloperoxidase and membrane pump activities," *Renal Failure,* vol. 32, pp. 1216-1222, 2010.

[55]   W. Jue, P. Jian, and Z. Daping, "Research on Dynamic Reputation Management Model Based on PageRank," in *Computer Science and Software Engineering, 2008 International Conference on*, 2008, pp. 814-817.

[56]   S. Vaddiraju, D. J. Burgess, I. Tomazos, F. C. Jain, and F. Papadimitrakopoulos, "Technologies for continuous glucose monitoring: current problems and future promises," *J Diabetes Sci Technol,* vol. 4, pp. 1540-62, Nov 2010.

[57]   K. P. Loh, S. Liang Zhao, and W. De Zhang, "Diamond and carbon nanotube glucose sensors based on electropolymerization," *Diamond and Related Materials,* vol. 13, pp. 1075-1079, 4// 2004.

[58]   A. Bhattacharya, V. P. Rao, C. Jain, A. Ghose, and S. Banerjee, "Bio-sensing property of gold coated ZnO nanorods," *Materials Letters,* vol. 117, pp. 128-130, 2/15/ 2014.

[59] W. Xue and T. Cui, "A thin-film transistor based acetylcholine sensor using self-assembled carbon nanotubes and SiO2 nanoparticles," *Sensors and Actuators B: Chemical,* vol. 134, pp. 981-987, 9/25/ 2008.

[60] U. Yogeswaran, S. Thiagarajan, and S.-M. Chen, "Nanocomposite of functionalized multiwall carbon nanotubes with nafion, nano platinum, and nano gold biosensing film for simultaneous determination of ascorbic acid, epinephrine, and uric acid," *Analytical Biochemistry,* vol. 365, pp. 122-131, 6/1/ 2007.

[61] S. Dong, S. Zhang, L. Chi, P. He, Q. Wang, and Y. Fang, "Electrochemical behaviors of amino acids at multiwall carbon nanotubes and Cu2O modified carbon paste electrode," *Analytical Biochemistry,* vol. 381, pp. 199-204, 10/15/ 2008.

[62] J. Wang, T. Tangkuaram, S. Loyprasert, T. Vazquez-Alvarez, W. Veerasai, P. Kanatharana*, et al.*, "Electrocatalytic detection of insulin at RuOx/carbon nanotube-modified carbon electrodes," *Analytica Chimica Acta,* vol. 581, pp. 1-6, 1/2/ 2007.

[63] V. Serafín, L. Agüí, P. Yáñez-Sedeño, and J. M. Pingarrón, "Electrochemical immunosensor for the determination of insulin-like growth factor-1 using electrodes modified with carbon nanotubes–poly(pyrrole propionic acid) hybrids," *Biosensors and Bioelectronics,* vol. 52, pp. 98-104, 2/15/ 2014.

[64] M. Zheng, A. Jagota, M. S. Strano, A. P. Santos, P. Barone, S. G. Chou*, et al.*, "Structure-Based Carbon Nanotube Sorting by Sequence-Dependent DNA Assembly," *Science,* vol. 302, pp. 1545-1548, November 28, 2003 2003.

[65]   K. Keren, R. S. Berman, E. Buchstab, U. Sivan, and E. Braun, "DNA-Templated Carbon Nanotube Field-Effect Transistor," *Science,* vol. 302, pp. 1380-1382, November 21, 2003 2003.

[66]   X. Tang, S. Bansaruntip, N. Nakayama, E. Yenilmez, Y.-l. Chang, and Q. Wang, "Carbon Nanotube DNA Sensor and Sensing Mechanism," *Nano Letters,* vol. 6, pp. 1632-1636, 2006/08/01 2006.

[67]   M. Tominaga, S. Nomura, and I. Taniguchi, "d-Fructose detection based on the direct heterogeneous electron transfer reaction of fructose dehydrogenase adsorbed onto multi-walled carbon nanotubes synthesized on platinum electrode," *Biosensors and Bioelectronics,* vol. 24, pp. 1184-1188, 1/1/ 2009.

[68]   P. D. Tam, N. Van Hieu, N. D. Chien, A.-T. Le, and M. Anh Tuan, "DNA sensor development based on multi-wall carbon nanotubes for label-free influenza virus (type A) detection," *Journal of Immunological Methods,* vol. 350, pp. 118-124, 10/31/ 2009.

[69]   T. Dastagir, E. S. Forzani, R. Zhang, I. Amlani, L. A. Nagahara, R. Tsui*, et al.*, "Electrical detection of hepatitis C virus RNA on single wall carbon nanotube-field effect transistors," *Analyst,* vol. 132, pp. 738-740, 2007.

[70]   H. Karadeniz, A. Erdem, and A. Caliskan, "Electrochemical Monitoring of DNA Hybridization by Multiwalled Carbon Nanotube Based Screen Printed Electrodes," *Electroanalysis,* vol. 20, pp. 1932-1938, 2008.

[71]   Q. Shen and X. Wang, "Simultaneous determination of adenine, guanine and thymine based on β-cyclodextrin/MWNTs modified electrode," *Journal of Electroanalytical Chemistry,* vol. 632, pp. 149-153, 7/1/ 2009.

[72]   A. I. Gopalan, K.-P. Lee, and D. Ragupathy, "Development of a stable cholesterol biosensor based on multi-walled carbon nanotubes–gold nanoparticles composite covered with a layer of chitosan–room-temperature ionic liquid network," *Biosensors and Bioelectronics,* vol. 24, pp. 2211-2217, 3/15/ 2009.

[73]   K. A. Mahmoud, S. Hrapovic, and J. H. T. Luong, "Picomolar Detection of Protease Using Peptide/Single Walled Carbon Nanotube/Gold Nanoparticle-Modified Electrode," *ACS Nano,* vol. 2, pp. 1051-1057, 2008/05/01 2008.

[74]   J.-W. Shen, T. Wu, Q. Wang, and Y. Kang, "Induced stepwise conformational change of human serum albumin on carbon nanotube surfaces," *Biomaterials,* vol. 29, pp. 3847-3855, 10// 2008.

[75]   J. A. McCammon, B. R. Gelin, and M. Karplus, "Dynamics of folded proteins," *Nature,* vol. 267, pp. 585-90, Jun 16 1977.

[76]   A. T. Brunger, C. L. Brooks, 3rd, and M. Karplus, "Active site dynamics of ribonuclease," *Proc Natl Acad Sci U S A,* vol. 82, pp. 8458-62, Dec 1985.

[77]   H. Frauenfelder, H. Hartmann, M. Karplus, I. D. Kuntz, Jr., J. Kuriyan, F. Parak*, et al.*, "Thermal expansion of a protein," *Biochemistry,* vol. 26, pp. 254-61, Jan 13 1987.

[78]   B. Brooks and M. Karplus, "Harmonic dynamics of proteins: normal modes and fluctuations in bovine pancreatic trypsin inhibitor," *Proceedings of the National Academy of Sciences,* vol. 80, pp. 6571-6575, November 1, 1983 1983.

[79]   B. R. Brooks, R. E. Bruccoleri, B. D. Olafson, D. J. States, S. Swaminathan, and M. Karplus, "CHARMM: A program for macromolecular energy, minimization,

and dynamics calculations," *Journal of Computational Chemistry,* vol. 4, pp. 187-217, 1983.

[80]   P. K. Weiner and P. A. Kollman, "AMBER: Assisted model building with energy refinement. A general program for modeling molecules and their interactions," *Journal of Computational Chemistry,* vol. 2, pp. 287-303, 1981.

[81]   W. R. P. Scott, P. H. Hünenberger, I. G. Tironi, A. E. Mark, S. R. Billeter, J. Fennen*, et al.*, "The GROMOS Biomolecular Simulation Program Package," *The Journal of Physical Chemistry A,* vol. 103, pp. 3596-3607, 1999/05/01 1999.

[82]   M. Karplus and J. A. McCammon, "Molecular dynamics simulations of biomolecules," *Nat Struct Mol Biol,* vol. 9, pp. 646-652, 09//print 2002.

[83]   J. C. Phillips, R. Braun, W. Wang, J. Gumbart, E. Tajkhorshid, E. Villa*, et al.*, "Scalable molecular dynamics with NAMD," *Journal of Computational Chemistry,* vol. 26, pp. 1781-1802, 2005.

[84]   W. Humphrey, A. Dalke, and K. Schulten, "VMD: visual molecular dynamics," *J Mol Graph,* vol. 14, pp. 33-8, 27-8, Feb 1996.

[85]   J. F. Head, T. R. Mealy, F. X. McCormack, and B. A. Seaton, "Crystal Structure of Trimeric Carbohydrate Recognition and Neck Domains of Surfactant Protein A," *Journal of Biological Chemistry,* vol. 278, pp. 43254-43260, October 31, 2003 2003.

[86]   L. M. Gordon, K. Y. Lee, M. M. Lipp, J. A. Zasadzinski, F. J. Walther, M. A. Sherman*, et al.*, "Conformational mapping of the N-terminal segment of surfactant protein B in lipid using 13C-enhanced Fourier transform infrared spectroscopy," *J Pept Res,* vol. 55, pp. 330-47, Apr 2000.

[87]   J. Johansson, T. Szyperski, T. Curstedt, and K. Wuethrich, "The NMR Structure of the Pulmonary Surfactant-Associated Polypeptide SP-C in an Apolar Solvent Contains a Valyl-Rich .alpha.-Helix," *Biochemistry,* vol. 33, pp. 6015-6023, 1994/05/01 1994.

[88]   K. Håkansson, N. K. Lim, H.-J. Hoppe, and K. B. M. Reid, "Crystal structure of the trimeric α-helical coiled-coil and the three lectin domains of human lung surfactant protein D," *Structure,* vol. 7, pp. 255-264, 3/15/ 1999.

[89]   F. J. Walther, L. M. Gordon, J. A. Zasadzinski, M. A. Sherman, and A. J. Waring, "Surfactant protein B and C analogues," *Mol Genet Metab,* vol. 71, pp. 342-51, Sep-Oct 2000.

[90]   G. Lamoureux, E. Harder, I. V. Vorobyov, B. Roux, and A. D. MacKerell Jr, "A polarizable model of water for molecular dynamics simulations of biomolecules," *Chemical Physics Letters,* vol. 418, pp. 245-249, 1/25/ 2006.

[91]   B. A. Reva, A. V. Finkelstein, and J. Skolnick, "What is the probability of a chance prediction of a protein structure with an rmsd of 6 å?," *Folding and Design,* vol. 3, pp. 141-147, 4// 1998.

[92]   Y. H. Xie and A. K. Soh, "Investigation of non-covalent association of single-walled carbon nanotube with amylose by molecular dynamics simulation," *Materials Letters,* vol. 59, pp. 971-975, 4// 2005.

[93]   G. Stirnemann, S.-g. Kang, R. Zhou, and B. J. Berne, "How force unfolding differs from chemical denaturation," *Proceedings of the National Academy of Sciences,* vol. 111, pp. 3413-3418, March 4, 2014 2014.

[94]   M. M. Ouberai, K. Xu, and M. E. Welland, "Effect of the interplay between protein and surface on the properties of adsorbed protein layers," *Biomaterials,* vol. 35, pp. 6157-6163, 8// 2014.

[95]   M. L. Connolly, "Solvent-accessible surfaces of proteins and nucleic acids," *Science,* vol. 221, pp. 709-13, Aug 19 1983.

[96]   X. Yu, D. Chattopadhyay, I. Galeska, F. Papadimitrakopoulos, and J. F. Rusling, "Peroxidase activity of enzymes bound to the ends of single-wall carbon nanotube forest electrodes," *Electrochemistry Communications,* vol. 5, pp. 408-411, 5// 2003.

[97]   Z. Du, Y.-L. Yu, and J.-H. Wang, "Functionalization of Multi-Walled Carbon Nanotubes and their Application for Selective Isolation of Acidic Proteins," *Macromolecular Bioscience,* vol. 9, pp. 55-62, 2009.

[98]   Y. Cheng, G. R. Liu, Z. R. Li, and C. Lu, "Computational analysis of binding free energies between peptides and single-walled carbon nanotubes," *Physica A: Statistical Mechanics and its Applications,* vol. 367, pp. 293-304, 7/15/ 2006.

[99]   Y. Kang, Y.-C. Liu, Q. Wang, J.-W. Shen, T. Wu, and W.-J. Guan, "On the spontaneous encapsulation of proteins in carbon nanotubes," *Biomaterials,* vol. 30, pp. 2807-2815, 5// 2009.

[100]   W. L. Jorgensen, J. Chandrasekhar, J. D. Madura, R. W. Impey, and M. L. Klein, "Comparison of simple potential functions for simulating liquid water," *The Journal of Chemical Physics,* vol. 79, pp. 926-935, 1983.

[101] Z. He and J. Zhou, "Probing carbon nanotube–amino acid interactions in aqueous solution with molecular dynamics simulations," *Carbon,* vol. 78, pp. 500-509, 11// 2014.

[102] L. J. Lanticse, Y. Tanabe, K. Matsui, Y. Kaburagi, K. Suda, M. Hoteida*, et al.*, "Shear-induced preferential alignment of carbon nanotubes resulted in anisotropic electrical conductivity of polymer composites," *Carbon,* vol. 44, pp. 3078-3086, 11// 2006.

[103] P. Pötschke, S. M. Dudkin, and I. Alig, "Dielectric spectroscopy on melt processed polycarbonate—multiwalled carbon nanotube composites," *Polymer,* vol. 44, pp. 5023-5030, 8// 2003.

[104] A. Oberlin, M. Endo, and T. Koyama, "Filamentous growth of carbon through benzene decomposition," *Journal of Crystal Growth,* vol. 32, pp. 335-349, 3// 1976.

[105] M. Paradise and T. Goswami, "Carbon nanotubes – Production and industrial applications," *Materials & Design,* vol. 28, pp. 1477-1489, // 2007.

[106] L. E. Murr and P. A. Guerrero, "Carbon nanotubes in wood soot," *Atmospheric Science Letters,* vol. 7, pp. 93-95, 2006.

[107] A. C. Dillon, T. Gennett, K. M. Jones, J. L. Alleman, P. A. Parilla, and M. J. Heben, "A Simple and Complete Purification of Single-Walled Carbon Nanotube Materials," *Advanced Materials,* vol. 11, pp. 1354-1358, 1999.

[108] B. W. Smith, Z. Benes, D. E. Luzzi, J. E. Fischer, D. A. Walters, M. J. Casavant*, et al.*, "Structural anisotropy of magnetically aligned single wall carbon nanotube films," *Applied Physics Letters,* vol. 77, pp. 663-665, 2000.

[109] C. Park, J. Wilkinson, S. Banda, Z. Ounaies, K. E. Wise, G. Sauti*, et al.*, "Aligned single-wall carbon nanotube polymer composites using an electric field," *Journal of Polymer Science Part B: Polymer Physics,* vol. 44, pp. 1751-1762, 2006.

[110] Y. Kunitoshi, A. Seiji, and N. Yoshikazu, "Orientation and purification of carbon nanotubes using ac electrophoresis," *Journal of Physics D: Applied Physics,* vol. 31, p. L34, 1998.

[111] X. Xu, R. Ray, Y. Gu, H. J. Ploehn, L. Gearheart, K. Raker*, et al.*, "Electrophoretic Analysis and Purification of Fluorescent Single-Walled Carbon Nanotube Fragments," *Journal of the American Chemical Society,* vol. 126, pp. 12736-12737, 2004/10/01 2004.

[112] K. A. Ferguson, "STARCH-GEL ELECTROPHORESIS--APPLICATION TO THE CLASSIFICATION OF PITUITARY PROTEINS AND POLYPEPTIDES," *Metabolism,* vol. 13, pp. SUPPL:985-1002, Oct 1964.

[113] J. Fromageau, E. Brusseau, D. Vray, G. Gimenez, and P. Delachartre, "Characterization of PVA cryogel for intravascular ultrasound elasticity imaging," *IEEE Trans Ultrason Ferroelectr Freq Control,* vol. 50, pp. 1318-24, Oct 2003.

[114] W. Sun, H. Tomita, S. Hasegawa, Y. Kitamura, M. Nakano, and J. Suehiro, "An array of interdigitated parallel wire electrodes for preparing a large-scale nanocomposite film with aligned carbon nanotubes," *Journal of Physics D: Applied Physics,* vol. 44, p. 445303, 2011.

[115] W. Xue and P. Li, *Dielectrophoretic Deposition and Alignment of Carbon Nanotubes*, 2011.

[116] M. Gao, S. Huang, L. Dai, G. Wallace, R. Gao, and Z. Wang, "Aligned coaxial nanowires of carbon nanotubes sheathed with conducting polymers," *Angewandte Chemie,* vol. 39, pp. 3664-3667, 2000.

[117] D. M. Bigg and D. E. Stutz, "Plastic composites for electromagnetic interference shielding applications," *Polymer Composites,* vol. 4, pp. 40-46, 1983.

[118] Z. Ounaies, C. Park, K. E. Wise, E. J. Siochi, and J. S. Harrison, "Electrical properties of single wall carbon nanotube reinforced polyimide composites," *Composites Science and Technology,* vol. 63, pp. 1637-1646, 8// 2003.

[119] O. Meincke, D. Kaempfer, H. Weickmann, C. Friedrich, M. Vathauer, and H. Warth, "Mechanical properties and electrical conductivity of carbon-nanotube filled polyamide-6 and its blends with acrylonitrile/butadiene/styrene," *Polymer,* vol. 45, pp. 739-748, 2// 2004.

APPENDIX

A1. NAMD Molecular Dynamics

Atomic position obey Newton's second law:

$$m_i \frac{d^2}{dt^2} r_i(t) = -\nabla_i F\big(r_1(t), r_2(t), \ldots, r_N(t)\big)$$

- NAMD uses spatial decomposition algorithm to divides the simulation space into rectangular regions called patches
- Each patch is responsible for updating the coordinates of the atoms contained in its region of space
- Patch dimensions are greater than the cutoff radius for non-bonded interactions
- In parallel molecular dynamics, spatial decomposition evenly distributes computational load to causes the region of space mapped to each processor
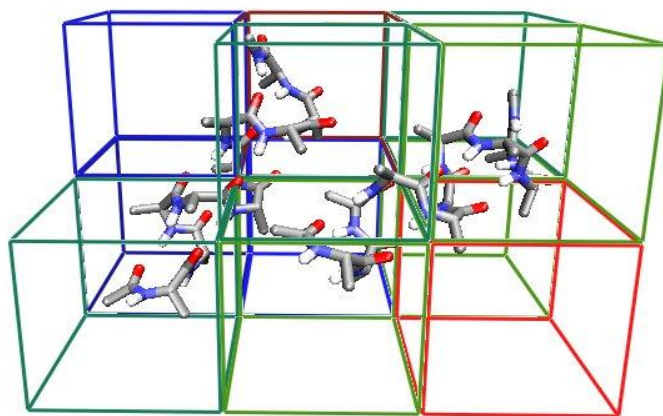
Figure A 1. NAMD patches using spatial decomposition algorithm

A2. Steps Involved in MD Computation
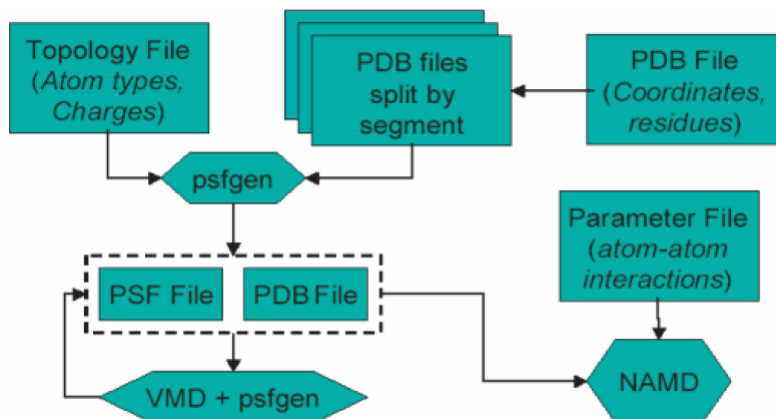
Figure A 2. Flowchart indicating the role of files as used by VMD, NAMD, and psfgen

A3. PSF Structure Building

```
package require psfgen
topology top_all27_prot_lipid.inp
pdbalias residue HIS HSE
pdbalias atom ILE CD1 CD
segment U {pdb adjustspa.pdb}
coordpdb adjustspa.pdb U
guesscoord
writepdb spa1.pdb
writepsf spa1.psf
```

A4. Tcl Script for preparing pdb/psf of Single walled carbon nanotube

```
package require nanotube
package require psfgen
proc writetop {{op ""}} {
  if {$op=="del"} {
    file delete tmp.top
```

137

```
  } else {
    set fz [open "tmp.top" w]
    puts $fz "* >>> Top File for C Cluster<<< "
    puts $fz "0   1                           "
    puts $fz "MASS    21 CA     12.01100 C \n  "
    puts $fz "RESI CNT          0.00          "
    puts $fz "GROUP                           "
    puts $fz "ATOM C    CA      0.00 \n        "
    puts $fz "PRES LINC         0.00          "
    puts $fz "BOND 1C 2C \n                    "
    puts $fz "END                             "
    close $fz
  }
}
proc nanotube2 {length n m {output nanotube}} {
  nanotube -l $length -n $n -m $m
  set sel1 [atomselect top all]
  $sel1 set resid [$sel1 get index]
  $sel1 writepdb tmp1.pdb
  writetop
  resetpsf
  topology tmp.top
  segment CCC {pdb tmp1.pdb}
  set xyz [$sel1 get {x y z}]
  foreach c1 [$sel1 get resid] {
    foreach c2 [$sel1 get resid] {
      set dist [vecdist [lindex $xyz $c1] [lindex $xyz $c2]]
      if {$c1 < $c2 && $dist < 1.8} {
        patch LINC CCC:$c1 CCC:$c2
      }
    }
  }
  coordpdb tmp1.pdb CCC
  regenerate angles dihedrals
  writepdb ${output}.pdb
  writepsf ${output}.psf
 writetop del
```

A5. Root mean square deviation (RMSD) of protein

$$rmsd = \sqrt{\frac{1}{N}\sum_{i-1}^{N}\left(R_i - R_{i+1}\right)^2}$$

N is number of atoms

R_i is atom coordinates of original protein structure

R_{i+1} is atom coordinate of protein structure in i+1 frame
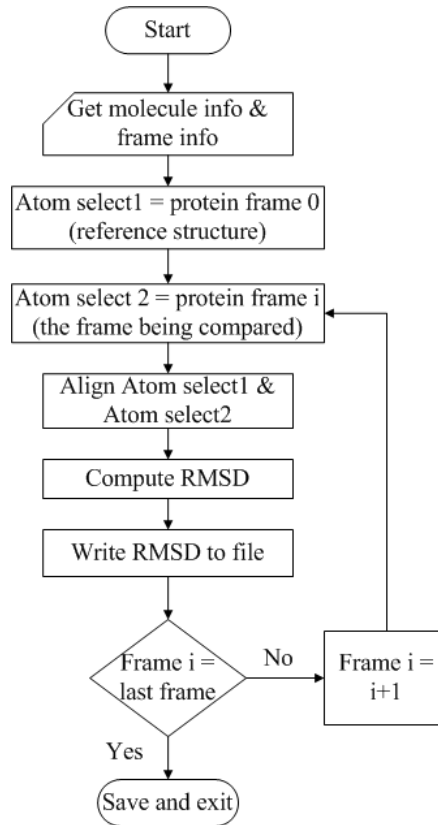
Figure A 3. Flow chart to calculate RMSD of protein

TCL Script to calculate RMSD

```
set outfile [open rmsd.dat w];
set nf [molinfo top get numframes]
set frame0 [atomselect top "index START to END and backbone and
noh" frame 0]
set sel [atomselect top "index START to END and backbone and
noh"]
# rmsd calculation loop
for {set i 1 } {$i < $nf } { incr i } {
    $sel frame $i
    $sel move [measure fit $sel $frame0]
    puts $outfile "[measure rmsd $sel $frame0]"
}
close $outfile
```

A6. TCL script to calculate distance between center of protein and center of carbon nanotube

```
set chan [open massdistance.dat w]
    set num_steps [molinfo top get numframes]
    puts $chan "$num_steps"
for {set frame 0} {$frame < $num_steps} {incr frame} {
    set sela [atomselect top "protein" frame $frame]
    set selb [atomselect top "index START to ENT of CNT" frame
    $frame]
    set gca [measure center $sela weight mass]
    set gcb [measure center $selb weight mass]
    set dist [veclength [vecsub $gca $gcb]]
    puts $chan "$dist"
    }
close $chan
```

A7. TCL script to calculate number of protein atoms adsorbed on CNT surface

```
set outfile [open number.dat w];
set a [molinfo top get numframes]
for {set i 0 } {$i <= $a} { incr i } {
set b [atomselect top "(protein within 5 of index START to END OF
CNT) and not hydrogen" frame $i]
    set c [$b num]
    puts $outfile "$c"
}
close $outfile
```
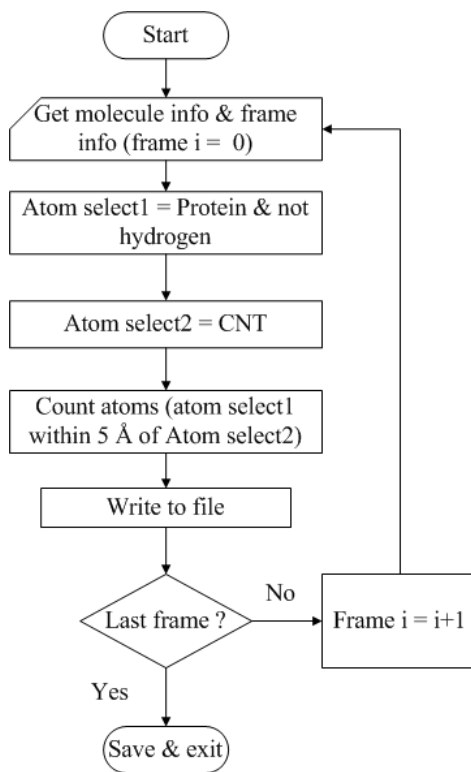

Figure A 4. Flow chart to calculate number of protein atoms adsorbed on CNT surface

A8. TCL script to calculate radius of gyration

```tcl
set gr [open Rg.dat w];
 set nf [molinfo top get numframes]
 # gyration is sqrt( sum((r(i) - r(center_of_mass))^2) / N)
for {set i 1 } {$i < $nf } { incr i } {
  set sel [atomselect top protein frame $i]
  set com [measure center $sel]
  set sum 0
  foreach coord [$sel get {x y z}] {
    set sum [vecadd $sum [veclength2 [vecsub $coord $com]]]
  }
  set b [expr sqrt($sum / ([$sel num] + 0.0))]
   puts $gr "$b"
 }
close $gr
```

A9. Configuration file for fix process run

```
#############################################################
## JOB DESCRIPTION                                         ##
#############################################################
# Minimization and Equilibration of
# Protein in a Water Box
#############################################################
## ADJUSTABLE PARAMETERS                                   ##
#############################################################
structure          File.psf
coordinates        File.pdb
set temperature    300
set outputname     results_FixProcess
firsttimestep      0
```

142

```
##############################################################
## SIMULATION PARAMETERS                                    ##
##############################################################
# Input
paraTypeCharmm      on
parameters          par_all27_prot_lipid.inp
temperature         $temperature


# Force-Field Parameters
exclude             scaled1-4
1-4scaling          1.0
cutoff              12.0
switching           on
switchdist          10.0
pairlistdist        14.0


# Integrator Parameters
timestep            2.0  ;# 2fs/step
rigidBonds          all  ;# needed for 2fs steps
nonbondedFreq       1
fullElectFrequency  2
stepspercycle       10
# Constant Temperature Control
langevin            on    ;# do langevin dynamics
langevinDamping     1     ;# damping coefficient (gamma) of 1/ps
langevinTemp        $temperature
langevinHydrogen     off      ;# don't couple langevin bath to
hydrogens


# Periodic Boundary Conditions
cellBasisVector1    X    0.   0.0
cellBasisVector2    0.0  Y    0.0
cellBasisVector3    0.0   0    Z
cellOrigin          X' Y' Z'


wrapAll             on
```

143

```
# PME (for full-system periodic electrostatics)
PME                yes
PMEGridSpacing     1.0


# Constant Pressure Control (variable volume)
useGroupPressure       yes ;# needed for rigidBonds
useFlexibleCell        no
useConstantArea        no
langevinPiston         on
langevinPistonTarget   1.01325 ;#  in bar -> 1 atm
langevinPistonPeriod   150.0
langevinPistonDecay    75.0
langevinPistonTemp     $temperature


# Fixed Atoms Constraint (set PDB beta-column to 1)
if {1} {
fixedAtoms         on
fixedAtomsFile     fixFile.pdb
fixedAtomsCol      B
}
# Output
outputName         $outputname


restartfreq        500      ;# 500steps = every 1ps
dcdfreq            250
xstFreq            250
outputEnergies     100
outputPressure     100
############################################################
## EXECUTION SCRIPT                                      ##
############################################################


# Minimization
minimize           5000
reinitvels         $temperature
run 20000 ;# 40ps
```

A10. Configuration file for 100ns molecular dynamics run

```
##################################################################
## JOB DESCRIPTION                                            ##
##################################################################
# Perform MD run after completion of fix process run
##################################################################
## ADJUSTABLE PARAMETERS                                      ##
##################################################################


structure           File.psf
coordinates         File.pdb
outputName          output-result


#set temperature    300


# Continuing a job from the restart files
if {1} {

binCoordinates      results_FixProcess.restart.coor
binVelocities       results_FixProcess.restart.vel
extendedSystem      results_FixProcess.restart.xsc
}
firsttimestep       25000


##################################################################
## SIMULATION PARAMETERS                                      ##
##################################################################
## Input
paraTypeCharmm          on
parameters          par_all27_prot_lipid.inp
# NOTE: Do not set the initial velocity temperature if you
# have also specified a .vel restart file!
#temperature          $temperature
```

```
# Periodic Boundary conditions
# NOTE: Do not set the periodic cell basis if you have also
# specified an .xsc restart file!
if {0} {
cellBasisVector1    X      0.   0.0
cellBasisVector2    0.0    Y    0.0
cellBasisVector3    0.0    0    Z
cellOrigin          X' Y' Z'
}


wrapAll             on


# Force-Field Parameters
exclude             scaled1-4
1-4scaling          1.0
cutoff              12.0
switching           on
switchdist          10.0
pairlistdist        14.0


# Integrator Parameters
timestep            2.0  ;# 2fs/step
rigidBonds          all  ;# needed for 2fs steps
nonbondedFreq       1
fullElectFrequency  2
stepspercycle       10


#PME (for full-system periodic electrostatics)
if {1} {
PME                 yes
PMEGridSpacing      1.0
}


# Constant Temperature Control
langevin            on    ;# do langevin dynamics
langevinDamping     1     ;# damping coefficient (gamma) of 5/ps
langevinTemp        300
```

```
        langevinHydrogen       off      ;# don't couple langevin bath to
hydrogens

        # Constant Pressure Control (variable volume)
        if {1} {
        useGroupPressure       yes ;# needed for 2fs steps
        useFlexibleCell        no  ;# no for water box, yes for membrane
        useConstantArea        no  ;# no for water box, yes for membrane

        langevinPiston         on
        langevinPistonTarget   1.01325 ;#  in bar -> 1 atm
        langevinPistonPeriod   100.0
        langevinPistonDecay    50.0
        langevinPistonTemp     300
        }

        restartfreq            2500      ;# 500steps = every 1ps
        dcdfreq                2500
        xstFreq                2500
        outputEnergies         2500
        outputPressure         2500
        #############################################################
        ## EXECUTION SCRIPT                                       ##
        #############################################################

        # Minimization
        minimize     5000
        run 50000000 ;# 100ns
```